Swej Yogesh Shah was born in Mumbai, India, on March 14 1991. It was here that he completed his bachelor's degree in Chemical Engineering at the Institute of Chemical Engineering (ICT, formerly UDCT) in 2013. In the fall of that year he swapped Mumbai for Delft in The Netherlands. He pursued an MSc in Applied Earth Sciences at the Technische Universiteit Delft. He completed two internships before graduating Cum Laude with a specialisation in Petroleum Engineering two years later. For his internships, he worked at Chevron in The Hague and SINTEF in Oslo in the summer of 2014 and 2015, respectively. Following his graduation, Swej managed the Field Development Project course at TU Delft before pursuing his doctoral studies (PhD) under the supervision of Prof. Dr. William Rossen and Dr. Karl-Heinz Wolf.

A combination of wanderlust and his PhD project, took Swej to various parts of the world, which enabled him to explore new places and feed his appetite for adventure.

When Swej is not working, he enjoys playing sports. He is an active member of the Punch basketball club, and plays football with friends and colleagues after work. Additionally, Swej enjoys cooking and photography.

In Situ Foam Generation In Flow Across a Sharp Permeability Transition

Swej Yogesh Shah

In Situ Foam Generation In Flow Across a Sharp Permeability Transition

Swej Yogesh Shah

In Situ Foam Generation
In Flow Across a Sharp Permeability Transition

Swej Yogesh Shah

Invitation

To attend the public defense of my PhD thesis:

In Situ Foam Generation
In Flow Across a Sharp Permeability Transition

On:
Wednesday November 20th 2019
@
12:30 h in the Auditorium of the Technische Universiteit Delft

After the public defense you are welcome to join me
@
PSOR Café
Stevinweg 1
2628 CN Delft

for a reception

Don't hesitate to contact Swej or one of the paranymphs if you have any questions

Swej Shah
swej.shah@outlook.com
0649270889

Romy Meier
romymeier93@gmail.com
0646328464

Sian Jones
s.a.jones@tudelft.nl
0634059734

Propositions

accompanying the dissertation

IN SITU FOAM GENERATION

IN FLOW ACROSS A SHARP PERMEABILITY TRANSITION

by

Swej Yogesh SHAH

1. Foam, that would not be generated in a porous medium in steady flow at a low velocity, can be created at the same velocity in flow from low- to high-permeability provided that the permeability change is sharp and the contrast is great enough (Chapters 2 and 3).

2. Foam strength, when generated by snap-off in flow from low- to high-permeability, is greater when the permeability contrast is greater (Chapter 2).

3. Foam generation by snap-off across a permeability boundary is an intermittent process. This intermittency is greater with greater permeability contrasts, lower velocities and/or higher gas fractions (Chapters 2 and 3).

4. Brooks–Corey type drainage capillary-pressure (P_c) curves do not allow for snap-off to be modelled. Even during a drainage process, a brief moment of local imbibition causes snap-off. The corresponding reduction in P_c can be modelled only if van Genuchten type or imbibition curves are used (Chapter 3).

5. For a PhD candidate, learning to be critical is a precursor to, and a bigger achievement than, mastering a subject.

6. The impact of the students that a PhD candidate supervises should be considered among the achievements of a PhD candidate.

7. Writing a PhD dissertation involves multiple feedback loops in which the first iteration is invariably unintelligible. That gibberish is still useful, as it motivates a second wave of writing and the feedback loop continues.

8. A research group where confidentiality within the group is minimized and the exchange of ideas is promoted can produce more valuable results than its antithesis.

9. When a country has too many rules, something is missing in the flavour of its people, but a little bit of tolerance and open-mindedness in its people helps mitigate the blandness.

10. “Action isn’t just the effect of motivation, it’s the cause of it." - Mark Manson

11. Kobe Bryant is the greatest basketball player of all time.
12. In research, failure is also a valuable result.

These propositions are regarded as opposable and defendable, and have been approved as such by the promotor prof. dr. W. R. Rossen.

In Situ Foam Generation

In Flow Across a Sharp Permeability Transition

In Situ Foam Generation

In Flow Across a Sharp Permeability Transition

Proefschrift

ter verkrijging van de graad van doctor
aan de Technische Universiteit Delft,
op gezag van de Rector Magnificus prof. dr. ir. T.H.J.J. van der Hagen,
voorzitter van het College voor Promoties,
in het openbaar te verdedigen op
woensdag 20 november 2019 om 12:30 uur

door

Swej Yogesh Shah

Master of Science in Applied Earth Sciences,
Technische Universiteit Delft, Nederland,
geboren te Mumbai, India.

Dit proefschrift is goedgekeurd door de

promotor: prof. dr. W.R. Rossen
promotor: dr. K.-H.A.A. Wolf

Samenstelling promotiecommissie:

Rector Magnificus,	voorzitter
prof. dr. W.R. Rossen	Technische Universiteit Delft, promotor
Dr. K.-H.A.A. Wolf	Technische Universiteit Delft, promotor
Onafhankelijke leden:	
Prof. dr. ir. E. Schlangen,	Technische Universiteit Delft
Prof. dr. J.J.C. Geerlings,	Technische Universiteit Delft
Prof. dr. G.J. Hirasaki,	Rice University, USA
Dr. H. Hajibeygi,	Technische Universiteit Delft
Dr. R.D. Tewari	PETRONAS, Maleisië

This research work was sponsored by Universiti Teknologi PETRONAS.

Keywords: foam generation, snap-off, capillary heterogeneity, enhanced oil recovery, synthetic porous media

Printed by: Ipskamp Printing

Front & Back: Design by Romy Meier

ISBN 978-94-6366-221-5

An electronic version of this dissertation is available at
http://repository.tudelft.nl/.

Universal law is for lackeys
Context…is for kings.

Captain Lorca, Star Trek Discovery

PREFACE

This dissertation is the result of original work conducted at the Geoscience and Engineering Laboratory of the Delft University of Technology in the period November 2015 – November 2019. This work is directly related to the use of foam for subsurface displacement processes such as enhanced oil recovery (EOR), aquifer remediation and CO_2-storage. When I started working on this project, the idea was to examine a potential “Plan B" that aimed to sustain foam deep inside the reservoir. If foam does not propagate far from a well, this might bring the utility of foam as an effective agent for improving sweep efficiency into question. The mechanism studied in this work, namely snap-off across sharp permeability changes, is shown to be a useful mechanism for generating foam in situ, deep inside a reservoir. The results of this thesis imply positive consequences for the applicability of foam for the above-mentioned displacement processes.

In this book, the chapters succeeding “Introduction" are either published or submitted journal papers. Therefore, they can, in principle, be read individually. While I have tried to simplify the terminology used in this thesis as much as possible, it is expected that the reader is familiar with some basic nomenclature used in the petroleum-engineering community. It is also expected that the reader is aware of how oil is produced from the subsurface and what causes it to flow.

When I started my doctoral studies, the first order of business was to find the right porous medium for my experiments. Based on the experimental plan, after screening possible options, we chose to use porous sintered glass cores. To the best of my knowledge, sintered glass samples of comparable dimensions have never been used before for coreflooding experiments. As you will read through the rest of this thesis, we learned a great deal about cores made out of sintered glass and their applicability for a wide range of coreflooding experiments. We also investigated other methods to create synthetic porous media for future experimentalists.

Foam is a complicated system, and its behaviour in a porous medium is far more complicated than in bulk. We have been studying foam in porous media for over forty years and we still do not completely understand it. That is, in my opinion, the beauty of foam, for it will always keep your mind occupied. Foam is still not widely used as an EOR agent, but my experiences have led me to conclude that foam is effective, and safe, with respect to the displacement processes mentioned above. What we really need at this point is more data from field-scale implementations of this technology. We need a well-documented success story, one that prompts companies that invest in this research, to actually implement it.

Swej Yogesh Shah
Delft, October 2019

CONTENTS

SUMMARY

Liquid foams are a distribution of discontinuous gas bubbles separated by liquid lamellae, which are part of a continuous liquid phase. For subsurface applications, liquid foams can be used to displace a resident fluid, such as oil or water, from underground formations. For instance, for processes such as enhanced oil recovery (EOR), foam can be used to displace oil towards a producing well. For aquifer/soil remediation, foams can be used to displace non-aqueous liquids and clean the groundwater system.

In most cases, foam is a more efficient displacing fluid compared to those that are conventionally used, such as gas (for example, natural gas or CO_2) or water. Since creating foam requires gas, foam is especially attractive in processes where gas is already being used and is readily available on site. In the presence of foam, gas mobility is reduced. As a result, sweep efficiency is improved when compared to a gas-only injection process. The success of the foam application relies heavily on how far foam can propagate in the subsurface reservoir. The deeper it goes, the greater is the amount of resident fluid it can contact and displace from the pores of a rock.

Usually, foam is generated close to the well through which it is injected due to a high pressure-gradient in that region. When the pressure gradient is low, as is the case away from these wells, the resident fluids migrate at a lower velocity. Under those conditions, it is not certain how far foam can propagate or whether it can maintain its strength. In such a situation, some phenomena that occur in situ, can help generate foam, which can have a positive impact on the application.

In situ mechanisms of foam generation can help generate foam far from where it is being injected. These mechanisms depend on the properties of the rock and the fluids. One such mechanism is snap-off. Snap-off is the term given to the bridging of a pore throat (initially occupied by a non-wetting fluid such as gas) by a wetting fluid (water) through capillary action. This can happen in several different ways. In this work, we examine one particular mechanism of snap-off that can cause foam generation in flow across a sharp increase in permeability.

To motivate the research presented in this work, first, in Chapter 1, a general introduction to foam in porous media is presented. Snap-off, and other pore-level mechanisms responsible for creating bubbles in a porous medium are described. Previous work on snap-off in flow across a permeability boundary, both theoretical and experimental, is reviewed in detail. Possible modelling approaches for simulating the mechanism of snap-off studied in this work are also reviewed in this chapter. Considering the previous work, the existing gap in knowledge and the motivation behind this work is highlighted in this chapter. At the end, the research objectives are outlined.

Chapters 2 and 3 are the main body of this thesis. This is an experimental study where the process of foam generation is investigated through so-called coreflood experiments. Such experiments are conducted using cylindrical pieces of a porous medium. Fluids are injected from one end and produced from the other. Pressure and phase saturations are measured during the course of an experiment to observe flow generation and propagation. The cores used in this study are made from sintered glass and were initially designed to replicate the sharp changes in permeability found in nature.

At the beginning of Chapter 2, the experimental procedure is described in detail. Technical specifications of the various porous media used in this study, to perform foam-generation experiments, are also reported in the same section. Through Chapters 2 and 3, various experiments conducted during the course of this project are presented. These experiments were conducted to investigate the effect of permeability contrast, velocity and gas fraction on the process of snap-off in flow across an abrupt permeability increase. The experimental results are used to validate preceding theoretical work that explains this mechanism.

Through several experiments conducted as part of this work, the drawbacks of using long cylindrical sintered glass samples for coreflooding experiments are identified. As a result, a short study was undertaken in order to explore other possible options for creating well-characterized porous media with predetermined properties for laboratory studies. The results of this investigation are presented in Chapter 4, together with an overview of our experiences with using sintered glass porous media.

In Chapter 5, the main conclusions from this work are summarized. Additionally, some directions for future work in this field of research are proposed.

SAMENVATTING

Vloeibaar schuim is een verdeling van gasbellen gescheiden door vloeibare lamellen als onderdeel van een vloeistof. Voor ondergrondse toepassingen kan vloeibaar schuim gebruikt worden om aanwezige vloeistoffen, zoals olie en water, te verdringen uit de ondergrond. Bijvoorbeeld, voor processen zoals tertiaire oliewinning (enhanced oil recovery: EOR), kan schuim worden gebruikt om olie te verdringen naar een producerende olieput. In bodemsanering kan schuim gebruikt worden om vervuilende vloeistoffen uit het grondwatersysteem te verwijderen.

In de meeste gevallen is schuim een efficiëntere vloeistof verdringer dan wat normaliter gebruikt wordt, zoals bijvoorbeeld gas (aardgas of CO_2) of water. Omdat er gas nodig is om schuim te creëren, is het gebruik van schuim bijzonder aantrekkelijk daar waar al gas beschikbaar is. In de aanwezigheid van schuim, wordt de mobiliteit van gas verminderd. Als gevolg daarvan wordt de efficiëntie van de verdringing verbeterd in vergelijking met wanneer alleen gas wordt geïnjecteerd. Het succes van het toepassen van schuim is sterk afhankelijk van hoe ver het schuim zich kan verspreiden in het ondergrondse reservoir. Hoe dieper het schuim gaat, hoe groter de hoeveelheid vloeistof die in contact kan komen met het schuim en kan worden verplaatst uit de poriën van het gesteente.

Doorgaans wordt schuim dicht bij de injectie bron gegenereerd vanwege de hoge drukgradiënt in dat gebied. Wanneer de drukgradiënt laag is, wat het geval is ver van de bron, zullen de aanwezige vloeistoffen migreren met een lagere snelheid. Onder deze condities is het niet zeker hoe ver het schuim zich zal verspreiden en of het zijn sterkte blijft behouden. In zulke situaties, kunnen sommige fysische mechanismen die in de poriën plaatsvinden ook lokaal voor extra schuimvorming zorgen om zodoende de toepasbaarheid van schuim te helpen vergroten.

Lokale mechanismen voor schuim generatie kunnen dus helpen bij het maken van schuim ver van de plek waar het geïnjecteerd is. Deze mechanismen zijn afhankelijk van de eigenschappen van het gesteente en de vloeistoffen. Een zo'n mechanisme is "snap-off". Deze term wordt gebruikt als een porie vernauwing (in eerste instantie gevuld door een niet-bevochtigende vloeistof zoals gas) door capillaire werking wordt overbrugd door een bevochtigende vloeistof (water). Er zijn verschillende manieren waarop dit tot stand kan komen. In dit werk bekijken wij specifiek het zogenaamde snap-off mechanisme dat leidt tot schuimvorming in een stroming bij een sterke toename van de permeabiliteit (doorlatendheid).

Om het belang van het verrichtte onderzoek aan te geven wordt, allereerst, in hoofdstuk 1, een algemene introductie voor schuim in poreuze media gegeven. Snap-off, en andere mechanismen op porieniveau verantwoordelijk voor het creëren van bellen in poreuze media worden hier beschreven. Eerder werk aan snap-off in een

stroming over een permeabiliteitsgrens, zowel theoretisch als experimenteel, wordt gedetailleerd beschouwd. Mogelijke modelleringen voor het simuleren van snap-off mechanismen worden eveneens in dit hoofdstuk bestudeerd. Het bestaande werk, de nog ontbrekende kennis en het belang van het onderwerp komen aan de orde. Aan het einde van dit hoofdstuk worden de onderzoeksdoelen geschetst.

Hoofdstukken 2 and 3 zijn het voornaamste deel van dit proefschrift. Het is een experimentele studie waarin het proces van schuimvorming wordt onderzocht aan de hand van zogenaamde "coreflood" experimenten. Bij zulke experimenten wordt gebruik gemaakt van een cilindrisch poreus medium. Aan een kant wordt vloeistof geïnjecteerd en aan de andere kant geproduceerd. Gedurende het verloop van het experiment worden druk en saturatie van de verschillende fasen gemeten om de vorming en het voortbeweging van het schuim te bepalen. De in deze studie gebruikte kernen zijn gemaakt van gesinterd glas en zijn oorspronkelijk ontworpen om een sterk contrast in permeabiliteit te weerspiegelen zoals dat van nature voorkomt.

Aan het begin van hoofdstuk 2, wordt de experimentele procedure gedetailleerd beschreven. De technische specificaties van de verschillende poreuze media die in deze studie gebruikt worden voor schuimvormingsexperimenten worden hier ook genoemd. Verder in hoofdstukken 2 and 3, worden de verschillende, in de loop van het project uitgevoerde, experimenten gepresenteerd. Deze experimenten zijn uitgevoerd om te onderzoeken wat het effect is van permeabiliteitscontrast, snelheid en gasfractie op het proces van snap-off in stroming door een abrupte permeabiliteitsverhoging. De experimentele resultaten worden gebruikt om eerder theoretisch werk dat dit mechanisme verklaart te kunnen toetsen.

Door het uitvoeren van de verschillende experimenten als deel van dit werk worden de bezwaren van het gebruik van lange cilindrische gesinterde glasmonsters voor coreflood experimenten duidelijk. Dientengevolge is een korte studie opgezet die andere mogelijke manieren om goed gedefinieerde poreuze media met van te voren bepaalde eigenschappen voor laboratorium testen te maken beschrijft. De resultaten van dit onderzoek worden gepresenteerd in hoofdstuk 4, samen met een overzicht van onze ervaringen met het gebruik van poreuze media van gesinterd glas.

In hoofdstuk 5, worden de conclusies van dit werk samengevat. Daarnaast worden mogelijkheden voor toekomstig werk in dit onderzoeksveld voorgesteld

List of Figures

LIST OF TABLES

Abbreviations, Symbols and Nomenclature

a	=	Acceleration [m/s^2]
A	=	Cross-sectional area of the core [m^2]
c	=	Consolidation coefficient [m^2/s]
C	=	Sorting coefficient [-]
CMC	=	Critical micelle concentration [wt.%]
d	=	Grain diameter [m]
dl	=	Infinitesimal distance [m]
e	=	Voidage [-]
g	=	Acceleration due to gravity [9.81 m/s^2]
h	=	Height of a sample e.g. sandpack [m]
HU	=	X-ray CT measurement in Hounsfield units [HU]
k	=	Absolute permeability [m^2]
k_{rg}	=	Gas relative permeability [-]
k_{rw}	=	Liquid (water or surfactant solution) relative permeability [-]
l	=	Distance, from central axis of the centrifuge [m]
L	=	Core Length [m]
m	=	Cementation coefficient [-]
P	=	Absolute pressure [Pa]
P_c	=	Capillary pressure [Pa]
PVI	=	Pore volumes injected [-]
∇P	=	Pressure gradient [Pa/m]
r	=	Pore size [μm]
q	=	Flow rate [ml/min]
S	=	Phase saturation [-]
t	=	Time [s]
T	=	Dimensionless time [-]
u	=	Superficial (Darcy) velocity [m/s]
W	=	Weight [kg]
x	=	Distance along the core [m]
ϕ	=	Porosity [-]
μ	=	Viscosity [cP]
σ	=	Stress [N/m^2]
ρ	=	Bulk density [kg/m^3]
ω	=	Angular velocity [rad/s]

Superscripts

e	=	Entry-pressure, used to denote capillary entry pressure for a porous medium
L	=	Low-permeability region
LH	=	Region with low- to high-permeability transition
H	=	High-permeability region
min	=	Minimum, used to denote minimum ∇P or velocity required to generate foam
sn	=	Snap-off, used to denote critical capillary pressure required for snap-off
vb	=	Van Baaren, used to denote estimated permeability
0	=	Used to denote a property (ex: relative permeability) away from the permeability transition in the absence of foam

Subscripts

app	=	Apparent
dry	=	Denotes a dry core
exp	=	Denotes a measurement (e.g. CT attenuation) during an experiment
g	=	Gas
l	=	Liquid
liq	=	Denotes CT measurement of the liquid-saturated core
pre	=	Denotes the pre-centrifuge value of a property
post	=	Denotes the post-centrifuge value of a property
rock	=	Denotes a measurement for a rock
t	=	Total
v	=	Vertical direction
vt	=	Total in the vertical direction
w	=	Water
0	=	Denotes distance from the central axis of centrifuge to the top of the sample
50	=	Denotes median grain size

1

INTRODUCTION

In 2018, oil consumption worldwide rose by 1.5%, equivalent to roughly 1.4 million barrels per day (bbl/d). China and USA were the largest contributors to this growth, while the European Union maintained its 2017 consumption level (British Petroleum, 2019). While the demand for energy (including fossil fuels and modern renewables used to generate electricity) has increased steadily over the last year, gas and renewables have shown the most remarkable growth. Unfortunately, coal consumption has also increased despite the need, more now than ever, of the reduction of the human carbon footprint. Coal is primarily used to produce electricity, with increased consumption in developing countries such as India and Indonesia. With the current infrastructure, renewable sources cannot replace coal, let alone all fossil fuels, entirely in energy production. Using cleaner fossil-fuel based energy sources such as natural gas and oil, instead of coal, can significantly reduce the carbon footprint. In the Middle East, oil and natural gas accounted for more than 95% of the total electricity generation in 2018. Global demand for oil and gas will only increase in the near future. Hydrocarbons are not only used for power generation, but also to produce tens of thousands of products, many of which are used in daily life, such as pharmaceuticals, cosmetics, resins and clothes, among others.

Conventional oil-recovery techniques involve the utilization of reservoir pressure (the pressure in an oil bearing formation deep underground) to extract the oil via a well at the surface. In most cases, the reservoir pressure decreases as a greater amount of oil is produced from the reservoir. As a result, the potential to bring fluids to the surface is reduced and production diminishes. In this case, pressure is maintained by injecting another fluid such as water or gas into the same reservoir through injection wells. Currently, on average, 60-70% of the oil originally in place (OOIP) in a petroleum reservoir is left behind (Muggeridge et al., 2013), mainly because of the technical challenges and additional costs involved with conventional techniques to extract any incremental oil. Coupled with the realization that new giant reservoirs are becoming exceedingly difficult to find, this increases the potential for enhanced oil recovery (EOR). EOR involves the use of chemicals, along with better engineering and project

1

management, to improve recovery factors in a petroleum reservoir. One such technique involves the injection of surfactant solution and gas into a reservoir in order to create foam. Foam can act as an efficient displacement agent, boosting oil recovery by pushing larger amounts of oil towards a producing well (Bernard and Holm, 1964; Kovscek and Radke, 1994; Rossen, 1996).

Aside from the energy sector, subsurface processes also include groundwater resources, which are an important part of larger social-ecological systems. Groundwater pollution can cause the spread of serious water-borne diseases and negatively impact the local environment. Foams can also be used to displace contaminants from underground water-bearing formations (Hirasaki et al., 1997b,a, 2000; Mamun et al., 2002). The success of any project where foam is used as a displacement agent, whether to improve oil recovery or to remediate groundwater, relies on the long-term stability of foam and its ability to propagate over (often large) inter-well distances. This thesis investigates one particular mechanism that helps generate foam in-situ and may help sustain strong foam away from wells in any underground formation. This mechanism can have a significant impact on the design of foam EOR and aquifer-remediation projects. Recently, the use of of CO_2 foams for carbon sequestration has also received a significant amount of attention (Naderi Beni, A. and Varavei, A. and Farajzadeh, R. and Delshad, M., 2012; Vitoonkijvanich et al., 2015; Clark and Santiso, 2018; Rognmo et al., 2018). CO_2 foams have favourable properties due to the low interfacial tension between the gaseous and aqueous phase at reservoir conditions.

Early research on foam started with the application of foam for enhanced oil recovery in mind. As a result, most of the literature on foam in porous media applies to EOR. Nonetheless, many of the lessons learned and much of the knowledge gained from previous work applies to all applications of foam in porous media. In the next section, a general overview on the use of foam for EOR is presented with a focus on the behaviour of foam in a porous medium.

1.1. FOAM ENHANCED OIL RECOVERY

The "reservoir", as used in this thesis, is a subsurface rock formation containing hydrocarbons (oil, natural gas or a combination of the two) trapped by surrounding geological features. The reservoir together with the fluids residing in it are typically under immense pressures (in excess of 100 bar) and at a high temperature (typically $\approx 90\ ^\circ C$) owing to its depth below the surface of the Earth. As briefly stated earlier, reservoir liquids have conventionally been produced through wells, with water pushing the hydrocarbons from an injection well to a producing well. Water is less viscous and denser than oil. As a result, it bypasses or channels through a large amount of the fluids in place, leaving a lot of oil behind. Wettability of reservoir formations and permeability heterogeneity further reduce the effectiveness of displacement agents such as water and complicate the design of the process.

Gas, if available on site, can in principle be a more effective and economic displacement fluid. Most of the world's enhanced oil recovery (EOR) production comes

from injecting gases. At reservoir conditions, the gas can interact with the reservoir liquids, developing miscibility and essentially forming a single nonaqueous phase where the fluids contact. This improves microscopic sweep efficiency (Orr et al., 1982; Lake et al., 2014), leaving less to almost no residual oil behind in the region where gas contacts the oil. The size of this region, while desired to be the size of the whole reservoir, is a much smaller fraction of it, owing to the same problems that plague waterflooding techniques. For instance, gas is lighter than oil and tends to segregate to the top of the reservoir. Gas tends to flow through regions of higher permeability leaving oil behind in regions of lower permeability.

Foams are a distribution of discontinuous gas bubbles in a continuous liquid phase, can help mitigate several problems associated with gas flooding. When present as a foam, gas mobility is significantly reduced (Bernard and Holm, 1964; Huh and Handy, 1989; Chambers and Radke, 1990; Kovscek and Radke, 1994; Rossen et al., 1995; Rossen, 1996) leading to a more "viscosified" gas that gives better macroscopic sweep efficiency. In some cases, foam reduces gas mobility by a factor of tens of thousands (Cheng et al., 2000; Boeije and Rossen, 2015; Rossen and Boeije, 2015). Foam appears to be stronger and reduces gas mobility more in the high-permeability zones (Hirasaki, 1989; Zhou and Rossen, 1995; Rossen et al., 1995; Bertin et al., 1999), diverting flow to the low-permeability zones containing oil, thereby improving sweep efficiency in layered or highly heterogeneous formations.

1.1.1. FOAM GENERATION IN POROUS MEDIA

Foams in porous media can be generated through various mechanisms (Falls et al., 1988; Ransohoff and Radke, 1988; Kovscek and Radke, 1994; Rossen, 1996). Lamellae (liquid films separating bubbles) are created in porous media in three ways: lamella leave-behind, lamella division or snap-off. Snap-off itself can occur in many different ways (Rossen, 2003), with the most-studied mechanism being Roof snap-off (Roof, 1970). Roof snap-off was initially used to describe the creation of oil droplets in a strongly water-wet medium. In the context of this study, we are more interested in the mechanism of snap-off at sharp transitions in permeability that typically arise out of changes in rock type or sedimentary facies (large-scale features such as layering) and changes in grain size during deposition (small-scale features such as internal laminations and cross-laminations). At heterogeneity boundaries, the condition of capillary continuity implies a discontinuity in phase saturations. For two-phase flow from low- to high-permeability, this corresponds to a narrow region of high wetting-phase saturation at the edge of the low-permeability zone. Consider the two phases to be gas and water. Assuming a water-wet porous medium, as gas makes its way through a region of high water saturation, lamellae are formed in the region of higher permeability, as observed experimentally in Hirasaki et al. (1997b,a). The extreme case of this phenomena is the capillary end-effect which often leads to foam being observed at the outlet of a porous medium in coreflood experiments.

For a homogeneous medium, lamella leave-behind is one reason why foam generation is easier to achieve during drainage than during steady state flow (Rossen and

Gauglitz, 1990). During steady-state flow, lamellae division, according to some studies, is thought to be the primary mechanism for strong foam generation (Rossen and Gauglitz, 1990; Friedmann et al., 1991; Rossen, 1990a; Gauglitz et al., 2002; Tanzil et al., 2002a; Kam and Rossen, 2003). With reference to flow in porous media, foam generation, its propagation and stability are sensitive to several parameters, including injection rates, local pressure gradient, porosity, permeability, capillary pressure, oil saturation and oil composition, among other things. Injection rates, the pore framework of the rock and the concentration of the surfactant solution determine the strength and texture of the injected foam. In-situ foam texture is a complicated function of many factors including flow rates and pore geometry. Friedmann et al. (1986) reported from their experiments that bubble size, seen leaving the porous medium, was inversely related to injection velocity. Related to the utility of foams for enhanced oil recovery, it is not yet clear if foam generated at high ∇P near an injection well can propagate over large distances at a lower pressure gradient (Friedmann et al., 1986, 1994; Ashoori et al., 2012a; Yu et al., 2019). It may be that new foam must be created in situ as the foam advances (Rossen, 1990a,b,c,d; Rossen et al., 1995). If foam cannot propagate over several hundred meters, and it cannot be created in situ, then it cannot be considered a good candidate for mobility-control applications. In-situ phenomena responsible for the generation of foam may be key towards a successful foam trial. This work looks at a foam generation by snap-off due to flow across heterogeneities (such as cross laminations) in a porous medium. The creation of lamellae in this way is thought to be independent of the imposed pressure gradient and may serve as a back-up plan in the case that a foam front fails to propagate over large distances in an EOR application.

Homogeneous media. Foam generation is easier if gas and surfactant solution are injected into a medium initially saturated with surfactant solution (Gauglitz et al., 2002). Several laboratory experiments show that creation of strong foam in steady flow requires exceeding either a minimum velocity (u^{min}) or a minimum pressure gradient, denoted as ∇P^{min} (Ransohoff and Radke, 1988; Gauglitz et al., 2002; Tanzil et al., 2002a). Data shows three foam states, a "coarse" or "weak" foam state below this critical pressure drop, a "strong" foam state above it and an unstable transient state in between (Gauglitz et al., 2002). ∇P^{min} (or u^{min}) depends primarily on interfacial tension and rock permeability. Gauglitz et al. (2002); Isaacs et al. (1988) report that the minimum velocity for steam-foam generation in Berea sandstone scales roughly with the inverse of permeability. Sayegh and Girard (1989) perform their experiments with CO_2 (gas and supercritical) using both glass beadpacks and Berea sandstone cores as the porous medium. They report the requirement of a minimum velocity for foam generation in some of their beadpack experiments. The experimental studies of Sayegh and Girard (1989); Gauglitz et al. (2002) indicate that there may be a very low ∇P^{min} (or u^{min}) criterion for generation of CO_2 foam because of the low interfacial tension between the gas and liquid phases at elevated temperatures and pressures. Recently, a minimum pressure gradient was reported for Ethomeen C12 and CO_2 foam at high temperature (120 °C) and pressure (3400 psi) in studies conducted with carbonate cores (Cui et al., 2016; Jian et al., 2019).

Rossen and Gauglitz (1990) argue that foam generation in steady gas-liquid flow results from mobilization of lamellae due to a minimum pressure gradient rather than a minimum velocity per se. They use percolation theory to show that one can expect ∇P^{min} to scale roughly as k^{-1} for unconsolidated porous media. Here "k" denotes the average absolute permeability of the porous medium. ∇P^{min} also scales with gas-water surface tension which helps explain easier foam generation for CO_2 foam. Tanzil et al. (2002a) report that ∇P^{min} scales proportional to $k^{-1/2}$. More specifically, they define a dimensionless group $N_{cL} = \frac{\Delta P}{\sigma}\sqrt{\frac{k}{\phi}}$, and report that foam generation begins at a critical value $N^*_{cL} = 2$. Gauglitz et al. (2002) verify, through experimental data acquired over 2.5 orders of magnitude change in permeability, that in sandpacks and beadpacks the variation in ∇P^{min} is proportional to k^{-1}. Rossen and Gauglitz (1990); Gauglitz et al. (2002) also verify that foam generation is easier as the flow gets wetter, as observed by some other studies (Persoff et al., 1991; Friedmann et al., 1991; Kovscek et al., 1995).

Heterogeneous media. Several studies indicate that foam can be created by snap-off as gas and liquid flow across a sharp and abrupt increase in permeability, even under conditions in which foam would not be created in homogeneous media (Falls et al., 1988; Ransohoff and Radke, 1988; Rossen, 1999; Hirasaki et al., 2000; Tanzil et al., 2002b; Li and Rossen, 2005). The capillary-pressure/saturation relation is different on either side of the boundary at such a permeability transition. Yortsos and Chang (1990) describe the saturation response to such a capillary heterogeneity. Assuming that the relative-permeability functions are defined by the same function independent of permeability and wettability does not change, the solution to the flow problem across such an interface allows a discontinuity in saturation and predicts the accumulation of liquid just upstream of the boundary (Yortsos and Chang, 1990; van Duijn et al., 1995). In the case of flow from high- to low-permeability, one could expect a large saturation of the non-wetting phase such as gas or oil at the boundary of the high-permeability region. These would not be favourable conditions for foam generation. Steady flow across the boundary might be impossible unless one considers capillary dynamics i.e. unsteady-state flow (van Duijn et al., 2002, 2007).

In the experiments conducted by Falls et al. (1988), they observe snap-off at a sudden permeability increase. The criterion for snap-off to occur at such an interface is that capillary pressure in the pore-necks is below a critical value (P_c^{sn}), which was found to be approximately half the capillary entry pressure of the medium ($P_c^{sn} \approx P_c^e/2$). This is consistent with theoretical approximations for circular pore throats blocked by snap-off (Roof, 1970; Lenormand et al., 1983). Rossen (1999) used this result to show that for snap-off to occur in flow from low- to high-permeability zones, capillary pressure in the high-permeability zone must be less than half the capillary pressure in the low-permeability zone ($P_c^H < P_c^L/2$). In other words, the high-permeability region is at least four times as permeable as the low-permeability region ($k^H \geq 4\ k^L$), assuming $P_c \propto \sqrt{1/k}$. This trigger for foam generation depends only on the relative magnitudes of capillary pressure resulting from the heterogeneity and not directly on the magnitude

of capillary forces in each region. Therefore, for two different gas-liquid fluid pairs, if the liquid is strongly wetting compared to gas, the ratio of capillary pressures is independent of the interfacial tension between the gas-liquid phases, since the $P_c(S_w)$ curves would scale but not change shape. This is beneficial for practical applications of foam for displacement processes since the gas available on site can be used and foam generation in flow across permeability changes can still be expected, assisting with mobility control. The mobilisation of the generated foam, however, *would* depend on the gas-liquid interfacial tension. For instance, as implied earlier, CO_2 foams can propagate at lower pressure gradients compared to N_2 foams.

A greater permeability contrast is required to generate strong foam in drier flow, i.e. higher foam quality. **Fig. 1.1** shows the calculations of Rossen (1999), where the permeability contrast required to block gas flow by snap-off (effectively causing foam generation) is plotted as a function of the gas-water relative-permeability ratio far from the transition zone in the absence of foam. The relative permeability ratio relates to the injected fractional flow, $f_w = [1 + (k_{rg}/k_{rw})^0(\mu_w/\mu_g)]^{-1}$. Therefore, if $f_g = 80\%$, and $\mu_w/\mu_g = 50$, $(k_{rg}/k_{rw})^0 = 0.08$. According to **Fig. 1.1**, a permeability jump slightly higher than 4, at $f_g = 80\%$, would cause foam generation, independent of velocity or pressure gradient. However, if the pore geometry deviates from a circular shape, the ratio of P_c^e/P_c^{sn} may be larger or smaller than 2 (Lenormand et al., 1983; Chambers and Radke, 1990; Rossen, 2003). As a result, a greater or lower permeability contrast, respectively, may be required to block gas flow by snap-off at the same flowing gas fraction. It is important to note that while capillary pressure falls at the edge of the low-permeability zone, gas bubbles are expected to form at the entrance to the high-permeability zone. There is no dependency on pressure gradient. However, mobilisation of the bubbles and subsequent propagation away from the heterogeneity would require such a driving force.

Tanzil et al. (2002a) observe foam generation across such a sharp transition in permeability in their experiments. They employ a permeability ratio of 4.4 at a sharp boundary between two sandpacks of different grain sizes. The injected fraction of gas in their experiments is 67%. Their porous medium was set up horizontally. They use the theory of Yortsos and Chang (1990) to describe how a gradual increase in permeability would affect the capillary effect of the boundary, and by implication, foam generation. As the transition zone for the permeability rise becomes broader, the magnitude of change required to accumulate liquid and reduce capillary pressure below P_c^{sn} just upstream of the change, also increases. The theory of Yortsos and Chang (1990) indicates that strong foam can be generated by snap-off even when the permeability increase is gradual, although this may call for a greater permeability contrast.

Contrary to the findings of Tanzil et al. (2002a), Li and Rossen (2005), in their experiments, report *no* foam generation in sandpacks with permeability contrasts of 4.3:1 and 5.1:1. Instead, foam generation is reported when the permeability contrast was significantly greater, at 20:1. The mobilisation of this foam was periodic. Li and Rossen (2005) reports that the failure to obtain strong foam across the transition in permeability may be due to inefficient packing near the wall of the sandpack. For the

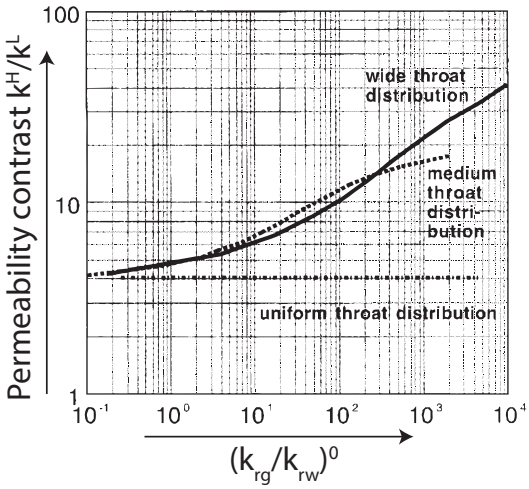

Figure 1.1: Theoretically computed permeability contrast required to completely block gas flow as a function of gas-water relative permeability ratio $(k_{rg}/k_{rw})^0$, with the superscript denoting its value far from the transition zone (Rossen, 1999). Left to right on the x-axis also represents an increase in gas fraction, as $f_w = [1 + (k_{rg}/k_{rw})^0(\mu_w/\mu_g)]^{-1}$.

lowest pressure drops employed in their experiments, injected gas fraction varied from approximately 75% to 85%. Additionally, the core was set up vertically, with flow from top to bottom. While Li and Rossen (2005) employ fixed pressure drops (for the gas phase) in their experiments, Tanzil et al. (2002a) employ fixed injection rates and gas fractions. Additionally, while Tanzil et al. (2002a) inject gas and surfactant solution into a column initially saturated with surfactant solution, Li and Rossen (2005) follow a different procedure, which might be the reason as to why they do not observe foam generation at similar permeability contrasts. In their experiments, the pack is initially saturated with brine. Then, brine is injected at a fixed rate and gas is co-injected at a fixed injection pressure. After steady state is achieved, surfactant solution replaces the brine.

1.1.2. LAMELLA DESTRUCTION

Lamellae can be destroyed either by rupturing of the liquid film between two bubbles or by gas diffusion from smaller bubbles to larger bubbles due to differences in gas pressure. A third mechanism, the drainage of liquid through the lamellae, can be neglected at pore scale. Foam coarsening, also known as Ostwald ripening, occurs when gas diffuses from smaller bubbles (higher pressure) that have to larger bubbles (lower pressure), with the consequence that smaller bubbles eventually disappear. Gas diffusion at higher foam qualities, once a bubble reaches pore size, is only appreciable through the thin, relatively flat sections of the liquid film in a pore throat. Bubble coarsening is a consequence of foams evolving towards a thermodynamic equilibrium by reducing their total surface area. In porous media, once bubbles grow to roughly the

same size as the pores, lamella destruction by diffusion ceases for both moving (Leeftink et al., 2015) and trapped bubbles. This is because lamellae in the middle of pore throats have zero mean curvature (Rossen, 1996).

Films can rupture due to mechanical disturbances or high capillary pressure. Film rupture by capillary suction is thought to be the primary mechanism of foam breakage in porous media (Jiménez and Radke, 1989; Chambers and Radke, 1990; Kovscek and Radke, 1994). The capillary pressure above which lamellae break is lower as the rate of lamella movement increases. This is because movement from pore body to pore constriction causes changes in lamella thickness. If the changes are rapid enough, there is not enough time for the liquid to flow into the lamella, causing it to rupture (Jiménez and Radke, 1989). As the rate of movement increases, a higher local liquid saturation (or lower capillary pressure) is required to refill the stretched lamella in time.

1.1.3. FIELD EXAMPLES

Several steam-flooding applications (Chad et al., 1988; Patzek et al., 1989; Patzek and Koinis, 1990; Castanier and Brigham, 1991; Friedmann et al., 1994; Patzek, 1996; Martinsen and Vassenden, 1999) demonstrate the ability of foam in reducing gravity override and channelling in conventional steam flooding applications. Chad et al. (1988) describe the injection sequence for foam with a gaseous phase of lean natural gas applied to the Pembina Ostracot 'G' Pool in west-central Alberta. They report an increment in production rate of approximately 32%, from 25 m^3/d to 33 m^3/d, over a 3-month period upon the injection of a 97 m^3 slug of brine mixed with surfactant. The ratio of liquid to gas injection rate was 5%, computed at reservoir conditions. Friedmann et al. (1994) report foam front propagation of up to 40 feet away from the injection well in a steam foam trial. Martinsen and Vassenden (1999) describe the FAWAG (Foam assisted water alternating gas) process applied to the Snorre field. Several other foam field trials have been reviewed by Shan (2001); Sheng (2013). Recently, a cost-effective way of creating blocking foams by injecting surfactant dispersed in hydrocarbon gas stream was tested in the field with success (Rossen et al., 2017; Ocampo et al., 2018).

1.1.4. MODELLING FOAM BEHAVIOUR IN POROUS MEDIA

Foam behaviour can be modelled in several ways, ranging from local-steady state models to more thorough, fully mechanistic approaches using population-balance or pore-network models. While the content of this thesis is purely experimental, we are interested in modelling foam generation by capillary snap-off and representing the same in a field-scale process. Therefore, a short summary of modelling approaches for foam in porous media is presented.

Method of characteristics or fractional-flow approach. The method of characteristics is an analytical technique for solving first-order PDE's by converting them into a system of ODE's. When applied to two-phase flow, it gives rise to fractional-flow theory, first introduced by Buckley and Leverett (1942) for oil/water systems. It can also be used to solve equations for foam flow (Zhou and Rossen, 1995; Rossen et al., 1999; Rossen and

Bruining, 2007; Namdar Zanganeh, 2011). This approach can provide accurate solutions for 1D test cases and can be used to benchmark simulators. It is important to note that since this approach has many assumptions, it often represents the best-case scenario and, possibly, the objective, of an EOR project. In spite of its assumptions, it can provide a valuable insight into foam behaviour.

Pore-network models. Chou (1990) attempted to build a completely mechanistic model for foam by linking foam generation to pore-size distribution based on percolation theory. In his model, it is assumed that lamellae are either stationary, or breaking or reforming at pore throats. Rossen and Gauglitz (1990) also used percolation theory to obtain an expression for the minimum pressure gradient (∇P^{min}) required for foam generation. As mentioned before, it stresses the importance of lamella mobilization and consequent division as a mechanism for foam generation. Chen et al. (2005a) propose a pore-network model, extending the work of Kharabaf and Yortsos (1997), to study the flow of fluids with a yield stress in a porous medium. The study of provides significant insights into the pore-level mechanics of foam generation in porous media. Fully dynamic pore-network models are computationally very expensive and a complete pore-network model for foam in porous media is yet to be developed.

Implicit-texture approach. Implicit-texture foam models represent the dependence of foam strength or gas mobility on foam texture or bubble size, implicitly. In fully mechanistic prediction of foam flow, foam texture is represented as lamella (or bubble) density. The next paragraph explains how this is achieved and why lamella density is important. Lamella density is defined as the number of lamellae per unit volume of the gas phase. Gas mobility in the implicit-texture modelling approach is an explicit function of a variety of local properties such as surfactant concentration, flow rates and water saturation, among others. These are believed to determine local lamella density. Since such a model assumes local steady state; it cannot account for dynamic foam generation and destruction. In other words, all implicit-texture models implicitly assume local equilibrium which means that the local rate of foam generation and destruction are equal and flow has reached a steady-state corresponding to local conditions (Islam and Ali, 1988; Kular et al., 1989; Patzek et al., 1989; Fisher et al., 1990; Law et al., 1992; Cheng et al., 2000; Lotfollahi et al., 2016). The implicit-texture approach as employed in the STARS^{TM} simulator of Computer Modelling Group Ltd. (CMG) (Vassenden et al., 1998; Shrivastava et al., 1999; Cheng et al., 2000) is widely used. In contrast, population-balance models employ an extra spatio-temporal differential equation to determine bubble size based on lamella creation and destruction rates, which in turn depend on local conditions. It is possible to adapt a population-balance model to local equilibrium (LE) by setting the expressions for lamella creation and destruction equal to each other (Kam et al., 2007; Myers and Radke, 2000; Chen et al., 2010; Ashoori et al., 2011).

Population-balance models. Population-balance models (Patzek, 1988; Falls et al., 1988; Friedmann et al., 1991; Kovscek et al., 1994, 1995, 1997; Fergui et al., 1998; Kam and Rossen, 2003; Zitha et al., 2006; Kam et al., 2007; Kam, 2008; Zitha and Du, 2010) provide a

framework to describe all mechanisms of foam behaviour. They explicitly represent how foam texture i.e. bubble size controls gas mobility. Foam texture depends on various mechanisms of foam generation and destruction.

In the population balance model describing foam behaviour in porous media, foam texture is represented as lamella or bubble density, as a separate variable. Population-balance models describe dynamics of lamella creation and bubble coalescence by introducing a conservation equation for the number of lamellae at each location (lamella density) in the porous medium. This is in addition to the usual time-dependent material balances on water, gas, surfactant, and oil, as in conventional reservoir simulation. This balance on lamellae includes convection, generation and destruction, and can include bubble trapping and liberation if these processes are represented explicitly. The model then represents gas mobility as a function of lamella density as well as other factors such as superficial velocity or capillary number. For instance, if gas in foam is modelled as a non-Newtonian fluid, gas mobility, in this modelling approach, can be modified to account for that. The dynamics of lamellae creation and destruction work on a shorter time scale compared to fluid transport Ashoori et al. (2011). This makes the system of equations "poorly conditioned" and "stiff", similar to a coupled geomechanics and fluid-flow problem.

Different population-balance models can be distinguished based on the lamellae-generation function they use. Some assume Roof snap-off to be a primary foam generation mechanism and therefore include gas and liquid velocities in their lamellae-generation function (Kovscek et al., 1997, 1995, 1994). Rossen (2003) points out that generation of lamellae by snap-off can occur in several different ways, with one of them being "Roof snap-off". Later, Kovscek et al. (2007) described a micro-model experiment which they claim verifies that roof snap-off is the primary mechanism for lamella creation in steady-state foam flow in porous media. Rossen (2008) points out some inconsistencies in this verification. Falls et al. (1988) include snap-off at a layer boundary as a mechanism for foam generation in their population balance model. They verify their model and the underlying assumptions through two elegant experiments. Their model, however, lacks generality, as there is no representation for lamella destruction by coalescence or coarsening or generation by mechanisms other than snap-off at layer boundaries. Friedmann et al. (1991) require a minimum velocity for foam generation in their model. Ransohoff and Radke (1988) propose a "germination-site" model to describe the onset of Roof snap-off and foam generation. Kam and Rossen (2003), for the first time, used a lamellae-generation function dependent on pressure gradient. This model was developed further to study the multiple steady-states of foam in porous media and to examine long distance propagation of foam in a reservoir (Kam et al., 2007; Kam, 2008; Ashoori et al., 2011; Ashoori and Rossen, 2012; Ashoori et al., 2012a). Modelling lamella creation in such a way makes the set of equations extremely stiff, and numerical dispersion can alter the strong-foam state (Ashoori et al., 2012b).

The approach of Falls et al. (1988) is well suited for application to foam generation across a sharp increase in permeability. Connecting capillary dynamics with lamella creation together with a shear-thinning foam rheology model could be the key to

modelling the experiments reported in this thesis.

1.2. SUBSURFACE HETEROGENEITY

Heterogeneity in petroleum reservoirs can scale from micrometers to kilometres. Small-scale (millimetre to metre) heterogeneity, such as stratification and cross-stratification, is known to reduce the efficiency of primary oil recovery due to capillary entrapment (van Lingen, 1998). The same kind of heterogeneity can induce snap-off and cause foam generation in a porous formation during flow of surfactant solution and gas, thereby improving the efficiency of oil recovery in a foam EOR application. As reported in the next chapters, foam generation in flow across an abrupt increase in permeability was observed in coreflood tests. The experiments were conducted at low superficial velocities and gas volume fractions, comparable to subsurface values. The permeability transition zone measured to be approximately 0.5 mm (or two coarse-grain diameters). Four different permeability contrasts were considered, comparable to measurements of small-scale heterogeneities found in the literature. Flow of gas across the heterogeneity is required for snap-off and foam generation to occur due to a sudden change in capillary pressure across the transition. In a layered reservoir, one can imagine that this may happen when gas migrates upwards across laminations or layer boundaries due to gravity. Vertical connectivity between the layers is assumed in this scenario. The primary viscous driving force in petroleum reservoirs, however, is in the horizontal direction, which is parallel to the typical orientation of laminations and layer boundaries. Therefore, vertical anisotropy may not be the most important type of heterogeneity with regards to foam generation. Horizontal anisotropy, though often less pronounced than vertical anisotropy, may play a crucial role in a subsurface foam application.

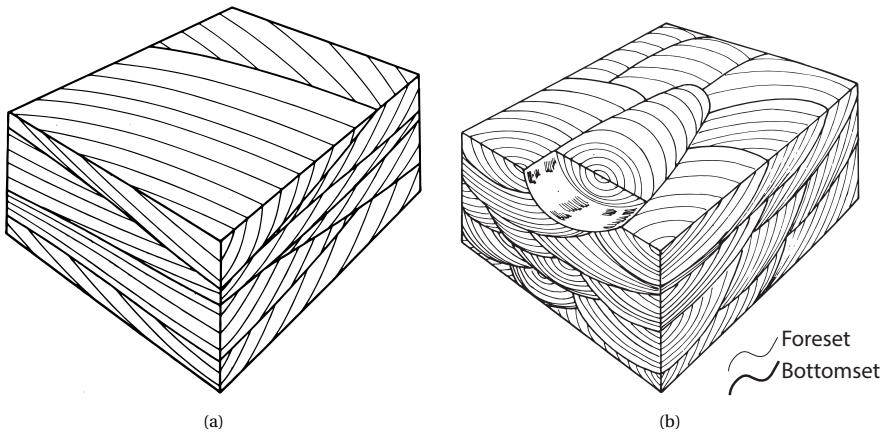

Figure 1.2: (a) Planar cross-bedding with tabular-to-wedge-shaped units and planar bedding surfaces, (b) Trough cross-bedding with festoon-shaped units. Well-developed troughs and strongly curved bedding surfaces in transverse direction. *From Reineck and Singh (1980).*

1

Cross-bedding (also called cross-stratification or cross-lamination) is one of the most common form of bedding encountered in geological formations. When present, it is arguably the biggest contributor to horizontal anisotropy. Cross-bedded sandstones comprise internal laminae oriented perpendicular or at an incline to the lateral direction. Therefore, it is more likely that fluids travel across cross-lamination heterogeneities in conventional reservoir flow. Reineck and Singh (1980) define a crossbed as:

A single layer, or a single sedimentation unit consisting of internal laminae (foreset laminae) inclined to the principal surface of sedimentation.

Erosion, non-deposition or an abrupt change in characteristics marks the bounding surface between adjacent sedimentation units. Based on the nature of this bounding surface, a cross-bedded unit is classified into two major types – planar crossbed and trough crossbed, as shown in **Fig. 1.2**. Fluvial deposits and deltaic deposits with a strong fluvial influence are commonly crossbedded. Fluvial systems occur together with aeolian, lacustrine or near-shore marine environments (Hartkamp-Bakker, 1993). Many conventional oil and gas reservoirs contain one or more formations deposited under a fluvial environment. The Snorre field in the Norwegian North Sea; Prudhoe Bay and Endicott, North Slope Alaska; the Tern field in the UK North Sea; and the Lakwa Field, Assam, India are some examples (Martin, 1993; van Lingen, 1998). Hartkamp-Bakker (1993) lists several outcrop examples of such formations in great detail, describing important geometrical and petrophysical parameters with respect to hydrocarbon recovery.

Characteristics of crossbedded reservoirs. Crossbedded sand-bodies form a subfacies within a larger geological setting. **Fig. 1.3** (van Lingen, 1998) shows a vertically stacked flow unit and gives an indication of the scales involved. Each sedimentary facies is bounded by sharper layer boundaries that mark large variations in characteristics. Within a sedimentary facies, one example of a trough crossbedding is demonstrated. The dimensions of the crossbeds shown can vary over several orders of magnitude. Thickness, width and length of the crossbeds may be related. For trough crossbeds, length:thickness ratios ranging from 10 to 30 and width:thickness ratios of 4 to 16 have been reported. For planar crossbeds, width:thickness ratios of around 20 are reported (Hartkamp-Bakker, 1993). Typical foreset inclination with respect to the bottomset is 35°. Foreset laminae thickness varies from less than a millimetre to a couple of centimetres (van Lingen, 1998).

Permeability contrast within crossbed laminae is usually a result of zones with contrasting grain size. Hartkamp-Bakker (1993) reports mini-permeameter and coreflood measurements of the permeability contrast in crossbedded sandstones acquired from outcrops and reservoir cores. She reports higher variability in foreset permeability values compared to the bottomset. From close to 2600 measurements taken from different fluvial outcrop locations in the Tertiary Loranca basin in central Spain, permeability distributions in foreset laminae show two distinct peaks associated with coarse-grained foreset laminae (CFL) and fine-grained foreset laminae (FFL).

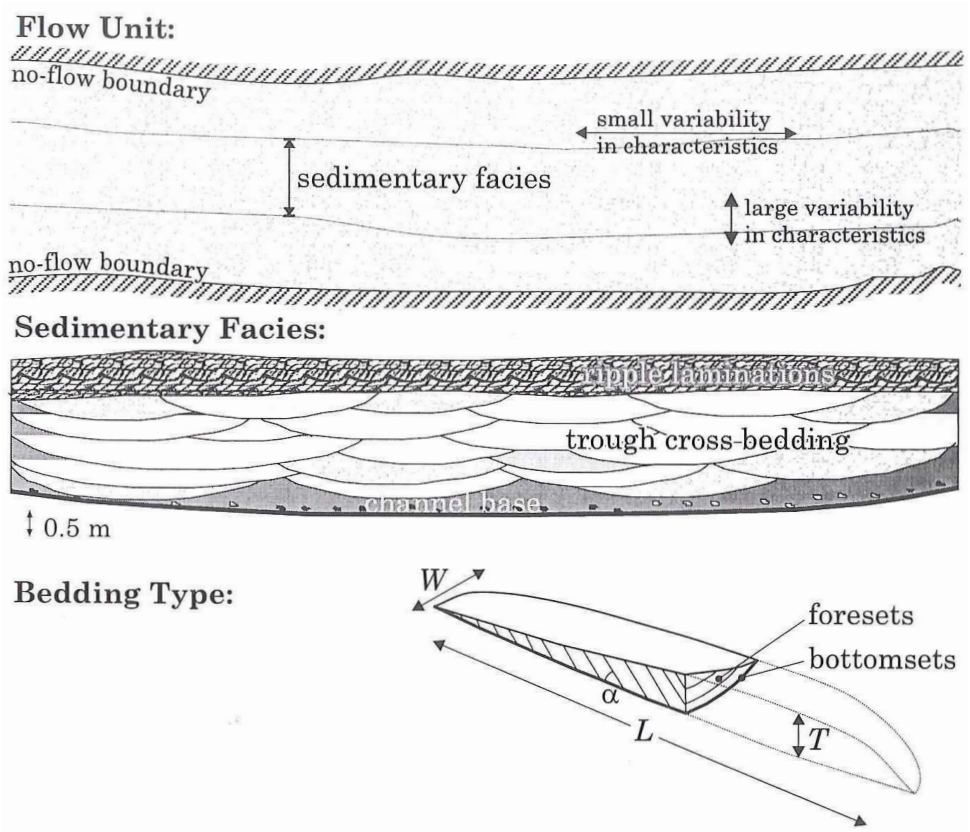

Figure 1.3: A reservoir flow unit with trough crossbedded subfacies. *From van Lingen (1998).*

Bottomset laminae (BL), on average, have a lower permeability compared to foreset laminae. In permeability distributions for bottomset laminae, the peak lies close to the FFL peak in the same distributions for foreset laminae. On average, the contrasts were 2:1.25:1 (CFL:FFL:BL). Similar measurements were also performed using core samples from offshore gas fields in the Dutch North Sea. Cores were extracted from the Upper Slochteren sandstone formation of the Upper Rotliegendes group and from the Vollpriehausen sandstone member of the Main Bundsandstein formation, which is arguably the most important reservoir rock of the Lower Triassic in the North Sea basin. Average permeability contrasts varying between 1.7:1.1:1 (CFL:FFL:BL) to 27.9:9.6:1 (CFL:FFL:BL) were reported. Permeability ratios between finer-grained foreset laminae and coarser-grained foreset laminae varied between 1.3:1 (CFL:FFL) and 5.4:1 (CFL:FFL).

1

1.3. RESEARCH OBJECTIVES

Based on the gap in knowledge addressed in the previous sections, the primary research objectives of this work are to:

- *Examine the process of foam generation in steady simultaneous two-phase flow across a sharp increase in permeability.*
- *Verify theoretical predictions (Rossen, 1999) and validate the underlying physical mechanisms through experimental data.*
- *Investigate the effect of permeability contrast, fractional flow and velocity on this process with a focus on field-relevance.*

In addition to the above, it is desired to generate an extensive set of experimental data that can be used to model this phenomenon through core-scale simulation followed by an upscaled representation on a field scale. The experiments were also designed to observe whether the foam mobilizes and propagates from the permeability boundary towards the outlet of the core at the field-like velocities employed.

To achieve these objectives, the following intermediate steps were followed:

- Acquire a synthetic porous medium, tailor-made to represent the sharp heterogeneities that result in foam generation. Characterize the petrophysical properties of the core.
- Design an experimental protocol where the chances of foam generation by mechanisms other than snap-off at a permeability boundary are minimized.
- Conduct a series of coreflood tests, with varying injection conditions, measuring local pressure and saturation (through X-ray computed tomography [CT]).

1.4. OUTLINE

This thesis comprises five chapters including this introduction and a conclusion. The remaining three chapters (Chapters 2-4) are based on peer-reviewed journal articles that are either published or to be published, reporting various results obtained from this study. While the article's have been edited to ensure continuity with the rest of the thesis, the reader might find possible repetition when compared with this chapter.

In Chapter 2, the experimental procedure employed to study foam generation by snap-off across sharp permeability boundaries is described in detail. Additionally, the effect of permeability contrast is investigated through four different core samples. Some of the shortcomings of using long, cylindrical, sintered-glass samples for corefloods are also highlighted, motivating Chapter 4.

In Chapter 3 the effect of fractional flow and velocity on this process is investigated.

Chapter 4 reports our attempts at creating synthetic porous media by sintering clay-rich grain aggregates and by consolidating sandpacks in a geo-centrifuge. Lessons learned from using sintered glass for corefloods are also presented.

Finally, in Chapter 5, relevant conclusions from the results of this study are presented with suggestions for future work.

2

Foam Generation by Snap-off in Flow Across a Sharp Permeability Transition: Effect of Permeability Contrast

Foam reduces gas mobility and can improve sweep efficiency in an enhanced oil recovery process. Previous studies show that foam can be generated in porous media by exceeding a critical velocity or pressure gradient. This requirement is typically met only near the wellbore and it is uncertain whether foam can propagate several tens of meters away from wells as the local pressure gradient and superficial velocity decreases. Theoretical studies show that foam can be generated, independent of pressure gradient, during flow across an abrupt increase in permeability. In this study, we validate theoretical predictions through a variety of experimental evidence. Coreflood experiments involving simultaneous injection of gas and surfactant solution at field-like velocities are presented. We use model consolidated porous media made out of sintered glass, with a well-characterized permeability transition in each core. The permeability change in these artificial cores is analogous to sharp, small-scale heterogeneities, such as laminations and cross-laminations. Pressure gradient is measured across several sections of the core to identify foam-generation events and the subsequent propagation of foam. X-ray computerized tomography (CT) provides dynamic images of the coreflood with an indication of foam presence through phase saturations. We investigate the effects of the magnitude of permeability contrast on foam generation and mobilization. Experiments demonstrate foam generation during simultaneous flow of gas and surfactant solution across a sharp increase in

permeability, at field-like velocities. The experimental observations also validate theoretical predictions of the permeability contrast required for foam generation by snap-off to occur at a certain gas fractional flow. Pressure-gradient measurements across different sections of the core indicate the presence or absence of foam and the onset of foam generation at the permeability change. There is no foam present in the system prior to generation at the boundary. CT measurements help visualize foam generation and propagation in terms of a region of high gas saturation developing at the permeability transition and moving downstream. If a coarse foam is formed upstream, it's transformed into a stronger foam at the transition. Significant fluctuations are observed in the pressure gradient across the permeability transition, suggesting intermittent plugging and mobilization of flow there. This is the first CT-assisted experimental study of foam generation by snap-off only, at a sharp permeability increase in a consolidated medium. The results of experiments reported in this paper have important consequences for a foam application in highly heterogeneous or layered formations. Not including the effect of heterogeneities on gas mobility reduction in the presence of surfactant could underestimate the efficiency of the displacement process.

2.1. INTRODUCTION

Foams are a distribution of discontinuous gas bubbles in a continuous liquid phase. They can be considered as an example of multiphase 'condensed soft-matter' systems. Foams have numerous applications in the food and chemical industries and in material science. This work focusses on the application of foam to enhanced oil recovery (EOR); more specifically, to capillary-dominated mechanisms of foam generation in porous media. Much of the world's EOR production can be attributed to the injection of gases, especially CO_2 and steam. Gas-injection processes, however, are often cursed by unfavourable mobility ratios and differences in fluid densities, which can lead to poor sweep efficiency. In the presence of foam, gas mobility is significantly reduced (Bernard and Holm, 1964; Huh and Handy, 1989; Rossen, 1996), leading to a more "viscosified" gas that gives better sweep efficiency.

There are three main mechanisms of creation of lamellae (liquid films separating bubbles): namely, lamella division, snap-off and leave-behind (Kovscek and Radke, 1994; Rossen, 1996). Lamella division, as can be inferred from **Fig. 2.1**, requires that at least one lamella or lens be initially present. Leave-behind primarily occurs during gas invasion through a liquid-filled medium and is more prevalent during a drainage process. Snap-off can occur by several mechanisms (Rossen, 2003). One mechanism is Roof snap-off (Ransohoff and Radke, 1988), which occurs as gas penetrates a narrow pore throat and drains liquid from a wide pore body, as illustrated in **Fig. 2.1b**. Another mechanism is snap-off as gas flows across a sharp increase in permeability (Falls et al., 1988; Rossen, 1999; Hirasaki et al., 2000; Tanzil et al., 2002b; Li and Rossen, 2005). This mechanism and the impact of permeability contrast on it is the subject of this chapter and is discussed further below.

Foams can be destroyed either by rupturing of the lamellae, for example, through

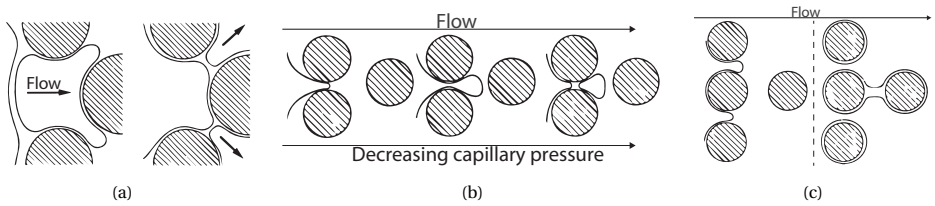

Figure 2.1: Mechanisms of lamella creation in porous media. *From Kovscek and Radke (1994).* (a) Lamella division. (b) Snap-off. (c) Leave-behind

mechanical disturbances or high capillary pressure, or by gas diffusion from smaller to larger bubbles within a pore due to differences in gas pressure. With respect to flow in porous media, foam generation, its propagation and stability, are sensitive to several parameters, including injection rates, local pressure gradient, porosity, permeability, capillary pressure, and oil saturation and composition, among other things. Laboratory experiments show that creation of strong foam in steady gas-liquid flow requires exceeding either a minimum velocity (u^{min}) or a minimum pressure gradient, denoted as ∇P^{min} (Ransohoff and Radke, 1988; Rossen and Gauglitz, 1990; Gauglitz et al., 2002; Tanzil et al., 2002a). Creation of foam in this case is thought to depend on mobilization of lenses and lamellae and subsequent lamella division. This criterion depends on the experimental procedure followed, and the threshold may be lower for a drainage process (for example, co-injection of gas and surfactant solution into a liquid-saturated core) owing to creation of lamellae by Roof snap-off and leave-behind (Rossen and Gauglitz, 1990). Nevertheless, the minimum-velocity or pressure-gradient threshold, as reported in the literature, may be overcome only near a well in a conventional reservoir and is much greater than that encountered away from wells deep inside the formation. This may have unfavourable consequences for foam propagation far from the injection well, as suggested by the experiments of Friedmann et al. (1994); Yu et al. (2019) and the modelling work of Ashoori et al. (2012a), who used the population balance model proposed by Kam (2008), where foam-generation rate is a function of pressure gradient only.

Several studies have indicated, however, that foam can be generated independent of pressure gradient, by snap-off, as gas and liquid flow across a sharp increase in permeability (Falls et al., 1988; Rossen, 1999; Hirasaki et al., 2000; Tanzil et al., 2002b; Li and Rossen, 2005). The extreme case of this phenomenon occurs at the outlet of the core in the form of foam generation as a consequence of the capillary end-effect. Yortsos and Chang (1990) presented the solution for steady gas-liquid flow across a permeability jump. Capillary continuity implies an increase in wetting-phase saturation (or reduction in capillary pressure) upstream of the permeability transition (van Lingen, 1998), which causes lamella creation by snap-off. In flow from high to low permeability, the opposite is expected to happen. Numerical simulations of two-phase flow from high to low permeability were reported by Chang and Yortsos (1992). The non-wetting phase accumulates immediately upstream of the boundary in the high-permeability zone. This

is similar to gas trapping as often witnessed in the void space upstream of the entrance to a core during gas-liquid injection. The same mechanism is responsible for the entrapment of oil in highly laminated sandstones as reported in the experiments of van Lingen et al. (1996). To summarise, during gas-liquid flow from high to low permeability, a dried out zone would exist at the boundary, creating conditions unfavourable for foam generation.

Sharp changes in permeability are quite common in petroleum reservoirs. Structural features that offer this sort of heterogeneity can exist across a large range of length scales. For example, in laminated and cross-laminated sandstones, the size of each unit could typically range from 1-1000 cm (Reineck and Singh, 1980). Unconformities such as layer boundaries can extend from a few metres to several hundred metres in length. Foam generation can occur as gas migrates upwards, due to gravity, across these layer boundaries, in the presence of surfactant solution. Gas and surfactant solution can also be driven to flow across vertical increments in permeability in the near-wellbore region when injected through highly deviated wells. While vertical anisotropy is more ubiquitous, laterally occurring permeability changes are also important as foam-generation sites because of the driving force of pressure gradient in the horizontal direction. Cross-laminations offer laterally occurring permeability changes oriented perpendicular or at an incline to the direction of fluid flow. **Fig. 2.2** shows two of the most-common classifications of crossbed units. As can be seen in the figure, the heterogeneity between consecutive laminae is usually a result of zones with contrasting grain size. Hartkamp-Bakker (1993) measured permeability contrasts in outcrop and reservoir core samples with crossbed laminae and reported contrasts ranging from 1:1 to 27:1 between different units.

Falls et al. (1988) observed foam generation and mobilization experimentally in a bead-pack with a permeability contrast of approximately 20:1. They also experimentally measured a critical capillary pressure for snap-off (P_c^{sn}) for the beadpacks used and found it to be approximately half the capillary entry pressure of the medium. For snap-off to occur, enough liquid must accumulate in the low-permeability section to cause the capillary pressure to drop below P_c^{sn}. Rossen (1999) uses this finding and a pore-network model to illustrate that for snap-off to occur at the boundary between two homogeneous regions differing in permeability; the minimum permeability ratio required is 4. A greater permeability contrast is required for drier flow. Once again, it is important to note that there is no pressure-gradient criterion for the creation of foam through this mechanism, though there may be such a condition for the mobilization of the foam. Tanzil et al. (2002b) report visual observations of foam generation and mobilization across such a sharp transition in permeability in their coreflood experiments with sand-packs inside a transparent glass column. They used a permeability ratio of 4.4:1 and an injected gas fraction of 67% for their experiments. Their experimental procedure, however, began with co-injection of gas and surfactant solution into a medium already saturated with surfactant solution, representing a drainage process. As discussed above, other mechanisms of foam generation (Roof snap-off and leave-behind) contribute towards the observed gas-mobility reduction during drainage. Contrary to the findings

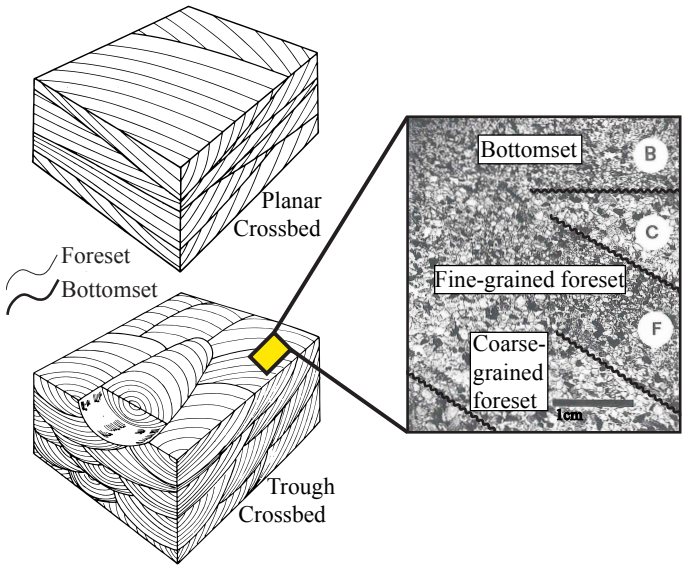

Figure 2.2: Left – Two common varieties of cross-stratification (*From (Reineck and Singh, 1980)*); Right – Changes in grain-size distribution across consecutive laminae as seen in a crossbed thin section from a fluvial outcrop (*From Hartkamp-Bakker (1993)*).

of Tanzil et al. (2002b), Li and Rossen (2005) did not observe foam generation in their sand-pack experiments with permeability contrasts of 4.3:1 and 5.1:1. Their experiment started with co-injection of gas and brine into a brine-saturated medium, followed by co-injection of gas and surfactant solution once steady-state has been reached. They suspected that gas bypass along the edges of the pack due to inevitable imperfect packing near a wall might have been the reason for failing to observe foam generation. They did, however, report foam generation during flow across a much greater permeability contrast of 20:1. The mobilization of this foam was periodic.

In this work, we follow an experimental procedure similar to the work of Li and Rossen (2005) and use a consolidated porous medium to examine the process of foam generation across an abrupt permeability jump. The main objective of this work is to validate the theoretical predictions of foam generation (Rossen, 1999) through coreflood experiments that isolate snap-off due to a capillary-pressure contrast as the only lamella-creation mechanism. We follow field-like superficial velocities to replicate the driving force encountered far from wells in a subsurface reservoir. We measure pressure gradient across several sections of the core to accurately identify the location for the first onset of foam generation and also to observe the propagation of this foam downstream. The experiments are assisted by X-ray computed tomography (CT) to help visualise phase saturations as foam generation and subsequent propagation commences.

This chapter is structured as follows. Section 2.2 describes the experimental set-up, the porous media used and the procedure followed in the experiments reported. Section 2.3 reports the results of the foam-generation experiments with pressure and

CT data obtained through the course of the experiment. The experimental results are analysed and discussed in Section 2.4, and the paper is concluded in Section 2.5.

2.2. EXPERIMENTAL METHODOLOGY

2.2.1. MATERIALS AND CHEMICALS

We perform coreflooding experiments with co-injection of gas and surfactant solution into an artificial porous medium made from sintered borosilicate glass. The cores were acquired from Hilgenberg GmbH, Malsfeld, Germany (www.hilgenberg-gmbh.de). The cores were prepared by sintering crushed, pure borosilicate glass and had a single sharp jump in permeability roughly a third of the way into the length of the core. In other words, roughly 1/3 of the core comprised a homogeneous low-permeability section whereas the rest of the core was made of a homogeneous high-permeability porous medium. The permeability change is achieved by sintering different grain sizes in the same core. The glass grains are angular as can be seen in the picture on the right in **Fig. 2.3**. While the cores were homogeneous in the axial direction, this was not always the case in the radial direction. On average, the porosity of the medium was 2-3% higher in a region roughly the size of a grain (0.1 to 0.5 mm for the cores used in this work) at the edges of the cylindrical core, compared to the bulk. This imperfection may be a result of differential expansion and contraction during the heating-up and cooling-down phase of the sintering process. Therefore, in the early stages of each experiment (described below), a significant amount of gas bypassed the brine-saturated core through the edge of the pack. Li and Rossen (2005) contend that this flow along the edges caused them to observe no foam generation across permeability contrasts of 4.3:1 and 5.1:1. However, this did not appear to affect our experiments, as we still observed foam generation across permeability contrasts, similar to those of Li and Rossen (2005), as reported in Section 2.4.

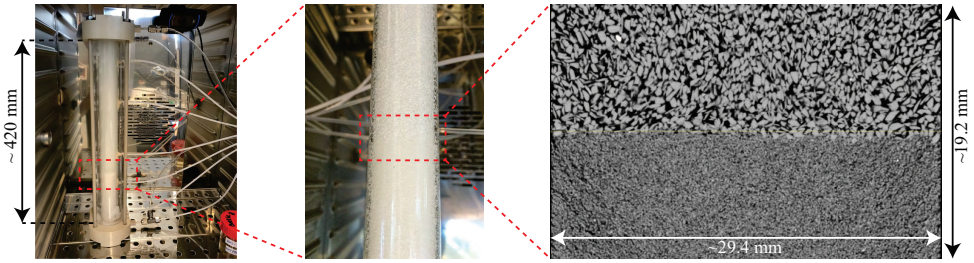

Figure 2.3: Core holder (left) with sintered-glass core (left and center) and μCT image (with a voxel size of 30 μm) of a vertical cross-section across the permeability change (right).

The cores were prepared in a glass tube with an internal diameter of 3 ± 0.1 cm and were cut after the sintering process to roughly 40 ± 2 cm in length. The core was enclosed in acrylic glass with polyether-ether-ketone (PEEK) end-caps. Four different core samples with different permeability ratios were acquired from the manufacturer, the details of which are mentioned in **Table 2.1**. The permeability to water is determined

from the slope of the straight line formed by a plot of superficial velocity versus the ratio of pressure gradient measured across the two core sections to viscosity (i.e. q/A vs $\nabla P/\mu$). The confidence interval for estimating this slope is also reported in darcies.

Table 2.1: Absolute permeability of individual sections and corresponding permeability contrast in heterogeneous sintered glass core samples used in the experiments. r represents average pore size, k is average permeability and superscripts L and H are used to denote average values for the low- and high-permeability regions, respectively.

Core sample	Pore size [μm] (Specified by manufacturer)	Approximate pore volume [ml]	Permeability [darcies]	$\langle \frac{k^H}{k^L} \rangle$
1	r^L: 16-40 r^H: 40-100	99	k^L: 5.4 ± 0.02 k^H: 20.7 ± 0.2	3.8
2	r^L: 40-60 r^H: 100-160	99	k^L: 10.9 ± 0.01 k^H: 59.3 ± 0.8	5.4
3	r^L: 16-40 r^H: 100-160	80	k^L: 3.1 ± 0.01 k^H: 43.2 ± 0.2	13.9
4	r^L: 16-40 r^H: 100-160	96	k^L: 1.7 ± 0.15 k^H: 46.7 ± 2.0	27.5

Anionic Alpha olefin sulfonate (AOS) $C_{14\text{-}16}$ with a molecular weight of 315 g/mol (Stepan® BIO-Terge AS-40 KSB) was used as a foamer at an active concentration of 0.5 wt.% (≈ 0.04 M). The surfactant solution was prepared using demineralized water also containing 1 wt.% (≈ 0.17 M) NaCl. The critical micelle concentration (CMC) of this surfactant in demineralized water with 1 wt.% NaCl was measured by Kahrobaei et al. (2017) using the Du Noüy ring method and reported to be 0.008 wt.%. Therefore, the experiments presented in this thesis are conducted at roughly 62 times the CMC. The properties of foam films stabilized by this surfactant in the presence of NaCl as an electrolyte are described by Farajzadeh et al. (2008). Nitrogen (N_2) with a purity of 99.98% was used as the gas phase in our experiments.

2.2.2. EXPERIMENTAL APPARATUS

A schematic flow diagram of the experimental set-up is shown in **Fig. 2.4**. The core is held horizontal in order to minimize the impact of beam-hardening effects and cross-artefacts while taking CT scans. Pressure gradient is measured every second across several sections of the core. In the low-permeability section, pressure gradient is used to confirm that there is no foam present or being generated as the experiment begins.

Across the permeability transition, pressure gradient indicates whether there is any foam being generated at the face of the heterogeneity. In the high-permeability section, pressure drop is used to monitor the mobilization of foam generated at the permeability change. We avoid the use of back-pressure regulators and employ atmospheric back-pressure instead, to avoid fluctuations introduced by multiphase flow through the back-pressure regulator. Any fluctuation in pressure at the downstream end could travel upstream, causing local fluctuations which would assist in foam generation. Therefore, the outlet of the core is open to atmosphere. The entire apparatus is placed on top of the CT scanner table. The medical CT scanner is housed in a temperature-controlled room at 21 ± 0.4 °C.

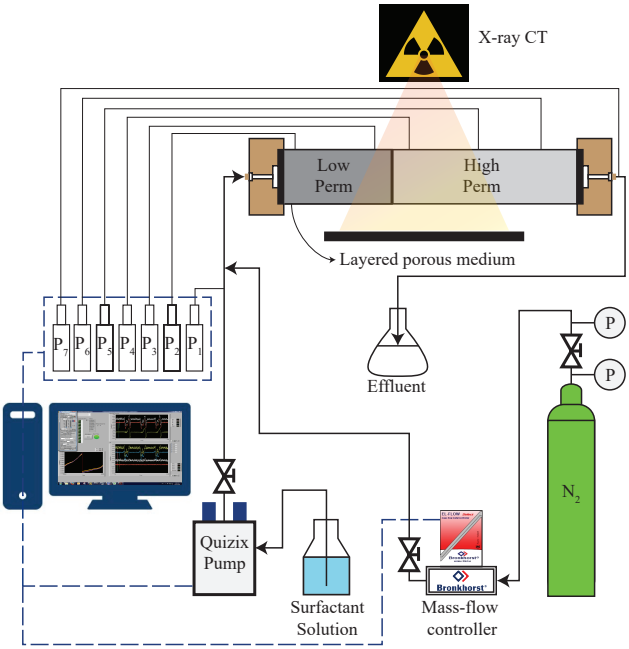

Figure 2.4: Schematic drawing of the experimental apparatus.

2.2.3. CT IMAGE ACQUISITION AND PROCESSING

The Siemens SOMATOM Definition Dual Energy CT scanner was used in this study. Since the experiments involved two-phase flow of fluids differing greatly in density, a single energy X-ray beam was used to scan the core. An overview of the image settings used is reported in **Table 2.2**. Single-slice helical CT scans were acquired with a pitch of 0.9, resulting in approximately 260 slices in each scan along the axis of a core, taken over a period of approximately 9 seconds for each core. A pitch less than 1.0 ensures X-ray beam overlap for the same scanned volume, resulting in a better image quality. One slice contains 512 × 512 pixels, a part of which contains the circular core cross-section. The images obtained were further processed to compute phase saturations using Fiji

Table 2.2: Overview of settings applied to the CT scanner

Parameter	Setting
Tube Voltage	140 KeV
Tube Current	250 mA
Pitch	0.9
Slice thickness	1.5 mm
Pixel size	1.5 × 1.5 mm^2
Scan mode	Spiral

(Schindelin et al., 2012), a distribution of the ImageJ software.

Raw CT data in terms of Hounsfield units (HU) are used to compute porosity and phase saturations as a voxel property for each image stack. Porosity can be obtained using the CT scans of a dry and water-saturated core (Mees et al., 2003). During the course of the experiment, liquid-phase saturation is computed for each scan as:

$$S_{liq} = \frac{HU_{exp} - HU_{dry}}{HU_{liq} - HU_{dry}} \tag{2.1}$$

where HU_{exp} denotes the CT measurement taken during the course of the multiphase flow experiment. HU_{dry} is the CT measurement of a dry core, obtained when the core is not yet saturated with any liquid, before each experiment. HU_{liq} represents the CT measurement for a core that is fully saturated with the liquid phase. In this work, HU_{liq} is recorded before the start of each experiment, when the core is fully saturated with brine solution. It is important to note that the accuracy of CT measurements depends on different parameters selected for the X-ray source, such as applied beam voltage, corresponding beam energy and the applied filters for shaping the beam. Once the liquid-phase saturations are computed for each multiphase scan, a colour scheme is applied to the images, where blue represents the aqueous phase and red represents the gas phase. The pixel size in each image slice is 195 × 195 μm^2 and each slice is 1.5 mm thick. The images are cropped to include only the circular cross-section of the core. Additionally, a distance of approximately 2 cm from the entrance and exit face has been cropped from the CT images of each core. This is done in order to avoid any misinterpretation due to the entrance and end-effects associated with corefloods. Moreover, anomalies in the saturation profile may arise from the fact that the first centimeter of each end of the core resides in the end-cap whereas the rest of the porous medium is only surrounded by the glass tube that houses it, as can be seen in **Fig. 2.3**. Liquid-phase saturation values are averaged in each cylindrical slice and plotted across the core length as shown in the next section. The saturation profile across the core can also be obtained by averaging values within each cylindrical image slice.

2.2.4. EXPERIMENTAL PROCEDURE

The basic sequence of steps carried out through each coreflooding experiment is as follows:

Permeability measurement. The setup is checked for leaks every time a new core is placed inside the core holder. Following the leak test, CO_2 is injected into the core for about 10 pore volumes (PV) to displace air present in the core. The last 2 PV of CO_2 are injected under vacuum. While under vacuum, demineralized, degassed water is injected at low flow rates of about 10^{-3} PV/min into the core to displace the CO_2. After water breakthrough, the core is brought to atmospheric pressure by closing the outlet and continuing water injection. Water injection is continued for another PV, following which the permeability of the core is measured by measuring pressure drop across different sections of the core at different flow rates. Next, the core is flushed with 1 wt.% NaCl brine and the permeability is calculated again. Measured permeability is used as the first indicator for the presence of any trapped gas in the core, especially when conducting multiple experiments with the same core.

Foam-generation experiment. At the end of the permeability measurement, the core is fully saturated with brine. To start the experiment, brine flow rate is set to the desired value and gas is introduced at the required fractional flow. Once gas-brine injection has reached steady-state, brine injection is replaced by surfactant injection. This procedure ensures that no foam is initially generated under drainage conditions. During the course of the experiment, we expect to see foam generation in the core. Once the experiment has reached steady state or sufficient data has been acquired, injection is stopped and the core cleaning procedure commences.

Core-cleaning procedure. After each experiment, the core is flushed with approximately 10 PV of 50 wt.% iso-propanol solution to kill the foam. This is followed by around ≈20-50 PV of demineralized water injection to remove all the alcohol and remaining surfactant solution from the system. If more experiments are to be performed with the same core, this step is followed by CO_2 injection and the permeability-measurement protocol.

2.3. RESULTS

Foam generation was observed in each experiment performed. All the experiments reported in this paper were carried out at a total injection rate (q_t) of 0.1 ml/min and a gas fractional flow of 80%. On average, this translates to about about 1.4 PV/day of total fluid injection for each core, which corresponds to a superficial (Darcy) velocity of 2.36 μm/s (0.67 ft/d) for each core. This superficial velocity was selected based on observations from a series of tests conducted at different flow rates. The objective of these tests was to select a velocity that was low enough to cause foam generation across the permeability transition only, registered by a pressure greater than the accuracy of the transducers, and in an experiment completed within a reasonable time frame. The "incubation effect" reported by Baghdikian and Handy (1991) and more recently observed by Kahrobaei et al. (2017) could result in foam generation throughout the

core when injection of surfactant solution and gas continues for long periods of time equivalent to several tens of pore volumes. At a velocity of 3.34 ft/d (0.5 ml/min), foam generation was observed in the inlet low-permeability section itself; evidently the pressure gradient in the low-permeability section was higher than the minimum pressure gradient required for foam generation. At a velocity of 1.34 ft/d (0.2 ml/min), foam generation was observed across the permeability transition and not in the inlet section. However, this total superficial velocity was still higher than that for fields with larger well spacing, as is often the case in offshore developments. At a superficial velocity of 0.67 ft/d (0.1 ml/min), we observed foam generation across the permeability jump and no foam in the inlet section, at least at the onset of foam generation across the heterogeneity. At flow rates lower than this, the experiment would take several weeks to conclude and the fluid velocities through the core would no longer be representative of conventional reservoir flow. Therefore, we selected a total superficial velocity of 0.67 ft/d for all subsequent experiments. Injected gas fraction was fixed at 80% in order to align with the theoretical predictions of Rossen (1999), who showed that snap-off in flow across an abrupt permeability increase depends on both gas fractional flow and permeability contrast. In his model, for foam generation to be observed at 80% gas fractional flow, the permeability contrast must be 4:1 or higher. Conversely, in flow across a permeability contrast of 4:1, the gas fractional flow must be 80% or lower in order to see foam generation. With the objective of validating this threshold in mind, since the lowest permeability contrast considered in this study was close to 4:1, an injected gas volume fraction of 80% was selected. In order to maintain consistency while studying the effect of permeability contrast, fractional flow was fixed at this value for all experiments.

Core 1. A foam-generation experiment was conducted with core sample 1, which has a permeability contrast of 3.8:1, close to the theoretical prediction of 4 required to cause foam generation by snap-off at 80% gas fractional flow (Rossen, 1999). **Fig. 2.6** shows the measured absolute pressures and the corresponding pressure gradient across various sections of the core. The origin of the plot represents the start of surfactant injection into the core, after steady-state has been achieved for the co-injection of gas and brine. Absolute pressure is measured at 7 locations across the length of the core, schematically shown in **Figs. 2.4** and **2.5**. The pressure transducers are connected to the top of the horizontally placed glass core. In the bottom plot (**Fig. 2.6b**), pressure gradient across 4 sections of the core is plotted: the inlet and outlet sections are ignored for the sake of readability.

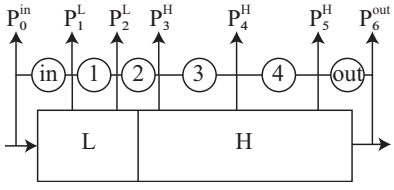

Figure 2.5: Schematic showing labelling scheme used to denote local pressure and pressure gradient.

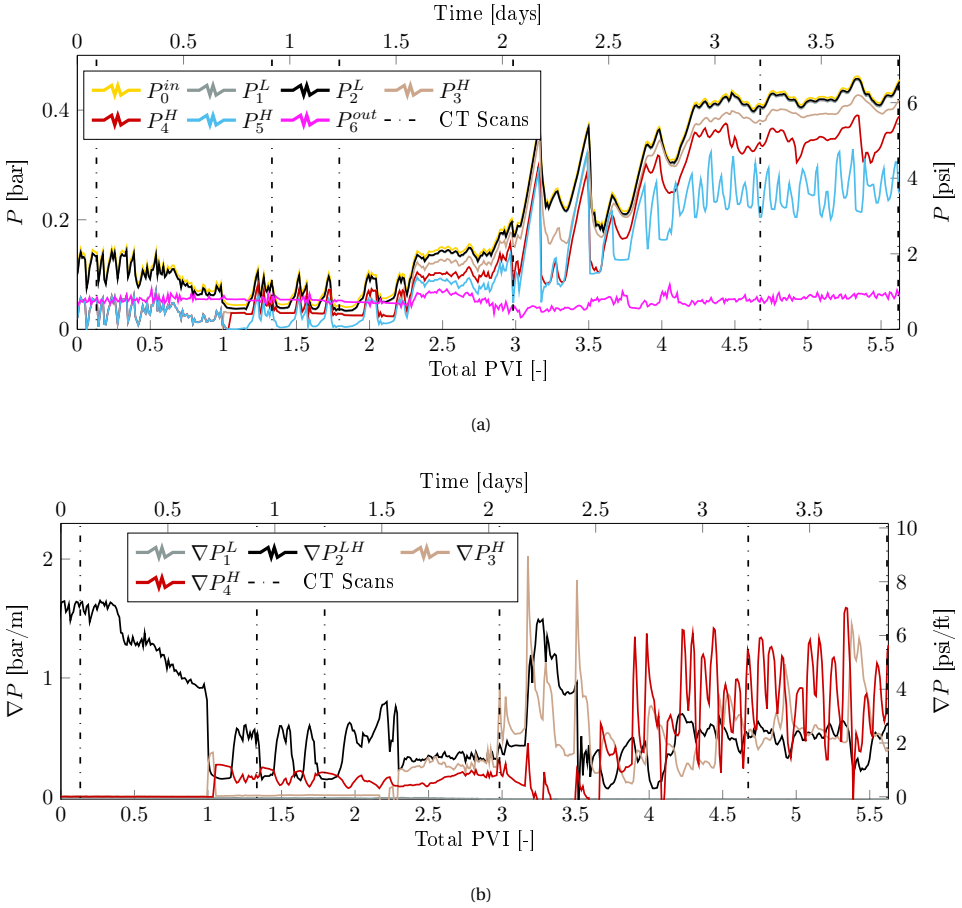

Figure 2.6: (a) Absolute pressure and (b) pressure gradient across various sections of core 1 during foam-generation experiment. Dash-dotted lines indicate times at which CT scans were taken to generate saturation maps across the length of the core. Superscript *L* represents a measurement in the low-permeability section, whereas superscript *H* represents data acquired from the high-permeability zone. *LH* represents the interval with the boundary.

Following **Fig. 2.6**, pressure gradient across the permeability transition rises sharply soon after gas is introduced into the core at 80% volume fraction. As co-injection of gas and brine reaches steady-state, ∇P_2^{LH} continues to register an unusually high pressure gradient. We believe that this is due to pressure taps across the permeability transition sensing different phases (McCool et al., 1983; Chen et al., 2016). This is further aggravated by gas trapping and the capillary effect caused by a sharp difference in capillary pressure between the two zones in this section. After surfactant injection begins, the measured pressure gradient shows a mild and gradual drop from about 0.3 PV to 1.0 PV of total injection. We suspect that this is because of a diffused surfactant front reducing the interfacial tension and subsequently, the capillary pressure between

the two phases at the pressure tap. It could also be due to a gradual build-up in gas saturation near the pressure tap in the high-permeability zone (McCool et al., 1983). In bulk, an increase in surfactant concentration reduces interfacial tension only below the CMC. At concentrations beyond the CMC, surfactant concentration has negligible effect on interfacial tension. Therefore, only a small amount of surfactant solution at a concentration much higher than its CMC would be enough to drastically reduce surface tension and capillary pressure.

Pressure gradient ∇P_1^L across the low-permeability zone is negligible through the course of the experiment, which suggests that there is no significant reduction in mobility or indication of strong foam present or being generated in the inlet section of the core. Dash-dotted lines in **Fig. 2.6** indicate times at which CT scans were taken across the entire length of the core. Raw CT data in Hounsfield Units is processed to obtain phase saturations as described in Section 2.2.3 (**Eq. (2.1)**).

When gas and brine are injected into the core, most of the gas overrides to the top and bypasses a large part of the core, as can be seen in the saturation map at the top in **Fig. 2.7**. Once surfactant is introduced into the core, it appears that there is a build-up in gas saturation suggesting that foam is perhaps being generated in the first section itself, as can be seen in the CT image at 0.03 pore volumes of liquid injected (0.13 total PVI). This is most likely a very weak foam as it is not persistent and is absent in the images thereafter. Moreover, there is no significant rise in ∇P_1^L (**Fig. 2.6**) to demonstrate mobility reduction and the presence of foam downstream of the inlet. After 0.4 PV surfactant injection (1.8 total PVI), a modest reduction in gas mobility is recorded in the section with the permeability transition (**Fig. 2.6**). This shows up as a higher gas-phase saturation just at the entrance of the high-permeability zone, clearly discernable in **Fig. 2.8**. At roughly 2.3 PVI, pressure gradient downstream of the permeability jump, ∇P_3^H and ∇P_4^H, begin to rise (**Fig. 2.6**) indicating a reduction in gas mobility due to foam propagation. This is verified by the CT response, which shows a foam front propagating through the high-permeability zone at 0.6 PVI liquid (3.0 total PVI). At 0.9 PVI liquid, CT images show that the foam front has reached the outlet of the pack and there is still no foam in the low-permeability zone. This gives a clear indication of foam generation at the sharp permeability increase and subsequent propagation downstream towards the outlet of the core.

Core 2. A foam-generation experiment was performed in core sample 2, with a permeability contrast of 5.4:1 between the low- and high-permeability zones. The pressure gradient across different sections of the core developed with time in a manner similar to sample 1, as shown in **Fig. 2.9**.

Once again, the pressure gradient across the permeability change gradually declines after surfactant is introduced in the core. There is a sharp drop in ∇P_2^{LH} and a sharp jump in the downstream pressure gradient ∇P_3^H at around 1.7 total PVI. As shown in **Fig. 2.10**, CT images at 0.4 PVI surfactant solution (1.9 total PVI) show that this coincides with an increase in gas saturation in the high-permeability zone. The images also suggest that the preferred path for gas flow is along the edges of the core, which means that the

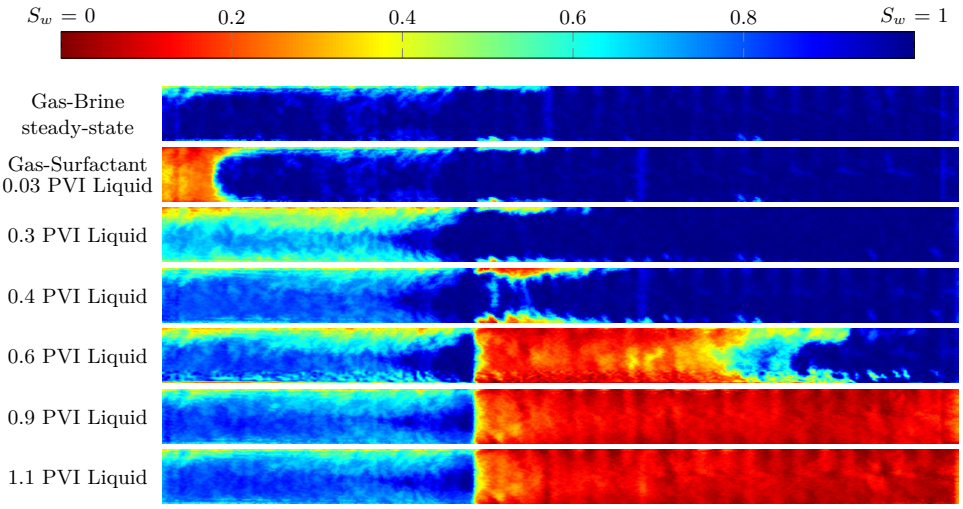

Figure 2.7: Average liquid saturation computed using X-ray CT imaging as seen in a vertical cross-section through the center of core 1. Color bar represents a liquid saturation range from 0 to 1. Blue represents a high liquid-phase saturation whereas red represents a high gas saturation, here interpreted as the CT response to the saturation change caused by foam. Top-most saturation map comes from the CT image taken during gas-brine injection and images thereafter were taken after surfactant solution was introduced in the core.

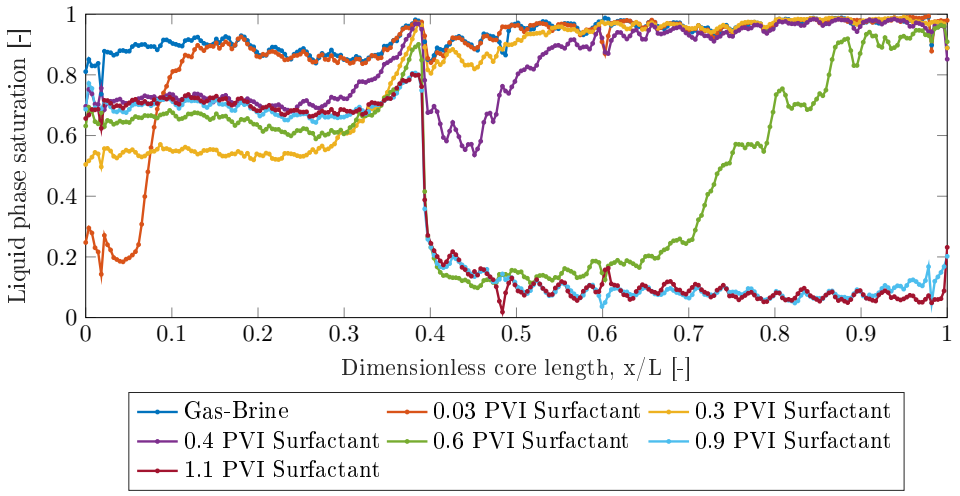

Figure 2.8: Average liquid-phase-saturation profile in core 1 at different pore volumes of injection (PVI) through the course of the foam-generation experiments in **Fig. 2.7**.

initial onset of foam generation takes place right at the entrance to the high-permeability zone near the walls of the core. This mobility reduction then forces the gas to flow through the center of the core, resulting in foam generation through the whole face of the heterogeneity.

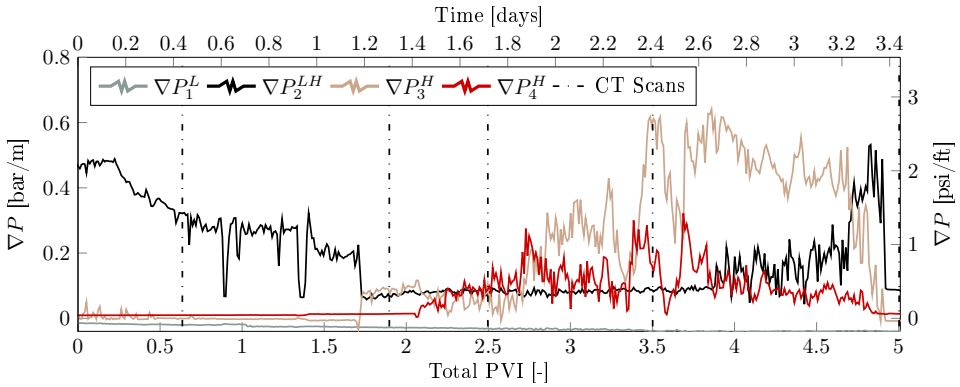

Figure 2.9: Pressure gradient across various sections of core 2 during foam-generation experiment. Dash-dotted lines indicate times at which CT scans were taken to generate saturation maps across the length of the core. Superscript L represents a measurement in the low-permeability section, whereas superscript H represents data acquired from the high-permeability zone. LH represents the interval with the boundary.

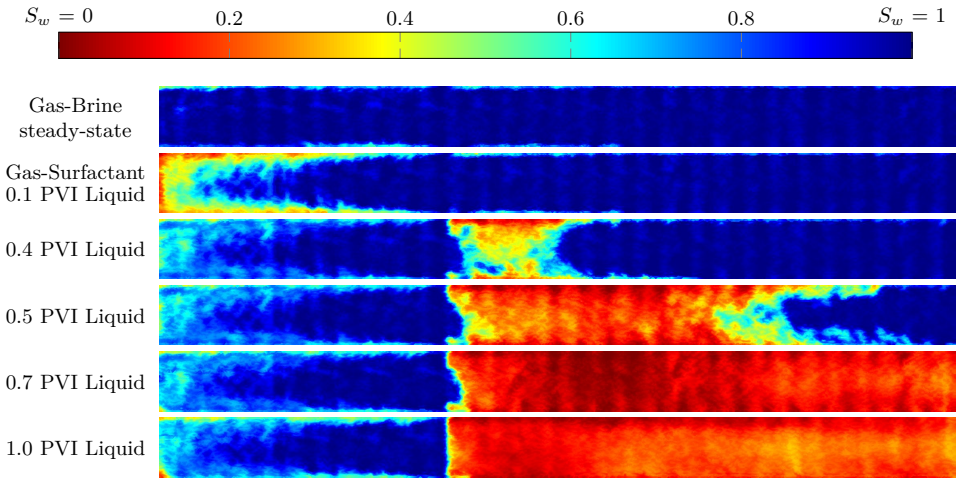

Figure 2.10: Average liquid saturation as seen in a vertical cross-section through the center of core 2 computed using X-ray CT imaging during the course of a foam-generation experiment. Top-most saturation map comes from the CT scan taken during gas-brine injection and images thereafter are from scans taken after surfactant solution was introduced in the core.

Saturation values per cylindrical slice are plotted against the dimensionless core position in **Fig. 2.11**. The core is almost completely saturated with liquid during co-injection of gas and brine, since most of the gas breaks through from the edges of the core, more from the top than from the bottom. At 0.4 PVI liquid injection, liquid saturation drops sharply at the entrance of the high-permeability zone, indicating foam generation. At 0.5 PVI of liquid, the foam front appears to have travelled from a dimensionless position of 0.6 to 0.9, roughly half the length of the high-permeability

zone, into the 4th section of the core. This is also evident from the pressure-gradient profile shown in **Fig. 2.9** as ∇P_4^H begins to rise and exhibit sharp fluctuations, starting at approximately 2.1 PVI. At 0.7 PVI liquid (3.5 total PVI), foam has propagated to the end of the pack and the gas saturation is about 90% in the high-permeability region. Gas saturation is roughly 20% in the low-permeability zone and no significant reduction in mobility is witnessed in terms of pressure gradient (**Fig. 2.9**).

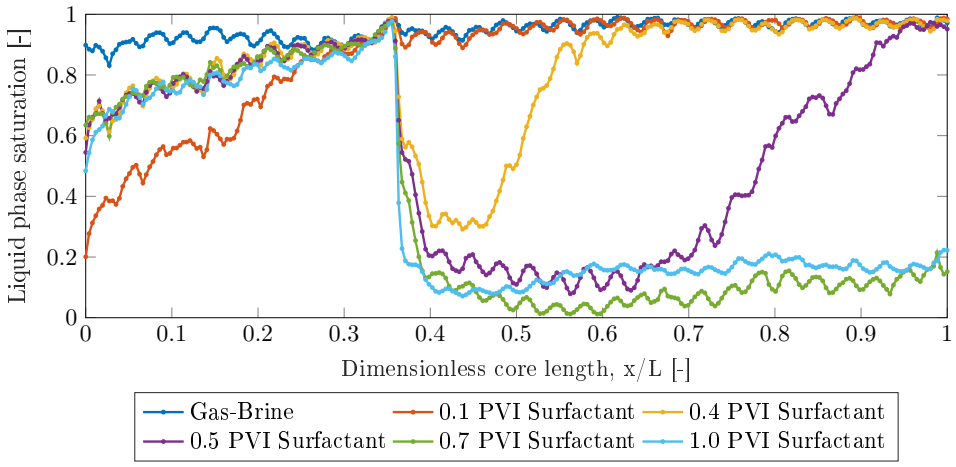

Figure 2.11: Average liquid-phase-saturation profile in core 2 at different pore volumes of injection (PVI) through the course of the foam-generation experiment.

Core 3. Foam generation was also observed in core sample 3 with a permeability contrast of 13.9:1. As shown in **Fig. 2.12**, pressure gradient across the permeability transition and further downstream showed distinct periods of rise and sharp drops, unlike the continuous and relatively mild fluctuating pattern observed in **Figs. 2.6** and **2.9**. The pressure gradient in the low-permeability section (∇P_1^L) stays low through the course of the experiment, suggesting there is no significant reduction in gas mobility. However, as shown in **Figs. 2.13** and **2.14**, the gas saturation is approximately 50% in the first section. This means that if there is any foam in the low-permeability section, it has little effect on gas mobility and is, therefore, weak foam. Evidently, even this weak foam transforms into strong foam at the permeability transition.

CT images in **Fig. 2.13** also indicate that, as with sample 2, there may be a region of high permeability along the edges of the core due to imperfect sintering of the glass grains with the tube wall. Gas prefers to flow along the edges of the core and foam generation also begins at the outer boundary of the cylindrical porous medium, shown clearly in the scan taken at 0.4 PVI of surfactant solution. Images at 0.5 and 0.7 PVI liquid (2.7 and 3.5 total PVI, respectively) show that the foam front propagates first along the edges, forcing gas to flow through the center of the porous medium, resulting in subsequent propagation of foam through the center of the core.

Core 4. Core sample 4 had the greatest permeability contrast among the tested cores

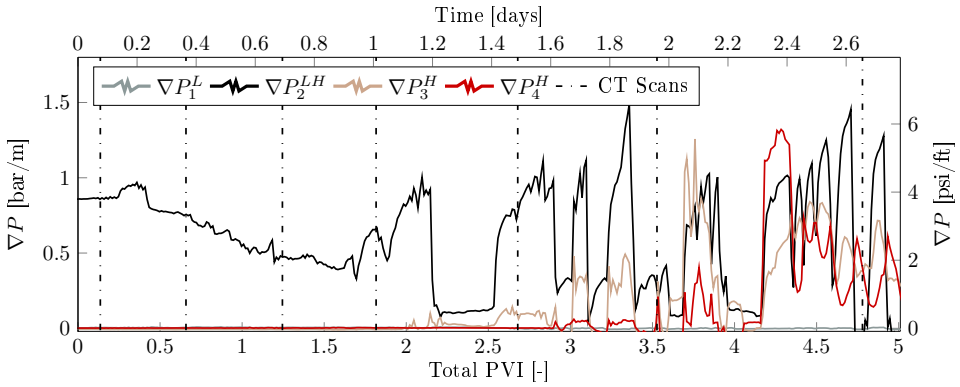

Figure 2.12: Pressure gradient across various sections of core 3 during foam-generation experiment. Dash-dotted lines indicate times at which CT scans were taken to generate saturation maps across the length of the core. Superscript L represents a measurement in the low-permeability section, whereas superscript H represents data acquired from the high-permeability zone. LH represents the interval with the boundary.

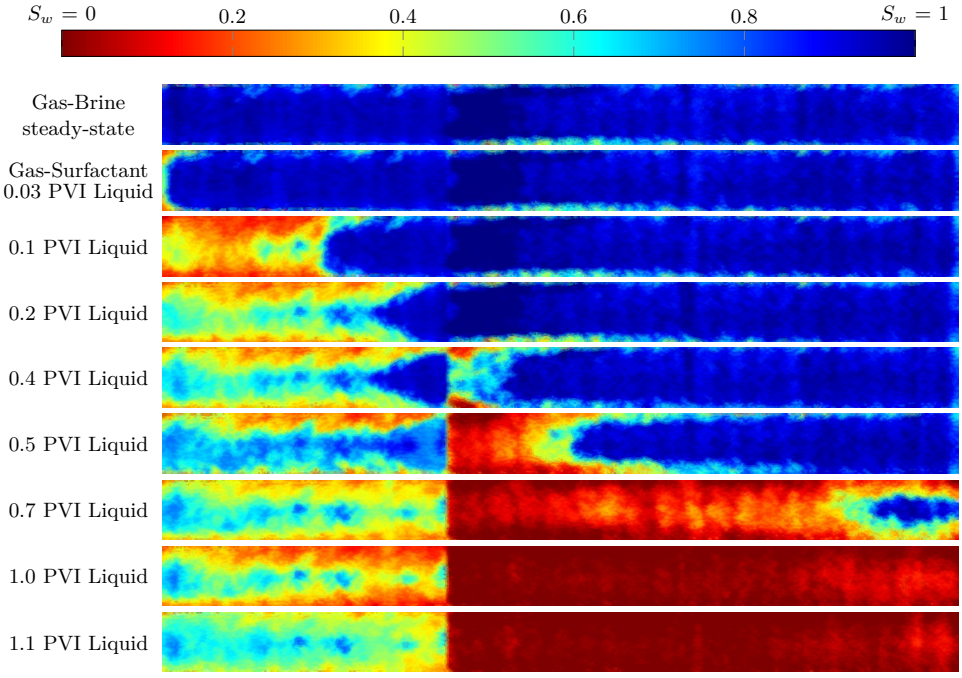

Figure 2.13: Average liquid saturation as seen in a vertical cross-section through the center of core 3 computed using X-ray CT imaging during the course of a foam-generation experiment. Top-most saturation map comes from the CT scan taken during gas-brine injection and images thereafter are from scans taken after surfactant solution was introduced in the core.

(27.5:1). We observe that strong foam is created across the permeability transition and it propagates through the high-permeability zone to the end of the core. While the

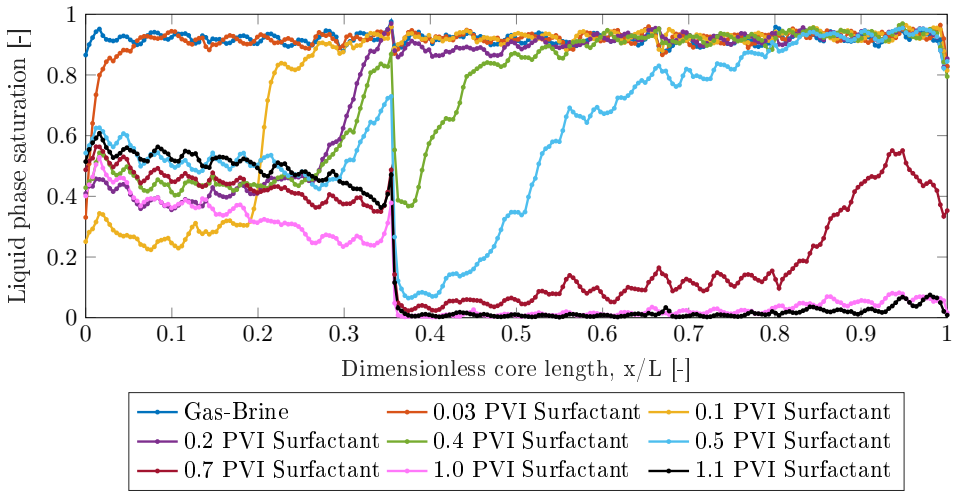

Figure 2.14: Average liquid saturation versus dimensionless core position during a foam-generation experiment in core 3.

measured pressure gradient across the inlet section, as shown in **Fig. 2.15**, shows no appreciable increase, indicating absence of strong foam, the saturation profile obtained through CT scans, as shown in **Fig. 2.16**, shows that the gas saturation is fairly high in the low-permeability zone towards the end of the experiment. Gas saturation is almost 70% in the low-permeability zone upstream of the transition as seen in the saturation profiles computed at 1.2 PVI of surfactant injection (6 Total PVI) and thereafter. This rise in gas saturation, however, is witnessed only after foam generation across the transition has been observed. In the high-permeability section, CT images show a gas saturation of almost 100% towards the end of the experiment, indicating the presence of strong foam with a significant reduction in gas mobility, in terms of pressure gradient, as discussed in the next section.

2.4. DISCUSSION

In the experiments reported, we show evidence of foam generation across a sharp permeability rise during simultaneous flow of gas and surfactant solution. We observe foam generation across a permeability contrast of slightly less than 4:1 at a gas fractional flow of 80%, in accordance with theoretical predictions. While in some of our experiments we see indications of foam generation in terms of high gas saturation in the low-permeability section itself, this foam may be classified as “weak foam”, or what Friedmann et al. (1991) call a “leave-behind foam”, as gas mobility remains high (in terms of measured pressure gradient) in this section throughout the course of the experiment.

Foam generation does result in a significant reduction in gas mobility in the high-permeability zone. We quantify this reduction in mobility in terms of apparent foam viscosity. Assuming a steady-state average pressure drop across the high-permeability

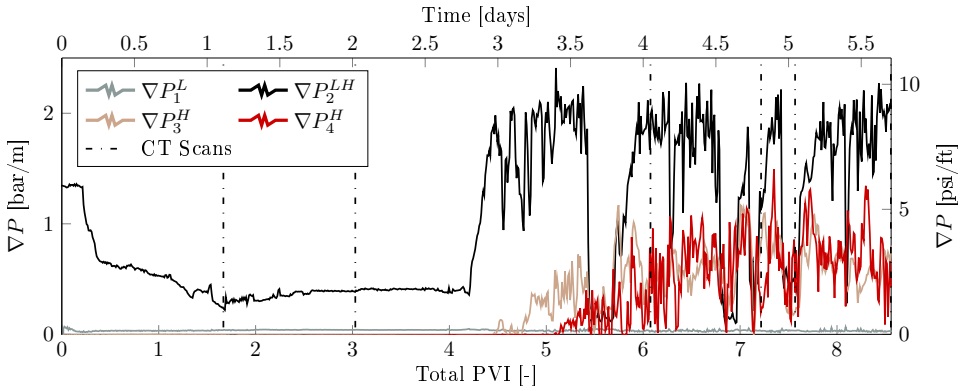

Figure 2.15: Pressure gradient across various sections of core 4 during foam-generation experiment. Dash-dotted lines indicate times at which CT scans were taken to generate saturation maps across the length of the core. Superscript L represents a measurement in the low-permeability section, whereas superscript H represents data acquired from the high-permeability zone. LH represents the interval with the boundary.

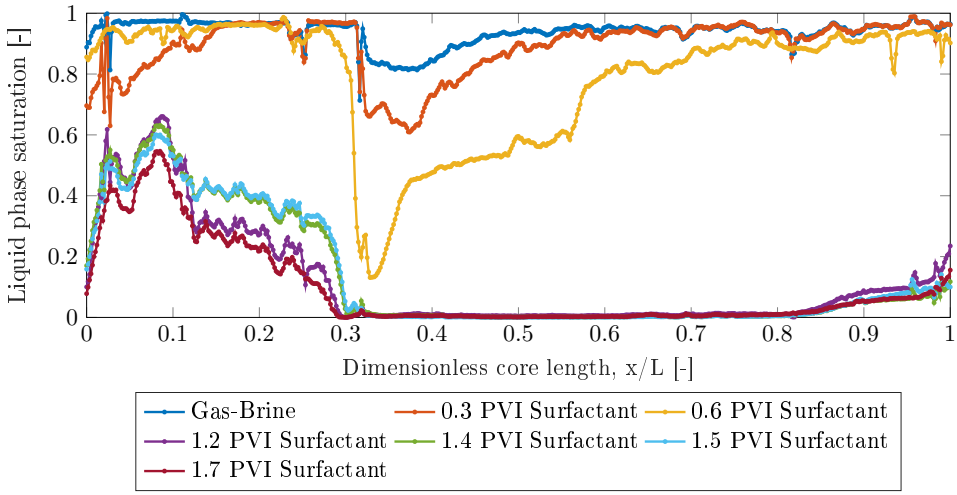

Figure 2.16: Average liquid saturation versus dimensionless core position during a foam-generation experiment in core 4.

zone, we use the pressure gradient across the entire zone (sections 3 and 4) and compute apparent viscosity as:

$$\mu_{app}^{H} = \frac{k^H \nabla P^H}{u_l + u_g} \tag{2.2}$$

where k^H is the measured permeability in the high-permeability section, ∇P^H is the pressure gradient across the same section during the experiment and u_g and u_l are the gas and liquid superficial velocities, respectively. The total superficial velocity (u_t) is the

sum of these two velocities and the denominator in **Eq. (2.2)**. The apparent viscosity was averaged over quarter-day periods and plotted against total injected pore volumes in **Fig. 2.17**. Since the measurements are taken every second, there is a spread in the data collected and averaged over a six hour period. This spread is plotted in terms of an error bar in each direction, which represents one standard deviation of all the viscosities computed from all the recorded pressure gradients within the six-hour measurement window.

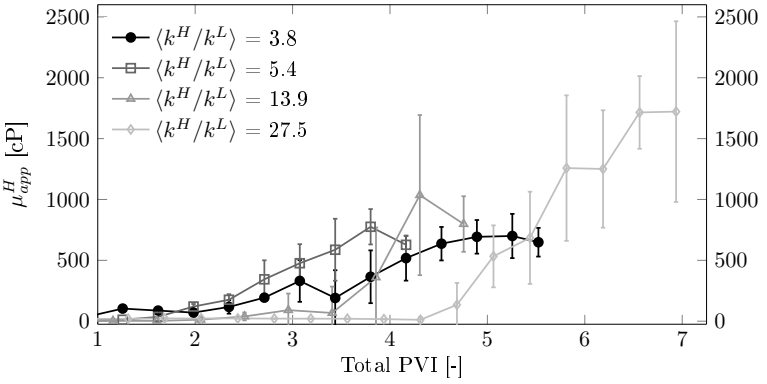

Figure 2.17: Apparent viscosity of foam in the high-permeability region of each core, generated by flow across the abrupt permeability increase, plotted against the total pore volumes of injection. u_t = 0.67 ft/d and f_g=80% in all the experiments.

The average apparent viscosity of foam, generated across a sharp permeability increase, ranges from about 600 cP to 1800 cP. Evidently, the greater the permeability contrast in the core, the larger the apparent viscosity of the generated foam. Additionally, we observe that at a greater permeability contrast, it takes longer to observe foam in the high-permeability section, especially in the core with the greatest permeability contrast, shown by the purple line in the above figure. We suspect that this may due to a greater intermittency in foam generation, as explained below, across greater permeability contrasts.

The measured pressure gradient in all our experiments exhibits large fluctuations. At a greater permeability contrast, the magnitude of these fluctuations is greater, as can be seen by the error bars in **Fig. 2.17**. These fluctuations occur because lamellae are not generated steadily across the face of the heterogeneity (Falls et al., 1988). Instead, foam generation across the sharp increase in permeability is intermittent. This can be explained as follows: foam generation causes a reduction in gas mobility, which in turn causes the flow to become drier; locally, capillary pressure then rises above the critical capillary pressure for snap-off and foam generation ceases. After foam generation ceases, liquid accumulates again and the cycle repeats. This coincides with our observations at the outlet of the core. Distinct periods of liquid production were followed by strong foam coming out of the core, followed by relatively weaker and drier foam with a large bubble size, followed by periods of only gas production. The nature

of produced fluids may also be affected by the capillary end-effect at the outlet. In a separate set of experiments, we have observed that the intermittency of foam generation and subsequent mobilization is less frequent at a higher liquid fractional flow and a higher flow rate.

While designing the experiments reported in this paper, the objective was to create conditions for a uniform, one-dimensional forced displacement across the permeability jump. However, as mentioned earlier, the porous medium was not perfectly homogeneous in the single-permeability regions and the unwanted artefact of imperfect sintering and higher porosity along the edges leads to preferential flow of gas near the walls of the core. While this may have resulted in unwanted experimental observations, complicating subsequent analysis, the aggravated effect of gravity (due to a low flow rate and high permeability), combined with this edge effect, brought the experimental conditions closer to realistic geological settings. In a realistic subsurface setting, gas may have other flow-paths available and may bypass the permeability boundary altogether, not contributing to the process of foam generation. In the experiments presented in this paper, regardless of the availability of a preferential flow-path for gas, foam generation was observed across the permeability jump. The experiments were designed so that foam was generated by snap-off and not due to drainage or a high pressure gradient. While Li and Rossen (2005) suggested that preferential flow along the edges of a core would make foam generation in such an experiment more difficult, this was not observed here. Snap-off still occurred at the permeability boundary at contrasts as low as 3.8:1 with a field-like total superficial velocity of 0.67 ft/d.

The results of this study can have important implications for the use of foam for mobility control in subsurface displacement processes. In a petroleum reservoir, ten metres away from the injection well, fluid velocity can be as much as 100 times lower than that in the immediate vicinity of the well. As a result, foam strength can be significantly lower and foam propagation may fail (Ashoori et al., 2012a; Friedmann et al., 1994). However, quite often there exist sharp heterogeneities in the formation. When they are present, foam strength can still be maintained by snap-off across these permeability contrasts. If the impact of these heterogeneities on foam generation and propagation are not accounted for, the effectiveness of foam in reducing gas mobility can be underestimated. In order to understand the consequences of this phenomenon in a more realistic, three-dimensional, subsurface setting with layered or secondary granulometry, the results of this study could be used to model foam generation by snap-off in a flow across a sharp permeability change and the model can be used to simulate the displacement process in the analogue system.

It is important to note that surfactant adsorption is negligible in our synthetic porous media made from borosilicate glass. Therefore, in our experiments, foam generation appears to be almost immediate once the surfactant arrives at the permeability transition. In the field, however, surfactant adsorption, whenever not satisfied, can delay the propagation of surfactant.

2.5. CONCLUSION

Simultaneous flow of gas and surfactant solution across a sharp permeability increase results in foam generation by snap-off, provided that the liquid volume fraction is high enough and permeability contrast is sufficient. Foam can be generated by this phenomenon at extremely low superficial velocities, close to and even lower than conventional field velocities encountered far from wells. This coincides with theory, which suggests that this mechanism is independent of pressure gradient. CT images clearly indicate that foam is generated at the permeability change and it propagates downstream towards the outlet of the core.

At the low flow rates used in these experiments, no effective foam was generated in the homogeneous core upstream of the permeability transition. Events of foam generation and subsequent mobilization are associated with sharp fluctuations in the pressure gradient across the permeability jump. Foam generation and propagation is not immediate as the surfactant front reaches the permeability jump. Instead, foam generates, propagates and mobilizes intermittently from the permeability transition. The intermittency appears to be greater for greater permeability contrasts.

Foam generation during flow across abrupt permeability changes in the vertical direction could significantly reduce gravity segregation. Foam created during flow across layer boundaries would block the upward movement of gas towards higher layers. This would reduce the gas mobility in the vertical direction, effectively reducing vertical permeability to gas and increasing the segregation length (Jenkins, 1984; Rossen and Bruining, 2004; Stone, 1982; Tanzil et al., 2002b).

3

Foam Generation by Snap-off in Flow Across a Sharp Permeability Transition: Effect of Velocity and Fractional Flow

Foam reduces gas mobility and can help improve sweep efficiency in an enhanced oil recovery process. For the latter, long-distance foam propagation is crucial. In porous media, strong foam generation requires that local pressure gradient exceeds a critical value (∇P^{min}). Normally, this only happens in the near-well region. Away from wells, these requirements may not be met, and foam propagation is uncertain. It has been shown theoretically that foam can be generated, independent of pressure gradient, during flow across an abrupt increase in permeability (Rossen, 1999). The objective of this study is to validate theoretical explanations through experimental evidence and to quantify the effect of fractional flow on this process.

This chapter (Shah et al., 2019a) extends the results of the previous chapter (Shah et al., 2019b) investigating the effect of permeability contrast on this process. In this study the effects of gas fractional flow (f_g) and total superficial velocity (u_t) are described. Coreflood experiments were performed in a cylindrical sintered glass porous medium with two homogeneous layers and a sharp permeability jump in between, representing a lamination or cross-lamination. Unlike previous studies of this foam-generation mechanism, in this study gas and surfactant solution were co-injected at field-like velocities into a medium first flooded to steady-state with gas-brine co-injection. Pressure gradient is measured across several sections of the core. X-ray computerized tomography (CT) is used to generate dynamic phase-saturation maps as

foam generates and propagates through the core. We investigate the effects of velocity and injected gas fractional flow on foam generation and mobilization by systematically changing these variables through multiple experiments. The core is thoroughly cleaned after each experiment to remove any trapped gas and to ensure no hysteresis.

Local pressure measurements and CT-based saturation maps confirm that foam is generated at the permeability transition, which then propagates downstream to the outlet of the core. A significant reduction in gas mobility is observed, even at low superficial velocities. Foam was generated in all cases, at all the injected conditions tested. However, at the lowest velocity tested, strong foam did not propagate all the way to the outlet of the core. Although foam generation was triggered across the permeability boundary at this velocity, it appeared that, for our system, the limit of foam propagation, in terms of a minimum-driving-force requirement, was reached at this low rate. CT images were used to quantify the accumulation of liquid near the permeability jump, causing local capillary pressure to fall below the critical capillary pressure required for snap-off. This leads to foam generation by snap-off. At the tested fractional flows, no clear trend was observed between foam strength and f_g. For a given permeability contrast, foam generation was observed at higher gas fractions than predicted by previous work (Rossen, 1999). Significant fluctuations in pressure gradient accompanied the process of foam generation, indicating a degree of intermittency in the generation rate - probably reflecting cycles of foam generation, dryout, imbibition, and then generation. The intermittency of foam generation was found to increase with decreasing injection velocities and increasing fractional flow. Within the range of conditions tested, the onset of foam generation (identified by the rise in ∇P and S_g) occurs after roughly the same amount of surfactant injection, independent of fractional flow or injection rate.

3.1. INTRODUCTION

Foams have numerous applications in the oil industry. They are used for drilling (Lyons et al., 2009), to divert acids in well-stimulation procedures (Chambers, 1994), for hydraulic fracturing of low-permeability formations (Gupta, 2009), to improve liquid lifting in low-pressure gas wells (Yang and Siddiqui, 1999) and for tertiary oil-recovery processes (Rossen, 1996). In aquifer-remediation processes (Hirasaki et al., 1997b,a, 2000), foam is used to improve sweep while removing dense non-aqueous phase liquids (DNAPLs). This work concerns the use of foam as a mobility-control agent in an enhanced oil recovery (EOR) process.

Most of the world's EOR production comes from injecting gases. Gas has a very low viscosity and density compared to oil and, therefore, in a displacement process, sweep efficiency is poor due to viscous fingering and gravity override. When used as a dispersed phase, as in foam, its apparent mobility is greatly reduced and sweep efficiency is improved. In a heterogeneous, layered system, as discussed by Tanzil et al. (2002b) and Shah et al. (2019b), the effective permeability in the vertical direction may be greatly reduced by foam generation in the high-permeability strata, reducing

the extent of gravity segregation. In porous media, foams can be generated in various ways (Ransohoff and Radke, 1988; Kovscek and Radke, 1994; Rossen, 1996). Several experimental studies (Gauglitz et al., 2002; Tanzil et al., 2002a) and theoretical models (Rossen and Gauglitz, 1990; Friedmann et al., 1991; Kam and Rossen, 2003; Rossen, 1990a) suggest that strong foam generation in porous media would require exceeding a critical pressure gradient or velocity threshold, which is typically only overcome in the near-well region. Creation of foam in these cases is thought to depend on mobilization of lenses and lamellae and subsequent lamella division. Mobilising the bubble train requires a minimum pressure gradient (Rossen, 1990b,a; Kharabaf and Yortsos, 1998; Chen et al., 2005b; Almajid and Kovscek, 2019). For CO_2 foams, this minimum pressure gradient might be so low at reservoir conditions (due to a lower interfacial tension) that it might not be observed in foam experiments.

Others argue that snap-off is the dominant mechanism of foam generation in a porous medium (Ransohoff and Radke, 1988; Kovscek and Radke, 1996, 2003). While snap-off can occur through several mechanisms (Rossen, 2003), in these studies, the increased frequency of snap-off is thought to be dependent on pore geometry and interfacial curvature as well as gas-phase and liquid-phase velocities. The relevant mechanism of snap-off in these experiments is Roof snap-off (Roof, 1970), which occurs as gas invades a narrow pore throat and drains liquid from a wider downstream pore body. These studies report no minimum-pressure-gradient requirement for foam generation but argue that snap-off may cease if the the newly created lamella or lenses cannot mobilise (Kovscek and Radke, 1996). As mentioned earlier, the mobilisation of lamellae from a snap-off site requires a minimum pressure gradient. Other research reporting similar findings was revisited by Almajid and Kovscek (2016). Foam experiments that start with a surfactant-saturated core, analogous to gas draining the preceding surfactant slug in a surfactant-alternating-gas (SAG) flood in the near-well region, might not observe this critical velocity or pressure-gradient dependence. There appears to be no clear consensus in the literature on the most dominant mechanisms of strong-foam generation in porous media. In this study, we are interested in foam-generation mechanisms that could dominate away from wells, where the pressure gradient is low and the darcy velocity is considered to be, in practice, approximately 1 ft/d (Dake, 1994); much lower than the reported thresholds in the studies referred to above. These are regions where the gas and surfactant slugs injected into a reservoir would have mixed and gas is not draining a surfactant-saturated zone.

If strong-foam generation is thought to depend on exceeding a threshold pressure gradient or velocity, conditions in these regions may not be favourable for foam to propagate or even exist (Ashoori et al., 2012a; Yu et al., 2019). We are addressing a hypothetical situation in which foam did not travel far from the wells despite injection of a sufficient amount of gas and surfactant solution in the reservoir. This work investigates foam generation by snap-off that is triggered by an abrupt contrast in permeability, and at that location, capillary pressure.

In the presence of sharp heterogeneities, foam can be generated by snap-off, independent of pressure gradient or velocity, as gas and surfactant solution flow across

an abrupt increase in permeability (Falls et al., 1988; Rossen, 1999; Hirasaki et al., 2000; Tanzil et al., 2002b; Li and Rossen, 2005; Shah et al., 2019b). Fortunately, sharp heterogeneities are quite common in petroleum reservoirs and exist over a large range of length scales. The most prevalent are unconformities such as sharp layer boundaries, which can extend from a few metres to several hundreds of metres in length (Reineck and Singh, 1980). Layered systems often also consist of internal laminations that add to the frequency of sharp changes in permeability in a given rock volume. Cross-laminations present abrupt permeability contrasts in the horizontal direction (Hartkamp-Bakker, 1993), offering locations for foam generation by snap-off during lateral pressure-driven flow. Hartkamp-Bakker (1993) measured the permeability variation across internal laminations in a variety of samples extracted from outcrops as well as reservoir cores. She reported permeability ratios across individual units ranging from 1:1 (change in grain framework but not in permeability) to 27:1 between different units.

In flow across such a heterogeneity, the wetting phase accumulates at the boundary of the low-permeability region (Yortsos and Chang, 1990) and local capillary pressure is reduced there. If the capillary pressure falls below the critical capillary pressure for snap-off, i.e. P_c^{sn} (Falls et al., 1988), foam generation can be expected. The extreme case of this phenomenon is the capillary end-effect encountered in coreflood experiments, which is also reported to have caused foam generation at the outlet of a core (Ransohoff and Radke, 1988). Falls et al. (1988) measured the capillary entry pressure (P_c^e) and P_c^{sn} for glass beadpacks using a variety of bead sizes. They found that $P_c^{sn} \approx P_c^e/2$, consistent with theoretical approximations for circular pore throats blocked by snap-off (Roof, 1970; Lenormand et al., 1983). Rossen (1999) used this result to show that for snap-off to occur in flow from low- to high-permeability zones, capillary pressure in the high-permeability zone must be less than half the capillary pressure in the low-permeability zone ($P_c^H < P_c^L/2$). In other words, the high-permeability region is at least four times as permeable as the low-permeability region ($k^H \geq 4\ k^L$), assuming $P_c \propto \sqrt{1/k}$. This trigger for foam generation depends only on the relative magnitudes of capillary pressure resulting from the heterogeneity and not directly on the magnitude of capillary forces in each region. Therefore, for two different gas-liquid fluid pairs, if the liquid is strongly wetting compared to gas, the ratio of capillary pressures is independent of the interfacial tension between the gas-liquid phases since the $P_c(S_w)$ curves would scale but not change shape. This is beneficial for practical applications of foam for displacement processes since the gas available on site can be used and foam generation in flow across permeability changes can still be expected, assisting with mobility control. The mobilisation of the generated foam, however, *would* depend on the gas-liquid interfacial tension. For instance, as implied earlier in Chapter 1, CO_2 foams can propagate at lower pressure gradients compared to N_2 foams.

As the flow gets drier, a greater permeability contrast may be required to cause foam generation. **Fig. 3.1** shows the calculations of Rossen (1999), where the permeability contrast required to block gas flow by snap-off (effectively causing foam generation) is plotted as a function of the gas-water relative-permeability ratio far from the transition zone in the absence of foam. The relative permeability ratio relates to the injected

fractional flow, $f_w = [1 + (k_{rg}/k_{rw})^0(\mu_w/\mu_g)]^{-1}$. Therefore, if f_g = 80%, and μ_w/μ_g = 50, $(k_{rg}/k_{rw})^0$ = 0.08. According to **Fig. 3.1**, a permeability jump slightly higher than 4, at f_g = 80%, would cause foam generation, independent of velocity or pressure gradient. However, if the pore geometry deviates from a circular shape, the ratio of P_c^e/P_c^{sn} may be larger or smaller than 2 (Lenormand et al., 1983; Chambers and Radke, 1990; Rossen, 2003). As a result, a greater or lower permeability contrast, respectively, may be required to block gas flow by snap-off at the same flowing gas fraction. It is important to note that while capillary pressure falls at the edge of the low-permeability zone, gas bubbles are expected to form at the entrance to the high-permeability zone. There is no dependency on pressure gradient. However, mobilisation of the bubbles and subsequent propagation away from the heterogeneity would require such a driving force.

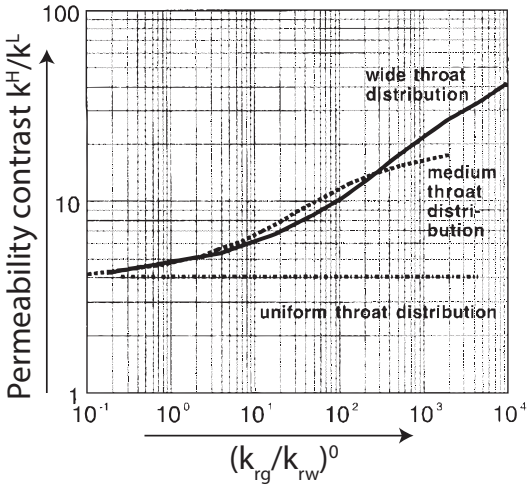

Figure 3.1: Theoretically computed permeability contrast required to completely block gas flow as a function of gas-water relative permeability ratio $(k_{rg}/k_{rw})^0$, with the superscript denoting its value far from the transition zone. Left to right on the x-axis also represents an increase in gas fraction, as $f_w = [1 + (k_{rg}/k_{rw})^0(\mu_w/\mu_g)]^{-1}$. *From Rossen (1999).*

In this work, foam-generation experiments are conducted by co-injecting surfactant solution and gas at field-like velocities, in a consolidated sintered glass porous medium with two layers perpendicular to the direction of flow. Local pressure gradient and saturation maps obtained through X-ray computed tomography are the primary measurements used to identify foam generation and mobilisation. Pressure gradient is used to quantify foam strength, whereas local saturation near the permeability contrast is used to quantify the reduction in capillary pressure that causes foam generation. A variety of injection rates and injection fractions are employed to validate the threshold conditions for foam generation. The previous work of Shah et al. (2019b) on the effect of permeability contrast is extended here to the effect of fractional flow and velocity.

The chapter is structured as follows. The next section describes the experimental set-up and procedure followed. Next, under Section 3.3, the outcome of foam-generation

experiments conducted at a variety of injection rates and gas fractional flow using a core with permeability contrast of approximately 3.8:1 are reported. In Section 3.4, an analytical examination of these results is presented and the main conclusions from these experiments are presented in final section.

3.2. EXPERIMENTAL METHODOLOGY

We conduct coreflooding experiments in a consolidated, sintered glass core with a low- and a high-permeability region, separated by a sharp, monotonic transition (**Fig. 2.3**). The core is 420 mm in length, with a 165 mm low-permeability section. The low-permeability section has a measured permeability (k^L) of 5.4 ± 0.02 darcies, whereas the high-permeability section has a permeability (k^H) of of 20.7 ± 0.2 darcies. Therefore, the permeability contrast ($\langle k^H/k^L \rangle$) is roughly 3.8:1, bordering the threshold predictions of (Rossen, 1999). The cores were acquired from Hilgenberg GmbH, Malsfeld, Germany (www.hilgenberg-gmbh.de). The materials used in this study, together with the experimental protocols followed, are identical to those described in detail in the previous chapter and by Shah et al. (2019b). Nevertheless, we highlight important aspects of the same to ensure an independent readability of this chapter.

Every experiment begins with multiple permeability measurements, using water, across the length of the core to ensure that there has been no grain migration and that there is no trapped gas in the core. Next, the core is saturated with brine solution (1 wt.% NaCl prepared in demineralized water) and the permeability is measured again. Once the core is saturated with brine, the flow rate is reset to the desired experimental value and gas (99.98% N_2) is co-injected at the desired fractional flow. After steady-state is achieved with the co-injection of gas and brine, the injected liquid phase is changed to the surfactant solution, and gas and surfactant solution are co-inected into the core. The surfactant solution comprises 0.5 wt.% (≈ 0.04 M) of the foaming surfactant anionic alpha olefin sulphonate (AOS) C_{14-16} with a molecular weight of 315 g/mol (Stepan® BIO-Terge AS-40 KSB) and 1 wt.% (≈ 0.17 M) NaCl. The surfactant concentration is roughly 62 times the CMC in 1 wt.% NaCl (Kahrobaei et al., 2017). For a variety of reasons including cost, detergency and low adsorption on sandstones, AOS is an excellent overall candidate for foam enhanced oil recovery in a conventional, mature oil reservoir (Farajzadeh et al., 2008). Since the experiments are conducted at field-like velocities; foam is not generated in the low-permeability section. Once the surfactant front reaches the permeability transition, foam generation is expected. The core is cleaned thoroughly after each experiment by flushing with 50 wt.% iso-propanol (IPA) solution for several pore volumes. IPA is known to kill foams. Therefore, after the core is cleaned with IPA, it is flushed with copius amounts (≈20-50 PV) of brine solution. Then the core is flushed with CO_2 (≈ 10 PV, with the last 2 PV under vacuum) to displace any remaining gas out of the core, followed by brine again to re-measure permeability before the start of an experiment. This treatment removes all trapped gas, traces of surfactant solution and IPA from the core. This minimizes chances of hysteresis effects affecting the foam-generation experiments (Kahrobaei et al., 2017).

The experimental procedure followed is similar to the experiments of Li and Rossen (2005). Unlike the experiments of Tanzil et al. (2002b), where gas and surfactant solution were injected into a surfactant-saturated sandpack, a drainage process, we inject gas and surfactant solution into a core at steady-state with gas and brine co-injection. As a result, gas does not drain a surfactant-saturated region of the core prior to foam generation at the boundary. This ensures that the chances of foam generation by mechanisms that dominate during drainage such as Roof snap-off (Roof, 1970) and leave-behind are minimal (Ransohoff and Radke, 1988; Kovscek and Radke, 1994; Kovscek et al., 1995; Rossen, 1996, 2003). In other words, the experiments were carefully designed not to allow foam generation by mechanisms other than snap-off at the permeability boundary in the core. After foam is generated at the heterogeneity, gas saturation in the high-permeability region can rise. This can then be considered a local drainage process and therefore, other mechanisms of foam generation may come into play as the foam mobilises and propagates through the high-permeability zone.

A schematic flow diagram of the experimental set-up was shown earlier in **Fig. 2.4**. **Fig. 2.3** shows the core in a vertical orientation, whereas in the dual-beam CT scanner the core is placed horizontally. This is not ideal for flow behaviour but is necessary in order to minimize the impact of beam-hardening effects and cross-artefacts while taking CT scans of a non-axisymmetrically placed object. Therefore, gravity-segregation affects the experiments conducted using the CT scanner, as discussed in the previous chapter and by Shah et al. (2019b). Along with saturation maps obtained through CT scans, pressure measurements in the low-permeability section are used to confirm that no foam is generated upstream of the permeability contrast. No back-pressure is applied, in order to avoid fluctuations caused by multiphase flow through the back-pressure-regulator assembly. These fluctuations may cause foam generation (Li and Rossen, 2005). For the image settings of the CT scanner and details about the image analysis procedure, we refer to the previous chapter (Section 2.2.3) and to Shah et al. (2019b).

3.3. RESULTS

Two sets of experiments are reported in this section. The first set of experiments were conducted with the objective of understanding the impact of superficial velocity on foam generation and mobilisation while validating the velocity independence of this process by operating at the lowest injection rates possible within the range of the flow-control equipment. These experiments were conducted at an injected gas fraction of 80%, with the highest total injection rate (q_t) tested being 0.1 ml/min. This corresponds to a superficial velocity (u_t) of 2.36 μm/s or 0.67 ft/d in field units. In total, four different injection velocities were considered. Starting at 0.67 ft/d, the rates were successively lowered in each experiment to 0.5 ft/d (q_t = 0.075 ml/min), 0.33 ft/d (q_t = 0.05 ml/min), and finally to 0.17 ft/d (q_t = 0.025 ml/min). The core was placed vertically in a temperature-controlled oven at 30°C to allow for a gravity-stable displacement at the lowest rates considered.

Through the second set of experiments, the effect of fractional flow on foam

generation was assessed. Extending the work of Shah et al. (2019b), these tests were conducted at u_t = 0.67 ft/d. Gas fraction was varied from 60% to 95%. Lower gas fractions are less relevant for field applications and, therefore, have not been reported. These experiments were conducted with the core placed horizontally on the CT scanner table.

3.3.1. EFFECT OF VELOCITY

Foam generation was observed at all the tested velocities at f_g = 80%. **Fig. 3.3a** shows a typical measurement of pressure gradient across various sections of the core as indicated in **Fig. 3.2**. The maximum pressure drop across the core in all experiments is close to 0.5 bar and the outlet of the core is at atmospheric pressure. **Fig. 3.3a** reports pressure gradient for the experiment conducted at u_t = 0.5 ft/d, whereas **Fig. 3.3b** reports the experiment conducted at the lowest velocity, i.e. u_t = 0.17 ft/d. The horizontal axis represents total pore volumes of injection (PVI) of surfactant solution and N_2 gas. The core has reached a steady state to gas-brine injection at the origin of the plot.

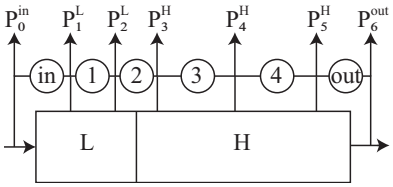

Figure 3.2: Schematic showing labelling scheme used to denote local pressure and pressure gradient.

As mentioned above, before surfactant is introduced into the core, each experiment starts with gas injection into a brine-saturated core. As gas drains the low-permeability section, the pressure transducers report a jump in pressure, indicating the arrival of gas. If each transducer measures the same phase once gas has arrived at the outlet of the core, then these jumps in absolute pressure correspond to spikes in terms of pressure gradient. However, in all the experiments conducted, regardless of the orientation of the core, the pressure gradient across the permeability transition ∇P_2^{LH} (black line in **Fig. 3.3**) is atypically high for gas-brine injection and the pressure gradient immediately downstream ∇P_1^L registers a slightly negative value. We believe that this is due to the pressure tap right before the permeability transition sensing a different phase compared to the rest of the ports (McCool et al., 1983; Chen et al., 2016; Shah et al., 2019b). Gas trapping and the capillary-pressure contrast within the core may add to this effect. The experimental data reported by As Syukri (2018) during gas-brine flow for similar experiments further supports this explanation. As more and more surfactant is injected, ∇P_2^{LH} gradually declines. When the surfactant arrives at the permeability contrast, foam is generated across the permeability transition. As the foam strength increases, the pressure taps in the high-permeability zone sense the reduction in gas mobility starting with the transducer immediately downstream of the transition. This is represented by

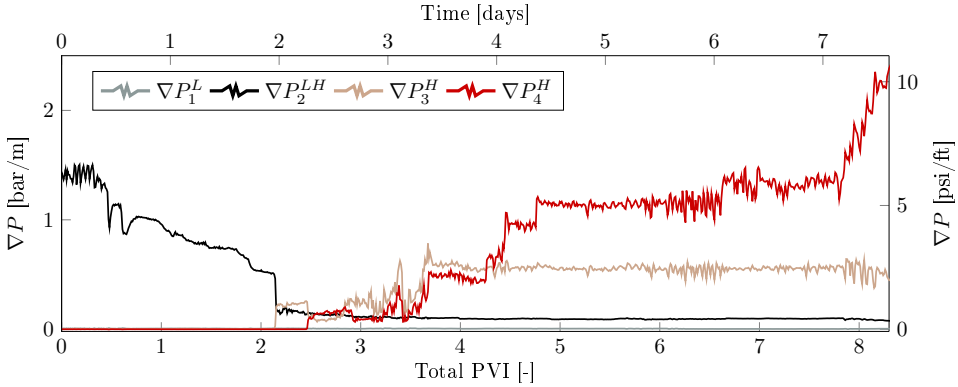

(a)

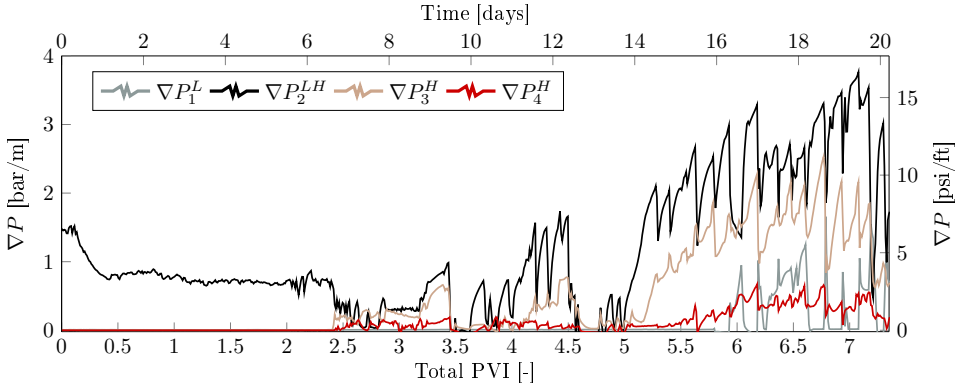

(b)

Figure 3.3: Pressure gradient across various sections of the core during the foam-generation experiment conducted at (a) u_t=0.5 ft/d and (b) u_t=0.17 ft/d at a fixed gas fractional flow of 80%. Superscript L represents a measurement in the low-permeability section, whereas superscript H represents data acquired from the high-permeability zone. LH represents the interval with the boundary.

the sharp drop in ∇P_2^{LH}, and jump in ∇P_3^H, at about 2.2 total PVI (0.44 PVI liquid) in **Fig. 3.3a** and 2.4 total PVI (0.4 PVI liquid) in **Fig. 3.3b**. ∇P_4^H rises shortly after. In **Fig. 3.3a**, ∇P_4^H rises further into the experiment, at around 4.5 PVI total. This corresponds to the passage of foam across the final section in the high-permeability zone followed by its arrival at the outlet of the core.

At the end of the experiment at u_t = 0.17 ft/d (**Fig. 3.3b**), at about 5.9 total PVI, pressure gradient in the low-permeability section begins to rise. Since ∇P_1^L is low until that point, we can conclude that no strong foam is generated in the low-permeability section prior to generation at the boundary. No significant rise in ∇P_1^L was observed in any other experiment reported in this paper. Since this experiment is conducted at

a lower velocity compared to all the other experiments reported in this paper, where no such rise in pressure gradient was observed, it is reasonable to conclude that the injection rate was not so high so as to cause foam generation in the low-permeability section unintentionally. We contend that this rise in pressure gradient is due to a secondary, upstream build-up in pressure gradient, indicating an apparent backward propagation of foam, similar to that observed in previous work (Apaydin and Kovscek, 2001; Simjoo et al., 2013).

Apaydin and Kovscek (2001) observe a secondary rise in pressure gradient, travelling upstream, after breakthrough of the initial foam front in their experiments with surfactant concentrations higher than 0.1 wt.%. They reason that this front propagation against the direction of flow may be originating from increased gas trapping near the outlet of the core. The original generation of stronger foam at the outlet they ascribe to the capillary end-effect. The backward propagation begins soon after breakthrough. The time taken to achieve a steady-state pressure profile throughout the core is much larger than in other experiments because the build-up of pressure drop against the direction of flow is a slow process. Simjoo et al. (2013) observed what they called a “secondary desaturation front" travelling from outlet to inlet in their experiments, after breakthrough. In our experiments, we have a finite transition in permeability inside the core, which is effectively an internal capillary end-effect. The rise in ∇P_1^L happens after several pore volumes of injection. In the field, the region around such a heterogeneity may experience several pore volumes of surfactant and gas. If the surfactant concentrations are high enough (Apaydin and Kovscek, 2001) and the velocities are low enough (to allow incremental gas trapping), one can expect foam generation and propagation in the low-permeability regions as well.

Not including the case discussed above, it is important to note that the pressure gradient in the low-permeability zone ∇P_1^L is low and does not indicate any reduction in gas mobility due to foam generation upstream of the permeability jump. Comparing **Fig. 3.3a** and **Fig. 3.3b**, it is evident that the magnitude of fluctuations in pressure gradient is greater at the lower velocity or injection rate. This subject of intermittency of the process shown by fluctuations in pressure gradient will be discussed later in this paper. For the foam-generation experiments conducted at u_t = 0.67 ft/d, u_t = 0.5 ft/d (**Fig. 3.3a**) and u_t = 0.33 ft/d, pressure gradient in the final section inside the high-permeability zone, ∇P_4^H, is either similar to or greater than ∇P_3^H in magnitude. In these experiments, the strength of foam generated at the permeability transition is maintained as it propagates downstream to the outlet of the core. However, as shown in **Fig. 3.3b**, at u_t = 0.17 ft/d, ∇P_4^H is lower than ∇P_3^H, indicating a drop in foam strength upon propagation. At this velocity, we appear to reach the limit of foam propagation and the foam generated at the permeability contrast is unable to steadily reach the outlet of the core.

This is confirmed by observations made at the outlet of the core (**Fig. 3.4**). A typical observation made at the outlet of the core is shown in **Fig. 3.4a** for u_t = 0.33 ft/d. At this velocity (and higher velocities), steady foam production is observed with infrequent, short, intermittent bursts of only gas and liquid production. At u_t = 0.17 ft/d,

however, short periods (few minutes to an hour) of relatively coarse foam production is observed (**Fig. 3.4b**) followed by a large amount of gas production (several hours to a day, corresponding to a few PVI) as shown in **Fig. 3.4c**, followed by liquid for a similar time interval, as shown in **Fig. 3.4d**.

(a) (b) (c) (d)

Figure 3.4: Snapshots of the outlet tubing showing fluids produced from the core as a typical observation of steady foam production at (a) u_t = 0.33 ft/d. At (b) u_t = 0.17 ft/d, short bursts of foam production preceded by liquid, followed by a few pore volumes of (c) gas production, followed by (d) liquid production, is observed.

3.3.2. EFFECT OF FRACTIONAL FLOW

Fig. 3.5 shows two foam-generation experiments performed at the same injection rate but with different fractional flow. The core has been placed horizontally on the medical CT scanner table. **Fig. 3.5a** shows pressure gradient versus pore volumes injected at u_t = 0.67 ft/d and f_g = 60%. The lower horizontal axis represents pore volumes of surfactant solution injected into the core. Close to around 1 PVI total or 0.4 PVI liquid, foam generation takes place across the permeability transition indicated by the drop in ∇P_2^{LH} and jump in ∇P_3^H, similar to the experiments reported above. The dash-dotted lines in the plot indicate times at which CT scans were taken across the core. Foam generation inferred from changes in sectional pressure-gradient measurements is also confirmed through phase-saturation profiles (**Fig. 3.6**). As explained in the previous section, the saturations are computed using X-ray CT images (Mees et al., 2003), with blue representing a high liquid saturation and red representing a high gas saturation. The images display phase saturation in a vertical cross-section through the center of the core. In the image at 0.5 PVI surfactant solution, gas saturation begins to rise in the high-permeability zone immediately downstream of the permeability transition. This confirms that the drop in ∇P_2^{LH} and jump in ∇P_3^H mark the onset of foam generation across the permeability contrast. At the start of surfactant injection, we observe an ambiguous build-up in gas saturation near the inlet of the core, as seen in the image at 0.08 PVI liquid. However, this does not correspond to a reduction in gas mobility in terms of pressure gradient, as there is no evident rise in ∇P_1^L (grey line in **Fig. 3.5a**). This region of high gas saturation does not appear in subsequent CT images, confirming that foam is indeed generated at the permeability transition, seen clearly as a sharp contrast in gas

saturation in the CT images. There is no strong foam present in the low-permeability zone. After 1.2 pore volumes of surfactant injection, foam has propagated downstream from the permeability contrast to the final section in the high-permeability region and ∇P_4^H gradually rises. The experiment is ended shortly after 2.2 PVI liquid as foam arrives at the outlet of the core.

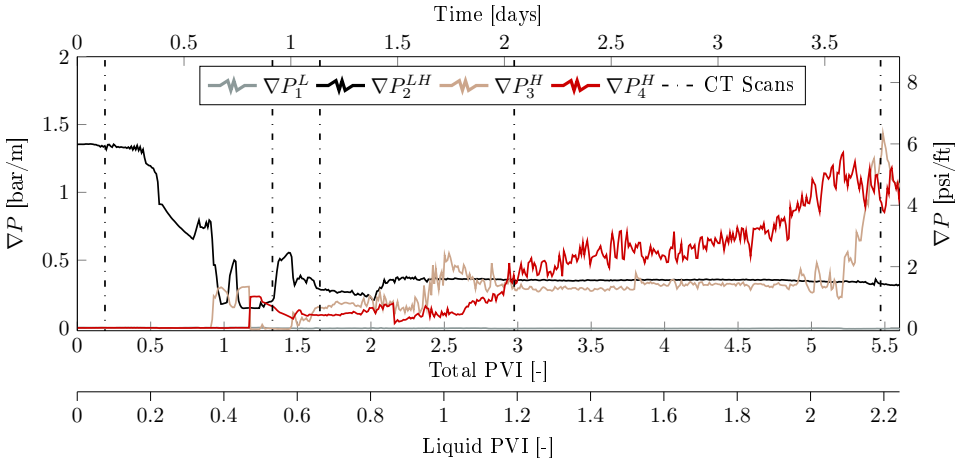

(a)

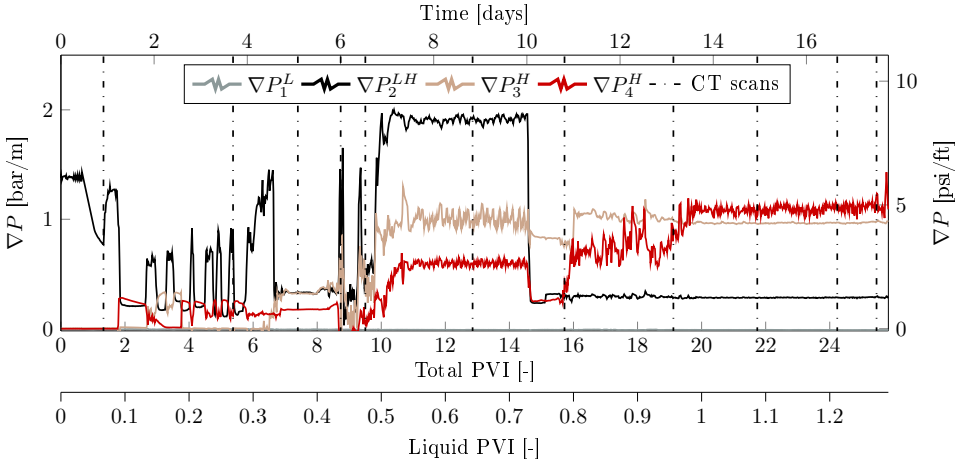

(b)

Figure 3.5: Pressure gradient across various sections of the core plotted against both total and surfactant (secondary horizontal axis) pore volumes injected during the foam-generation experiment conducted at (a) f_g=60% and (b) f_g=95% at a fixed total superficial velocity of 0.67 ft/d. Superscript L represents a measurement in the low-permeability section, whereas superscript H represents data acquired from the high-permeability zone. LH represents the interval with the boundary.

Fig. 3.5b shows pressure gradient versus pore volumes of injection for an experiment performed at the same injection rate (u_t = 0.67 ft/d) but a higher injected gas fraction (f_g = 95%). **Fig. 3.7** reports phase saturations for this experiment, computed using X-ray CT imaging, as seen in a vertical cross-section through the center of the core. Evidently, pressure gradient across the permeability transition exhibits larger fluctuations while foam arrives at the outlet faster (in terms of liquid injected) compared to the experiment conducted at f_g = 60%. At roughly 0.1 pore volumes of surfactant injection, pressure gradient in the high-permeability zone appears to rise. In this case, however, it does not mark the onset of foam generation, as the CT image taken at 0.27 PVI liquid does not indicate foam in the high-permeability zone. The next CT image, at 0.37 PVI liquid, shows a foam front propagating through the high-permeability zone. Therefore, the onset of foam generation is marked by the sharp drop in ∇P_2^{LH} or rise in ∇P_3^H at approximately 0.33 pore volumes of surfactant injection. Gas saturation in the low-permeability region increases substantially after surfactant is introduced in the core. The CT images at 0.48 PVI liquid and 0.64 PVI liquid show a gas saturation of almost 85% in the low-permeability zone, close to the permeability transition. Later in the experiment, the gas saturation is lower, at about 60%. The relatively high gas saturation, however, does not correspond to a significant reduction in gas mobility, as ∇P_1^L stays low. Pressure drop in the low-permeability section gradually rises from about 1 mBar to 10 mBar through the experiment. The absolute pressure transducers are accurate up to 3 mBar. This allows for a maximum mobility reduction by a factor of 16. We think that the relatively high gas saturation in the low-permeability zone, in this experiment, is due to the creation of a continuous-gas foam. If the foam were discontinuous, blocked flow-paths and moving lamellae would register a higher pressure gradient in the low-permeability section, closer to the measurements in the high-permeability zone. Moving lamellae would multiply by lamella division and this would abruptly increase pressure gradient as the experiment progressed. Thus it is a continuous gas phase without moving lamellae that reaches the permeability transition. Nevertheless, strong foam is generated in flow across the permeability transition and the foam propagates downstream from the heterogeneity towards the outlet of the core.

In both the experiments reported in **Fig. 3.5**, foam generation takes place after similar amounts of liquid injection, which conforms with the expected time of arrival of the surfactant solution at the permeability contrast. However, the pressure response is quite different. Pressure gradient across the permeability contrast exhibits large fluctuations at f_g = 95%. As mentioned above, when looking at the pressure measurements, it appears that a modest and arguably sporadic resistance to gas flow is witnessed in the high-permeability zone long before foam begins to appear in the CT images as a high-gas-saturation front moving through the region. At the end of both experiments, pressure gradient in the high-permeability zone is similar at around 1 bar/m. This indicates minimal to no sensitivity of the final mobility to the change in fractional flow. Experiments conducted at other gas fractions, as reported in the next section, also yielded similar observations. The theory of Rossen (1999) suggests that foam generation by snap-off in flow across a sharp permeability transition is easier

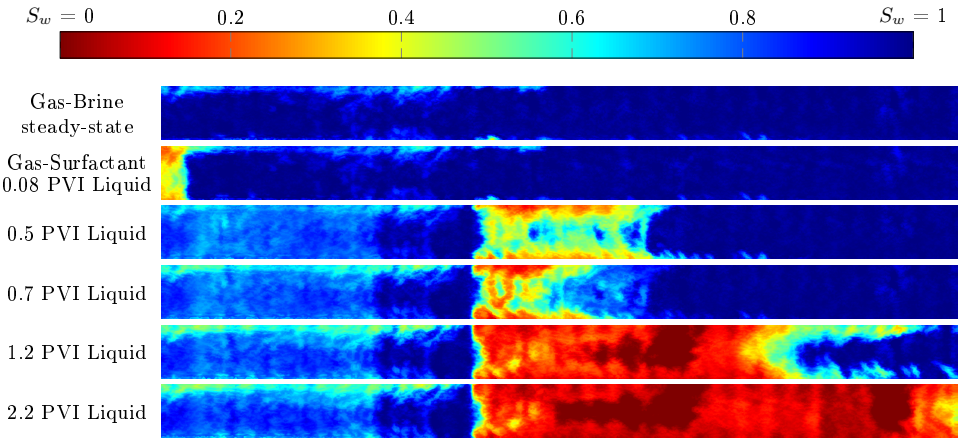

Figure 3.6: Average liquid saturation in a vertical cross-section through the center of the core obtained using X-ray CT imaging for the foam-generation experiment conducted at u_t = 0.67 ft/d and f_g=60%. The image at the top represents a measurement during steady-state gas-brine co-injection and the images thereafter were taken at times corresponding to dashed lines in **Fig. 3.5a**. Blue represents a high liquid saturation whereas red represents a high gas saturation, as indicated by the colorbar at the top.

in wetter flow. Some other studies indicate that the strength of steady-state foam in a sandstone can be higher during wetter flow (Persoff et al., 1991; Kovscek et al., 1995), while Huh and Handy (1989) report the opposite. In this study, with respect to foam generation by snap-off in flow across an abrupt permeability jump, we do not observe significant differences in foam strength or the time at which foam generation commences at lower gas fractions to support the findings of (Rossen, 1999). For a permeability contrast of approximately 3.8:1, foam generation is observed at higher gas fractions than predicted by theory (**Fig. 3.1**).

3.4. DISCUSSION

A series of injection rates and gas fractions were used to examine the effect of fractional flow and velocity on foam generation across a sharp permeability contrast of 3.8:1. Foam generation was observed at all the conditions tested. Snap-off in flow of gas and surfactant solution across an abrupt heterogeneity is intermittent in nature (Falls et al., 1988; Shah et al., 2019b). Foam is not created steadily across the interface as surfactant solution reaches the permeability jump. In our experiments, the onset of foam generation, and often the period thereafter, is accompanied by large fluctuations in measured pressure gradient across the permeability transition and in the high-permeability zone. As mentioned earlier, foam generation begins when capillary pressure at the edge of the low-permeability zone falls below P_c^{sn}. Snap-off in pore throats blocks the flow of gas causing the local gas fraction to increase and the flow to become drier. Locally, the capillary pressure may momentarily rise above P_c^{sn} and foam generation stops. Eventually, liquid convects or imbibes back to the boundary of the low-permeability zone and accumulates, creating favourable conditions for snap-off. This

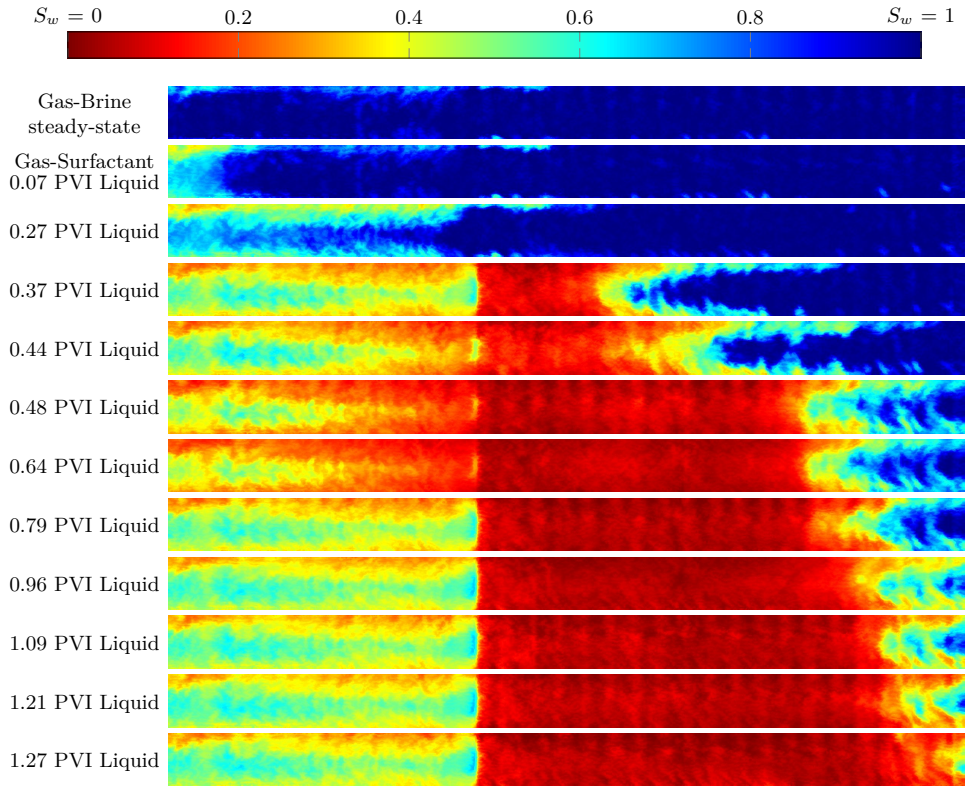

Figure 3.7: Average liquid saturation in a vertical cross-section through the center of the core obtained using X-ray CT imaging for the foam-generation experiment conducted at u_t = 0.67 ft/d and f_g=95%. The image at the top represents a measurement during steady-state gas-brine co-injection and the images thereafter were taken at times corresponding to dashed lines in **Fig.** 3.5b. Blue represents a high liquid saturation whereas red represents a high gas saturation, as indicated by the colorbar at the top.

cycle of events repeats itself and we think it is responsible for the large fluctuations in pressure gradient observed in our experiments.

We observe that this intermittency, in terms of magnitude and frequency of fluctuations in pressure gradient, is greater as the velocity decreases. **Fig.** 3.8 shows the measured pressure gradient across the entire high-permeability zone (**Fig.** 3.8a) and the corresponding apparent viscosity (**Fig.** 3.8b). Each data point represents all the measurements recorded and averaged over 0.05 PVI of surfactant solution (or 0.25 total PVI). The error bar in each direction represents one standard deviation of all the measurements within this window, representing the magnitude of fluctuation in pressure gradient. As the injection rate decreases, the magnitude of these fluctuations increases. For each case, the pressure gradient rises after roughly the same amount of liquid injected ($\approx$ 0.4 PV), corresponding to the time at which the surfactant solution arrives at the permeability contrast.

As reported in the previous chapter, apparent viscosity is computed as:

$$\mu_{app}^{H} = \frac{k^{H} \nabla P^{H}}{u_t} \tag{3.1}$$

where k^H is the measured permeability in the high-permeability section, ∇P^H is the pressure gradient across the same section during the experiment and u_t is the total superficial velocity. Therefore, if the pressure gradient remains the same, the computed apparent viscosity increases with decreasing velocity. While the experiment at u_t = 0.17 ft/d records the highest apparent viscosity, foam does not reach the outlet of the core, as reported in the previous section. Ignoring the experiment at the lowest velocity, **Fig. 3.8a** shows that the measured pressure gradient is, for the most part, higher at a lower injection rate. This is counter-intuitive for two-phase flow but can be explained as follows: As capillary number (or velocity in this case, as permeability is kept constant) increases, the impact of capillary heterogeneity decreases (Yortsos and Chang, 1990). For the same reason, coreflooding experiments are often conducted at high injection rates in order to minimize the influence of the capillary end-effect. Therefore, as velocity in our experiments increases, the rate of foam generation may be affected in a way that the strength of the resulting foam is reduced. Note that this would hold true only for foam created by snap-off across an abrupt increase in permeability. For other mechanisms of bubble generation, a higher velocity would lead to the creation of a stronger foam. The results of our experiments imply that a reduction in gas mobility can be expected far from wells in a foam EOR application, provided that sharp heterogeneities are present in the formation. For all practical purposes, it can be considered that this phenomenon is independent of velocity. While velocities as low as 0.17 ft/d may never be reached in a typical reservoir setting, we still observe foam generation across a permeability contrast of 3.8:1 at this superficial velocity. At velocities much greater than 1 ft/d, other mechanisms of foam generation come into play and the impact of snap-off across heterogeneities may be less significant.

Experiments with varying gas fractions were conducted with the core placed horizontally on the CT scanner table. CT images together with pressure measurements were used to identify when foam generation began and whether foam successfully propagated towards the outlet of the core. **Fig. 3.9** shows a plot of the apparent viscosity in the high-permeability section plotted against pore volumes of surfactant solution injected for three different fractional flows. Since the total velocity and absolute permeability remain constant between the experiments, the trend in apparent viscosity also reflects the trend in pressure gradient in the high-permeability zone. The CT images corresponding to f_g = 60% and f_g = 95% are shown in **Figs. 3.6** and **3.7**, respectively. As discussed in the previous section, for the experiments conducted at f_g = 80% and f_g = 95%, pressure gradient in the high-permeability zone rises before the CT images show a high gas saturation in that zone. Therefore, after ≈ 0.1 PVI liquid, the apparent viscosity (μ_{app}^{H}) is approximately 100 cP for these experiments (**Fig. 3.9**). However, the CT images visualize a foam front that begins to develop and move through the high-permeability zone after roughly the same liquid volume has been injected. This observation is

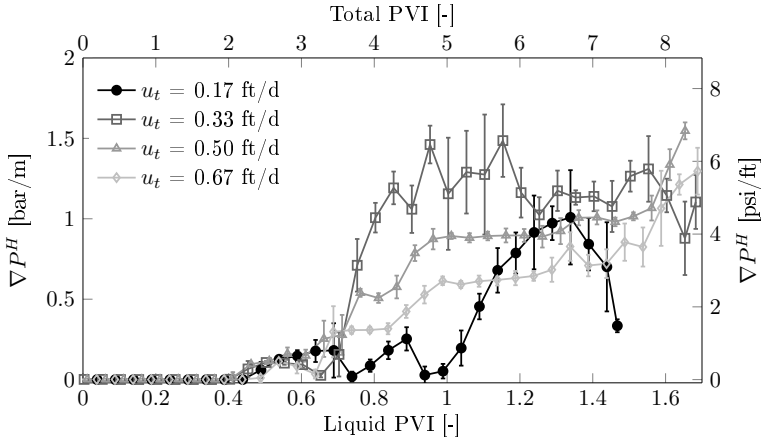

(a)

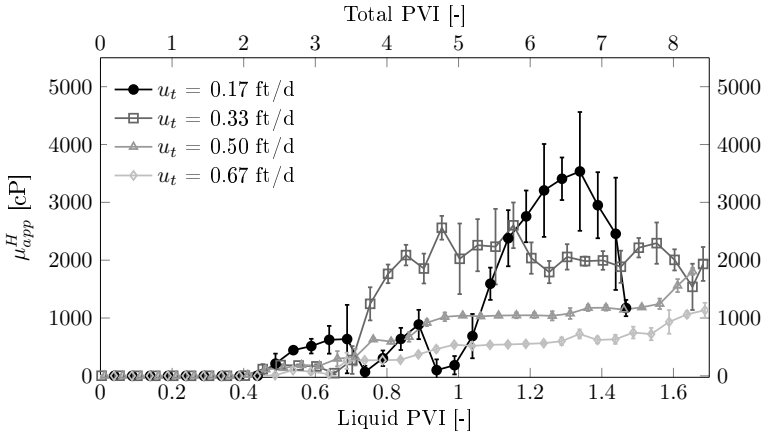

(b)

Figure 3.8: (a) Pressure gradient measured across the high-permeability section of the core at four different injection rates and (b) corresponding apparent viscosity. f_g = 80% in all the experiments.

independent of f_g, and, as mentioned above, u_t. Moreover, the onset of foam generation is accompanied by fluctuations in pressure gradient, which are more frequent, and larger in magnitude in these two experiments compared to the test at f_g = 60%. However, it takes longer (in terms of liquid PVI) for foam to propagate downstream to the outlet of the core at f_g = 60% compared to the other two experiments. In other words, it takes more surfactant solution for foam at 60% quality to travel the same distance as a foam at 95% quality.

At the end of the experiments shown in **Fig. 3.9**, $\mu^H_{app} \approx$ 900 cP for f_g = 95%, 700 cP for f_g = 80%, and 950 cP for f_g = 60%. It is not entirely clear why the foam apparent viscosity drops at 80% foam quality. It is possible that if the experiment was continued for an extended period of time, the apparent viscosity would reach a similar

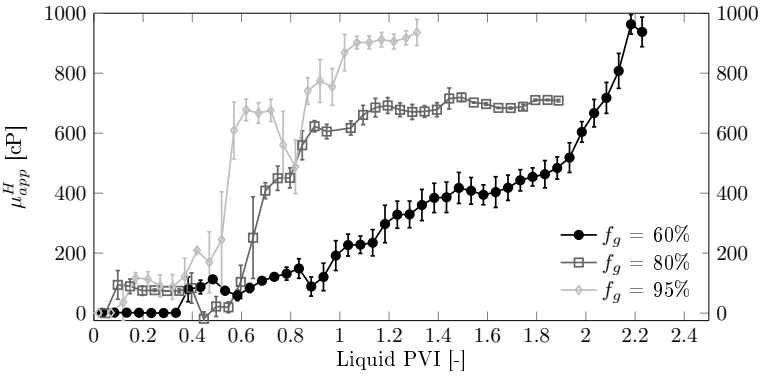

Figure 3.9: Apparent viscosity across the high-permeability section of the core through experiments conducted at three different injected gas fractions with the core placed horizontally in the CT scanner. u_t = 0.67 ft/d in all the experiments.

value. Nevertheless, this observation is inconsistent with the observations of Tanzil et al. (2002b) and Falls et al. (1988), who observed a decrease in pressure gradient and foam apparent viscosity with an increase in gas fraction. In both their experiments, foam was generated across a permeability discontinuity as a combination of gas and surfactant solution drained a medium already saturated with surfactant solution. Moreover, in the experiments of Tanzil et al. (2002b), a decrease in f_g between successive tests was also accompanied by an increase in u_t, since the gas velocity was kept constant. These differences in experimental protocols may be responsible for the contrast in experimental observations. As Syukri (2018) performed so-called foam-quality-scan experiments (Ma et al., 2013, 2014) with a homogeneous sintered glass core with the same permeability as the high-permeability region of the porous medium used in this study. In his foam scans, foam was generated under drainage conditions by injecting gas and surfactant solution into a surfactant-saturated core. The transition foam quality was 80% and the foam apparent viscosity was lower at a foam quality of 60% and 95% compared to 80%. The experiments at f_g = 60% and f_g = 95% were performed again to ensure repeatability. The experiment at f_g = 80% and u_t = 0.67 ft/d is a replication of an experiment performed by Shah et al. (2019b) under identical conditions. The results of all the experiments performed at the same injection conditions were similar and the discussion above holds, regardless of which experimental data we select.

In order to further investigate and validate the theory of foam generation across permeability contrasts by snap-off, we investigate the saturation profile in the core obtained through CT imaging, focusing on the permeability contrast. **Fig. 3.10** shows the average steady-state liquid saturation in the core plotted against dimensionless core length (x/L). Mean saturation values in the low- and high-permeability zones, and at the transition, are indicated. Every measurement on the graph represents average saturation inside a circular CT image slice, and each slice is 1.5 mm thick, as is the voxel size. Image settings identical to Shah et al. (2019b) were applied while scanning the core.

The permeability jump in the core takes place over one, or at most two, “coarse" grain diameters, equivalent to circa 0.5 mm. Since the voxel depth is more than this grain size, the CT measurement at the permeability contrast (at x/L ≈ 0.38 in **Fig. 3.10**) defines the average liquid saturation near the edge of the low-permeability zone. The exact liquid saturation one pore throat away from the heterogeneity can be higher. Nonetheless, the saturation profile gives a good indication of the behaviour across the heterogeneity in terms of liquid accumulation and local reduction in capillary pressure.

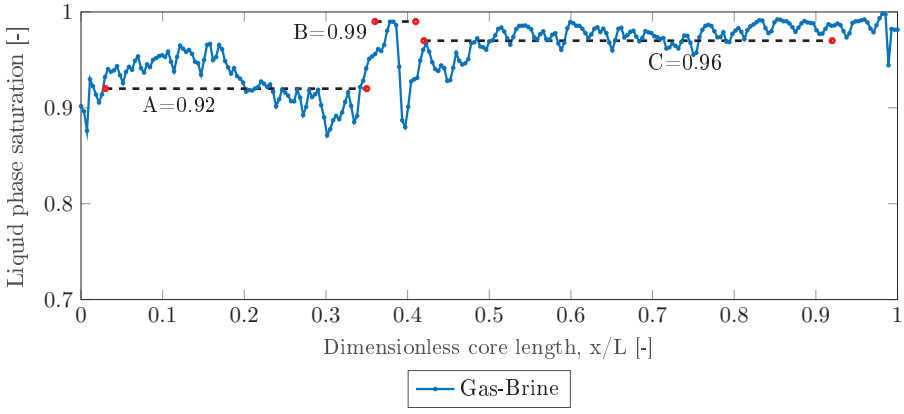

Figure 3.10: Steady-state liquid-saturation profile across the core during gas-brine co-injection. Dotted lines indicate average saturation in the low-permeability zone, at the transition, and in the high-permeability zone.

Berg et al. (2014) and Armstrong et al. (2016) measured capillary pressure as a function of saturation using mercury-intrusion porosimetry for sintered glass core plugs, as used in this study. We use the Leverett-J function (Leverett, 1941) to extend these measurements to the petrophysical and fluid properties of our experimental system and construct capillary-pressure curves for the two regions in the core. The curves are plotted on a semi-log scale in **Fig. 3.11a**. As indicated in the figure, capillary-pressure curves obtained through mercury-intrusion porosimetry include an entry-slope region. Several authors have investigated the physical meaning of this region (Nabawy et al., 2009; Katz and Thompson, 1986; Schowalter, 1979). The entry-slope region concerns pore throats near the edges of the porous medium that are being entered by the non-wetting phase. It is not representative of drainage in the bulk of the porous medium. Therefore, we estimate the capillary entry pressure of the low-permeability zone by extending the P_c curve (ignoring the entry-slope region) to intersect with the vertical line representing a water-saturated core (S_w=1), indicated by the dashed arrow in **Fig. 3.11a**. Note that to model snap-off across a permeability change, however, imbibition-type capillary pressure curves must be used which include the entry-slope region that allows capillary pressure to reach the critical value for snap-off at effective gas saturations between 0 and 1. Drainage capillary pressure curves would not allow for this type of snap-off since P_c is always higher than P_c^e, anywhere on the drainage P_c versus S_w curve (Falls et al., 1988). Even when occurring in a macroscopic drainage process, snap-off results from a

brief moment of local imbibition into appropriately sized pore constrictions that meet the strictly geometric criteria for static snap-off (Roof, 1970; Chambers and Radke, 1990; Ransohoff and Radke, 1988), which is a temporary deviation from drainage behaviour, in its exact sense.

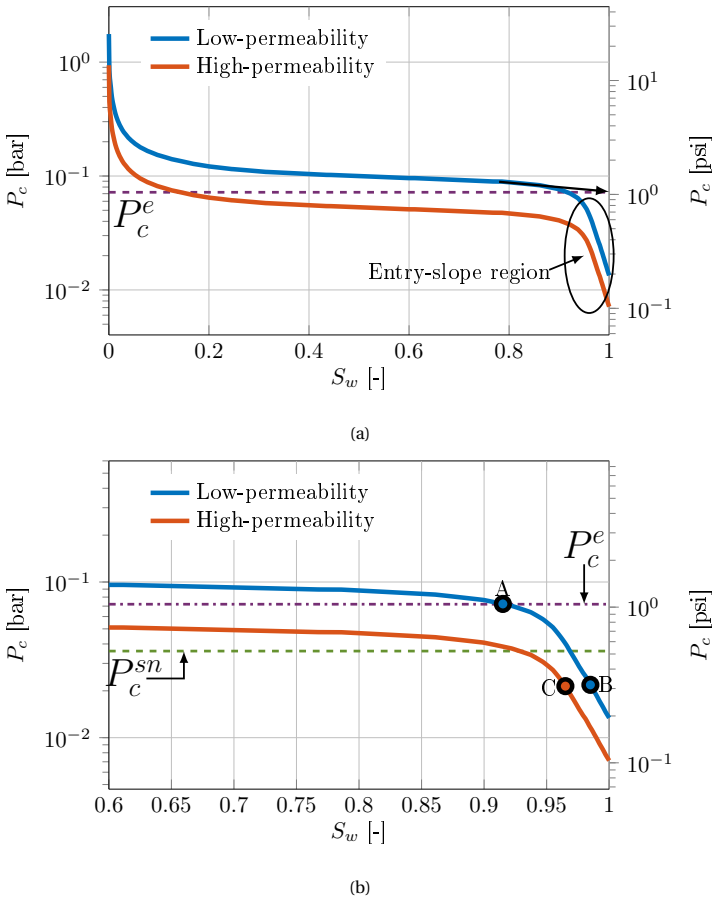

Figure 3.11: (a) Capillary-pressure curves for the high- and low-permeability regions in the core extracted from the measurements of Berg et al. (2014) and adjusted to the petrophysical and fluid properties of our system, (b) capillary pressure corresponding to average liquid saturations indicated in **Fig. 3.10**.

In **Fig. 3.11b**, the capillary-pressure curve is zoomed-in close to the liquid-saturated end. The average liquid saturations indicated in **Fig. 3.10** are plotted on the curve. $P_c^{sn} = 1/2\ P_c^e$ is assumed (Falls et al., 1988) and marked by the green dashed line on the plot. The capillary pressure corresponding to the average saturation in the low-permeability zone (A) is just above the entry pressure of the region. At the transition, liquid accumulates to maintain capillary continuity and it can be seen that the capillary pressure drops to below the capillary pressure for snap-off (B). The capillary pressure corresponding to the average liquid saturation in the high-permeability zone is close

to P_c at the transition. In alignment with the theory of Yortsos and Chang (1990), this response indicates that the permeability contrast is sharp and monotonic. Moreover, since the P_c at the transition is lower than P_c^{sn}, snap-off is observed as surfactant is introduced into the system. This is consistent with the work of Rossen (1999) and Falls et al. (1988). A similar investigation can be followed in all the experiments performed with CT-assisted saturation measurements and it is observed that capillary pressure at the boundary of the low-permeability zone drops below the critical capillary pressure for snap-off, resulting in foam generation across the permeability contrast. A complete analysis of the path followed along the P_c curve would include the edge effect on the measured drainage capillary pressure curves in **Fig. 3.11a** and the effect of imbibition on the low-permeability section at the boundary.

As mentioned earlier, the observations from the experiment conducted at u_t = 0.67 ft/d and f_g = 95% show that, for a given permeability contrast, foam was generated at a higher gas fraction than expected (**Fig. 3.1**). This disagreement with the work of Rossen (1999) could arise from the fact that Rossen employed a pore-network model with the effective medium approximation (Kirkpatrick, 1973) to compute relative permeability and model flow in homogeneous regions. For the porous medium used in this study, the flow behaviour is different and the relative permeabilities of the gas and liquid phases allow for the saturation response shown in **Fig. 3.10**. As a result, the reduction in P_c is sufficient to cause snap-off even at f_g = 95%.

3.5. CONCLUSION

Experiments at low superficial velocities were conducted with a variety of fractional flows in a layered core to observe foam generation by snap-off. In reservoirs where the geological setting allows for the presence of sharp changes in permeability, snap-off can help reduce gas mobility away from wells where the superficial velocities are low. These heterogeneities can exist in the form of layer boundaries or laminations and cross-laminations within individual layers. The permeability changes can be parallel or perpendicular to the direction of flow, or a combination of the two. When the contrast is parallel to the direction of flow, upward migration of gas due to gravity can cause foam generation in the high-permeability layers. Once foam is generated, gas mobility in the vertical direction will be reduced, effectively increasing the segregation length (Stone, 1982; Jenkins, 1984; Rossen and Bruining, 2007) and improving sweep efficiency in the low-permeability layers. In the presence of lateral changes in permeability, snap-off may help maintain foam strength and improve the mobility control deep inside the formation. Foam generation across sharp permeability contrasts can have important consequences for foam EOR applications and it must be accounted for to account for the improvement in overall sweep efficiency.

In this study, foam generation was observed almost immediately as the surfactant solution arrives at the permeability contrast, irrespective of f_g or u_t. However, in our synthetic porous medium, surfactant adsorption is almost negligible and in a more realistic setting adsorption must first be satisfied before foam generation commences. In

agreement with the observations of Falls et al. (1988), snap-off across the permeability contrast was an intermittent process. This is best indicated by periods of fluctuating pressure gradient that mark the onset of foam generation and subsequent propagation. This intermittency, in terms of magnitude and frequency of fluctuations in pressure gradient, was greater at higher gas fractions and lower velocities. The saturation maps constructed using CT imaging for some of our experiments help confirm that foam was indeed generated at the permeability transition and from there on it propagates downstream to the end of the core. The saturation maps also show that the local reduction in capillary pressure near the permeability jump is consistent with previous theory (Falls et al., 1988; Yortsos and Chang, 1990; Rossen, 1999).

4

Creating Synthetic Porous Media for Multiphase Flow Experiments Under Controlled Conditions

Heterogeneity in sedimentary rock makes prediction of subsurface flow behaviour difficult. Sharp changes in permeability can be found as unconformities such as layer boundaries or laminations and cross-laminations within individual subsurface formations. They contribute to effects such as capillary entrapment, channelling or early breakthrough and foam generation. They can have a significant impact on the successful application of a displacement process, be it for oil recovery or for aquifer remediation. It is desirable to conduct flow experiments under controlled conditions with predefined model porous media with the desired features of heterogeneity represented. Laboratory experiments studying subsurface processes are often conducted with tubular sand-packs or rock tubes called cores. Naturally found rocks often have a variety of structural features that affect experimental results and make the modelling of the effects of a single feature difficult. Sand-packs, on the other hand, are unconsolidated and extremely difficult to compact. Therefore, in this study, we explore several methods of preparing controlled synthetic pore frameworks of pre-defined dimensions in tubeshaped samples. The degrees of freedom in parameters are limited by the degree of resolution expected for certain type of experiments. In this work, our attempts are directed towards creating layered cores with homogeneous individual layers and sharp, uniform changes in permeability in between, for experiments concerning foam generation and gas trapping. We tested synthetic sintered glass samples with uniform and heterogeneous grain sizes with high/low permeability interfaces. We determined the quality of the interfaces, heterogeneity and pore surface qualities. Next to this,

high-temperature preparations of clay-rich grain-aggregates were prepared and their pore structure analysed by using micro-computed tomography. The grains are fused at elevated temperatures and contact points are transformed to contact planes. Lastly, well-characterized, compacted and consolidated sand-packs were created. In this study, consolidation means not necessarily the solidification of the packing of grains into a single solid object, but more efficient packing of grains with reduced porosity. These packs initially hold point contacts between the grains, creating a maximum porosity. Compaction is achieved using centrifugal force and consolidation is achieved by drainage of a wetting fluid under vacuum, during compaction. Advantages and disadvantages of these techniques, together with the suitability of the end-result with respect to our experimental requirements, is discussed. Every sample was analysed through permeability measurements and X-ray computed tomography. The layered sintered glass cores were also used to conduct core-flooding experiments with foam generation across abrupt increments in permeability. The sintering process is sensitive to the physical dimensions of the core such as length and diameter. Repeatability is limited and imperfect sintering near the edges of a core can significantly affect the relative permeability of individual phases. The structural integrity of cores made from sintered clay-rich grain-aggregates is sensitive to the heating and cooling cycles. Inhomogeneous temperature profiles often lead to fractures within the core and repeatability can not be ensured. The sand-packs, compacted using a centrifuge, produced the most promising results in terms of homogeneity within the samples. On average, a 15-35 % reduction in permeability is achieved as a result of compaction.

4.1. INTRODUCTION

Research investigating multiphase flow in subsurface porous media usually begins with experiments using naturally found rocks. The rocks are typically in the form of cylindrical tubes, known as cores, and the experiments are termed corefloods. Pressure, and often phase saturations through X-ray computerized tomography (CT), are the primary measurements as fluids flow through the porous medium during the experiment (Hove et al., 1987). The objective of these experiments might be to study a physical phenomenon (for instance, snap-off (Falls et al., 1988; Shah et al., 2019b), or reactive fluid transport (Ott et al., 2012)). In a study with different objectives, coreflood experiments were employed by Sorbie et al. (1987) to develop models that could represent the behaviour of a polymer in porous media. These experiments are also conducted to quantify the displacement efficiency of various fluids injected in a subsurface formation: for example, the use of surfactant to mobilize trapped oil in a petroleum reservoir (Hirasaki et al., 2005). Experimental data is then used to select appropriate agents for the displacement processes. Cores are also used to study the acoustic behaviour of various geological formations in the laboratory. Based on laboratory measurements, models are developed to extract information such as porosity, lithology and fluid saturation as a function of the acoustic response recorded in the field (Visser, 1988).

The reproducibility and reliability of coreflood results, however, is often limited because too many rock properties vary from one rock sample to another, even when extracted from the same formation. Mild contrasts in permeability and capillary-pressure can alter the results of displacement processes through, for instance, early breakthrough of high mobility fluids or by trapping of the non-wetting phase. The propagation of chemical agents such as foam and polymer is also affected by these features. No rock is truly homogeneous, and properties such as permeability and porosity vary locally within individual rock samples. As a result, conducting targeted experiments intended to develop models to describe physical phenomena as a function of their governing rock properties is difficult. For example, when analysing acoustic responses for formation evaluation, the allocation of a difference in response to a single rock property becomes unclear. Additionally, in coreflood experiments involving injection of chemicals, rock properties can altered through the course of the experiment and a fresh core is usually used for each experiment. This, once again, limits the reproducibility of results obtained through these experiments. Therefore, it is desirable to be able to produce well-characterized artificial porous media with predetermined properties for controlled experiments.

The objective of this work is to test and develop methods to create well-characterized, well-compacted and consolidated porous media, analogous to both homogeneous and layered subsurface systems. A review of methods to create artificial sandstones was presented by Visser (1988), whose work was driven by the investigation of acoustic behaviour of natural and synthetic rocks. In this case, it is necessitated by the need for a layered core with homogeneous individual layers required for experiments investigating foam generation in a porous medium with sharp permeability changes (Falls et al., 1988; Rossen, 1999). In an earlier publication (Shah et al., 2019b), similar experiments conducted using sintered glass cores are reported. In this chapter, experiences with using sintered glass will be discussed. Results from attempts at creating cores by sintering clay-rich grain-aggregates will be presented. A novel protocol to create centrifuge-consolidated sandpacks that meet the above mentioned requirements is also reported.

This chapter is structured as follows. In the next section, the foam-generation experiments that necessitated the investigation of methods to create artificial porous media are briefly described. Next, experiences with sintered-glass cores in these experiments is summarized. In the section that follows, attempts at creating artificial rock by sintering clay-rich grain-aggregates are reported. In the next section, a method to create long, homogeneous and layered sandpacks consolidated through increased stress and seepage suction using a geotechnical centrifuge is presented. Concluding remarks are put forward and recommendations for future work are proposed in the “Conclusions" section.

4.2. FOAM GENERATION EXPERIMENTS

Methods to create synthetic porous media were investigated in order to prepare cores to be used in a specific kind of foam-generation experiments, as described in detail in the previous two chapters of this thesis and summarised through this section. Foams are a distribution of trapped, discontinuous gas bubbles in a continuous liquid phase. Foams are used to achieve mobility control in displacement processes in porous media because they effectively “viscosify" the gas, allowing for a better sweep efficiency (Rossen, 1996). Therefore, foams are viable agents for enhanced oil recovery (EOR) in petroleum reservoirs and for incremental removal of non-aqueous phase liquids (NAPL's) in an aquifer-remediation process (Hirasaki et al., 1997b,a, 2000).

Foams can be generated in a porous medium through various mechanisms, as described by Ransohoff and Radke (1988); Kovscek and Radke (1994); Rossen (1996). Several studies indicate that creation of strong foam in porous media in steady gas-liquid flow requires that a critical pressure gradient threshold be exceeded (Rossen and Gauglitz, 1990; Rossen, 1990a; Friedmann et al., 1991; Gauglitz et al., 2002; Tanzil et al., 2002a; Kam and Rossen, 2003). Creation of strong foam in these cases is thought to depend on the continued mobilisation of liquid lenses that divide and create more lamellae as they mobilize. Others suggest foam generation is dominated by Roof snap-off (Roof, 1970), which dominates during a drainage process and does not require a threshold driving force (Ransohoff and Radke, 1988; Kovscek and Radke, 1996, 2003). There is no consensus in the literature about the dominant mechanism responsible for strong foam generation in porous media.

Near injection wells, since the surfactant and gas slugs are typically injected in an alternating fashion, gas drains the preceding surfactant slug. Moreover, the pressure gradient is quite large and the conditions for strong foam generation according to both convictions are easily met. Away from the wells, pressure gradient is much lower and the gas and surfactant slugs would have mixed. The requirements for foam generation and propagation may not be satisfied. In the presence of sharp heterogeneities, however, foam can be generated independent of pressure gradient during simultaneous flow of gas and surfactant solution (Falls et al., 1988; Rossen, 1999; Hirasaki et al., 2000; Tanzil et al., 2002b; Li and Rossen, 2005; Shah et al., 2019b). Our objective is to investigate this phenomenon and understand this mechanism of foam generation as it might be relevant for mobility reduction deep inside the reservoir.

Sharp changes in permeability are common in subsurface formations and can exist over a large range of length scales (Reineck and Singh, 1980; Hartkamp-Bakker, 1993). These heterogeneities, when found in natural formations, are quite frequent in the sense that one layered core of length 40 cm could have tens of permeability discontinuities. It is difficult to obtain natural cores with a single sharp change in permeability. Such a core is desirable when models describing the behaviour of fluids, as they flow across a permeability transition, are to be developed. It is also advantageous to have relatively homogeneous individual layers in order to minimize the impact of smaller permeability contrasts on the experimental results. Therefore, for our study of foam generation in flow across an abrupt increase in permeability, an artificially created core with a single,

well-characterized, sharp change in permeability was desired. A consolidated core was preferred since foam generation can create a high pressure gradient, which might result in the migration of grains in an unconsolidated medium.

As shown in Chapter 2, **Fig. 2.4** shows a schematic of the experimental setup employed to study foam generation across a sharp increase in permeability. This setup was used to study foam generation across abrupt heterogeneities in commercially acquired cores made from sintered glass. Some results from those experiments are reported in the next section with a focus on difficulties that lead us to explore other methods of creating synthetic porous media.

At the start of each experiment, brine (1 wt.% NaCl ≈ 0.17M) and gas (N_2) are injected into a layered porous medium with a low- and a high-permeability zone. Once steady-state is reached, surfactant solution (0.5 wt.% ≈ 0.04M Anionic α-olefin sulfonate [AOS] $C_{14\text{-}16}$ with a molecular weight of 315 g/mol and 1 wt.% NaCl ≈ 0.17M) and gas are co-injected into the core. This sequence is followed in order to avoid gas draining a surfactant saturated region in the core, thereby minimizing the chances of foam generation by mechanisms that occur during drainage (leave-behind, Roof snap-off). Fluids are injected into the low-permeability zone at low velocity in order to avoid foam generation by mechanisms that dominate at higher velocities (lamella division). Pressure is the main measurement through the course of an experiment. For select experiments, X-ray CT scanning is used to quantify phase saturations through the course of the experiment. For those cases, the core is placed horizontally, together with the rest of the setup, on the CT table in a temperature controlled room that houses the CT machine. For other experiments, the core is placed vertically in a temperature-controlled oven.

In order to reduce the impact of entrance- and end-effects on experimental measurements, a long core is desired. In addition to being longer than the size of the entrance region (Ettinger and Radke, 1992; Chen et al., 2010), the low-permeability section must be long enough to conclude that there is no significant reduction in gas mobility due to foam generation before the fluids arrive at the permeability transition. This is confirmed through multiple pressure measurements across the low-permeability zone. Additionally, pressure gradient must also be measured across various sections of the high-permeability region in order to examine mobilisation of foam from the boundary and subsequent propagation towards the outlet. As a result, the high- and low-permeability zones must be at least as long as a typical core length used in steady-state foam experiments (Osterloh and Jante, 1992; Alvarez et al., 2001; Simjoo et al., 2013). However, the longer the core, the more difficult it becomes to create relatively homogeneous individual sections artificially. We investigated methods to create cores where each section would be at least 30 cm long. For the samples discussed in this chapter, the maximum size of the core was limited to 50 cm due to a variety of reasons discussed under the dedicated section for each preparation method. The sintered-glass samples used to conduct foam-generation experiments were on average 40 cm long with a 15 cm low-permeability section.

In addition to size requirements, a well-compacted and -consolidated porous

medium was preferred. Compaction and consolidation can reduce the porosity and permeability of an artificially created core, making it more representative of naturally found sandstones. It can also limit the migration of grains during experiments, which can alter the properties of the medium with time. Moreover, at permeabilities representative of the subsurface, foam viscosity at typical field velocities would be indicative of what can be expected in the field. A lower permeability would reduce the extent of gravity segregation, a common issue faced in the lab when the core is placed horizontally, for example, on the CT scanner table. In order to study the impact of permeability contrast on foam generation, it was desired that the permeability of the core be controlled prior to fabrication. It was essential to have a monotonic change in permeability at the boundary between the low- and high-permeability layers, with no mixing of grains at the boundary between the two zones. The core needed to be water-wet for the foam generation experiments and any consolidation methods that might alter the wettability of the core (for example, using resins or chemically induced cementation) were discarded in this work. Finally, it was required that the porous medium be chemically inert to injected fluids and be stable at elevated temperatures and pressures in order to conduct experiments at field-like conditions.

4.3. EXPERIENCES WITH SINTERED GLASS CORES

The physics of sintering of glass, with the primary application of creating porous systems, have been extensively studied (Kuczynski, 1949, 1972; Scherer and Bachman, 1977a,b; Rabinovich, 1985). Fritted glass, which is essentially an extremely fine-grained sintered glass, is a commonly used filter in laboratories. Glass bead packs, both with and without sintering, have been used extensively to study flow in porous media with applications to the petroleum recovery and groundwater decontamination (Wong et al., 1984; Charlaix et al., 1987; Ransohoff and Radke, 1988; Datta et al., 2013; Datta and Weitz, 2013; Datta et al., 2014; Armstrong et al., 2014, 2016; Berg et al., 2016). Sintered glass is an excellent candidate as an artificial rock when the sample sizes involved are small. Uniform compaction and consolidation through the sintering processes requires a uniform temperature profile throughout the sample, which is increasingly difficult to obtain as the sample size increases. Note that for consolidation by sintering (this section and the next), the end result is a single solidified object. Maintaining a uniform packing density, and by that, porosity and permeability, through the sample becomes increasingly difficult as the length and width of the sample increases. A drawback of using cores made by sintering glass beads, or crushed glass, is that the specific grain surface is either much lower or higher, respectively, than natural sandstones. The interaction of sintered glass with injected chemicals (for example, surfactants) is different compared to naturally found rocks. Surfactant adsorbs on the grain surfaces of sandstones, but not significantly on glass. This can be advantageous when only the flow behaviour of injected fluids (that have a potential for adsorption) is the subject of investigation.

To conduct experiments examining foam generation in flow across sharp

heterogeneities, we acquired sintered glass cores from Hilgenberg GmbH, Malsfeld, Germany (www.hilgenberg-gmbh.de). Four core samples with different permeability contrasts were procured. The samples were prepared by sintering crushed, pure borosilicate glass in a tube of internal diameter 3 ± 0.1 cm made from the same material. As a result, the glass grains also sintered to the walls of the tube. The samples were 50 cm in length, with a 20-cm-long low-permeability region. Before use in foam-generation experiments, 5 cm was removed from each end of the core since the entrance and exit regions were of a lower permeability, an artefact of the manufacturing and subsequent cutting process. The low- and high-permeability sections were selected based on a pore-size classification as supplied by the manufacturer and listed in **Table 4.1**. These specifications hold only for filter discs, which are usually, at most, a few centimetres in length and diameter. The samples procured were much longer, and therefore, the properties of the final product differed from these specifications. The measured permeabilities of each core are listed in **Table 4.2**. The permeability change in these samples was monotonic, as verified by permeability measurements upstream, across (weighted harmonic average) and downstream of the transition. **Fig. 2.3** shows a sintered-glass core sample placed in the core-holder with various pressure-transducer lines connected through the length of the core. The figure also shows a μCT image of the permeability transition that confirms that the change in grain size is monotonic and takes place over one, or at most two, “coarse" grain diameters ($d_c \approx 0.5$ mm).

Table 4.1: Approximate pore size and permeability of the low- and high-permeability sections in each sample as specified by the manufacturer. Subscripts L and H represent the low- and high-permeability zones, respectively. r represents average pore size, k is average permeability and superscripts L and H are used to denote average values for the low- and high-permeability regions, respectively.

Core sample	Pore size (r [μm])	Expected permeability (k [darcies])
1	r^L: 16-40 r^H: 40-100	k^L: 6.4 k^H: 29.4
2	r^L: 40-60 r^H: 100-160	k^L: N/A k^H: 45
3	r^L: 16-40 r^H: 100-160	k^L: 6.4 k^H: 45
4	r^L: 16-40 r^H: 100-160	k^L: 6.4 k^H: 45

Experiments with the sintered glass cores produced valuable results, as discussed

Table 4.2: Measured properties of each heterogeneous core including the average permeability contrast. Superscripts L and H are used to denote average values for the low- and high-permeability regions, respectively.

Core sample	Approximate pore volume [ml]	Measured permeability (k [darcies])	$\langle \frac{k^H}{k^L} \rangle$
1	99	k^L: 5.4 ± 0.02 k^H: 20.7 ± 0.2	3.8
2	99	k^L: 10.9 ± 0.01 k^H: 59.3 ± 0.8	5.4
3	80	k^L: 3.1 ± 0.01 k^H: 43.2 ± 0.2	13.9
4	96	k^L: 1.7 ± 0.15 k^H: 46.7 ± 2.0	27.5

below, showing that foam can be generated in low-velocity flow across a sharp permeability contrast. However, characterization of the sample and experimental measurements such as local pressure gradient and phase saturations revealed inhomogeneous features with respect to the properties of the medium. Minor changes in permeability were measured through the length of the low- and high-permeability zones. CT images indicate that the porosity was in some cases higher near the walls of the core. These artefacts could be due to a variety of reasons, such as the packing method, grain-size distribution, and temperature changes and viscous flow of glass during the sintering process, among others. The relatively long length of the core aggravates the impact of these variables.

In order to quantify the increment in porosity towards the edges of the core, in comparison to the centre, a 20-cm homogeneous sample was acquired. The core length was reduced so that it could fit inside the more accurate μCT scanner. The grain size selected was larger and the resulting pore size ($r \approx$ 160-250 μm) was greater than in the samples listed in **Tables** 4.1 and 4.2, such that the CT machine was able to resolve the size of the pores. This allowed porosity to be estimated through image analysis. The resulting images had a voxel size of 30 × 30 × 30 μm^3. Over 1150 cylindrical image slices were acquired over a length of roughly 34 mm in the centre of the core.

The image stack was analysed using Fiji (Schindelin et al., 2012), a distribution of ImageJ, as follows. First the images are thresholded and converted to a binary image, separating the grains from the pore space, with the grain framework represented in

black. Next, salt-and-pepper noise is removed through an *open-and-close* operation. Salt-and-pepper noise refers to a form of image degradation in which "only a few pixels are noisy, but they are very noisy" (Boncelet, 2009). It appears in the form of a sparse distribution of black and white pixels in the binary image. The *open* operation (erosion followed by dilation) removes isolated pixels (salt noise) and the *close* operation (dilation followed by erosion) fills in small holes (pepper noise). Grains in the resulting image are segmented using the default watershed algorithm (Soille and Vincent, 1990) in the image-analysis software. Next, a circular mask is created to extract the annular regions of 3 mm width starting from the edge of the circular core. Porosity is computed in five different annular regions of thickness 3 mm. The the radius of the inner and outer circle bounding this annular region ranges from 0-12 mm and from 3-15 mm, respectively. Note that the inner radius of the core is 15 mm. This way, the annular region covers the entire cross-section of the core. A flow chart summarizing the image-analysis procedure is shown to the left of **Fig. 4.1**. Also shown in the chart on the right is a plot of average porosity in each annular region versus the distance of the inner circle from the centre of the core. The porosity of the core is smaller at the centre of the core compared to the regions near the walls of the core. While porosity varies by a small amount ($\approx$ 2%) through the first four measurements, it increases sharply in the annular region immediately next to the tube wall. This is consistent with the observation of a higher gas fraction flowing near the edges of the core, most notable in **Figs. 2.7**, **2.10** and **2.13**, as explained below.

Previous studies (Charlaix et al., 1987; Wong et al., 1984) have reported that coring (extracting a cylindrical sample with a specially designed drill bit) cylindrical samples out from a larger block and coating the outside with a resin would effectively remove the edge effect. Their samples were 50-150 mm in length with a diameter of 12.5 mm and were cored out of blocks with an approximate diameter of 100 mm. In our case, however, the core length required is much larger ($\geq$ 400 mm) and, therefore, requires an even larger block of porous sintered glass. To the best of our knowledge, sintering blocks of glass of such large dimensions, while maintaining consistency in properties throughout, had never been attempted and would be very difficult, if not impossible, to achieve. Additionally, coring a 400-mm tube of sintered glass would require specialized equipment and might result in fracturing inside the porous medium due to vibration-induced stresses. Nonetheless, if it can be achieved, porous sintered glass cores would be ideal candidates for low-pressure one-dimensional corefloods.

A range of foam-generation experiments were performed to understand the impact of permeability contrast, fractional flow and velocity (Shah et al., 2019b,a). Some of the experiments were accompanied by CT scans at important stages using the Siemens SOMATOM Definition Dual Energy CT scanner. The acquired CT images were used to quantify phase saturations through the length of the core during the course of a foam-generation experiment. All the sintered glass cores used in this study resulted in foam generation across the permeability contrast. While experiments at lower velocities ($u_t \leq 0.67$ ft/d) did not result in any foam generation in the low-permeability zone, in experiments conducted at higher velocities ($\geq$ 1 ft/d), foam was generated in the inlet

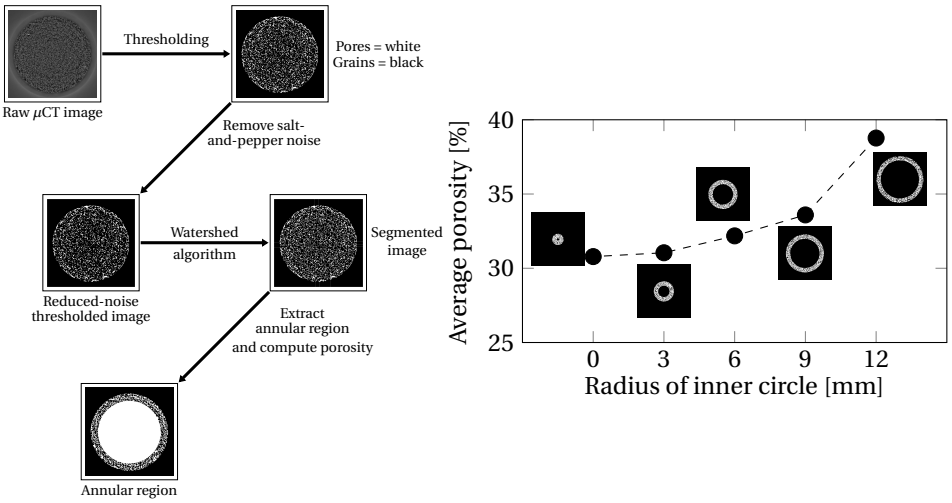

Figure 4.1: Flow diagram showing steps followed in computing porosity through image analysis of annular regions in the core (left). Average porosity in each annular region plotted against its distance from the centre of the core (right).

section itself prior to generation at the transition.

Liquid saturation during a foam-generation experiment can be computed using scans of a dry core, a wet core and a scan acquired during the experiment when multiple phases are flowing through the core (Mees et al., 2003). For further details about the experimental procedure, CT-scan settings and corresponding image analysis, we refer to Chapters 2 and 3 and Shah et al. (2019b). Consider **Fig. 2.7**, which shows the average liquid saturation as seen in a vertical cross-section through the centre of core 1 after various pore volumes of injection (PVI) of the liquid phase at a constant injected gas-liquid volume fraction of 80%. This particular experiment was conducted at a total injection rate (q_t) of 0.1 ml/min, which corresponds to a total velocity (u_t) of 0.67 ft/d. The experiment begins with co-injection of gas and brine (1 wt.% NaCl) into a brine-saturated core. Once steady-state is established, the core is scanned and the resulting liquid saturations are shown in the scan at the top in **Fig. 2.7**. At this stage, gas mobility is very high and gravity plays a dominant role, resulting in the injected gas overriding the liquid within the first few centimetres of the core. As a result, even though the injected fluids contain 80% gas, the CT image shows a high liquid saturation in the core, approximately 90% (Shah et al., 2019b). Once enough surfactant is injected such that it arrives at the permeability boundary, foam is generated in the high-permeability zone immediately downstream. The strength of the foam depends on the injection rate and the permeability contrast (Shah et al., 2019b,a).

In **Fig. 2.7**, a higher gas saturation is observed along the radial edge of the core, most notable in scans taken at 0.4 and 0.6 PVI liquid. This reflects the fact that the porosity along the edges of the core is higher compared to the bulk of the medium. This is an undesired artefact resulting from the imperfect sintering of the glass grains

to the walls of the core. As a result, the corefloods deviate from the assumption of a uniform, one-dimensional displacement that is typically employed when modelling the experiment. In results from other experiments reported by Shah et al. (2019b,a), evidence of inhomogeneities resulting from stage-wise packing of the glass grains when filling the tube prior to sintering can be seen. Additionally, signs of thermo-mechanical contraction and crystallization in the form of high-permeability streaks are visible in auxiliary samples that were procured but not reported those studies. Nonetheless, sintered glass cores were successfully used in the above-mentioned studies to demonstrate foam generation across a sharp contrast in permeability. Important conclusions could drawn from the experimental results, as reported by Shah et al. (2019b,a), independent of the imperfections in the core.

4.4. SINTERING CLAY-RICH GRAIN-AGGREGATES

With the hope of overcoming the difficulties involved in preparing large homogeneous porous sintered-glass samples, we attempted to create consolidated porous media by sintering clay-rich quartz and feldspar grain-aggregates. Multiple rock samples were acquired from various locations of the La Pitara outcrop near Teruel, Spain and from the Beringen and Zolder mines in Belgium. The samples from each location had varying amounts of clay and quartz. Several samples were used for the sintering experiment, of which the most promising result with samples from each location is reported. The rock sample from Spain is from the Cretaceous period and is from here-on referred to as rock A. The sample from Belgium is from the Carboniferous period and is henceforth referred to as rock B. The composition of these rocks obtained through X-ray diffraction/X-ray fluorescence (XRD/XRF) analysis is reported by Wolf (2006). Rock A comprises roughly 50-55% quartz, 10-20% organic matter with the remainder being clay and carbonates. Rock B consisted of 13-27% quartz, 60-70% clay with balance comprising of organic matter and carbonate minerals.

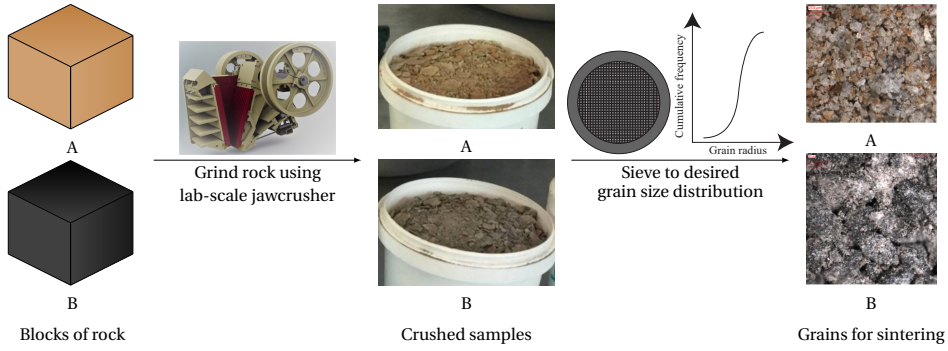

Figure 4.2: Schematic of procedure followed in going from cubic blocks of rock to grain-aggregates. Scale for microscope images to the right is indicated by the length of the white bar (A - 250 μm, B - 100 μm) on the top left corner of the two images.

The rock samples arrive from their respective locations in the form of cubic blocks. In

order to obtain grain aggregrates with a narrow, pre-determined size distribution, they are first crushed using a lab-scale jawcrusher to rocks of smaller sizes. At this point, the grain-size distribution is very wide, ranging from a tenth of a millimetre to tens of millimetres. Next, the crushed rock is sieved using an array of screens to arrive at the desired grain size for sintering. This procedure is depicted in **Fig.** 4.2. A grain size ranging from 90-250 μm was selected for the sintering tests. Next the grains are packed and prepared for sintering as shown in **Fig.** 4.3a. The grains are first poured into a ceramic tube that can withstand temperatures in excess of 1200 °C. While the grain-aggregates are gently poured into the tube, it is placed on top of a vibrating table set at an amplitude lower than the particle size, to achieve optimal packing. Graphite powder is poured on top of the pack to avoid oxidization of organic matter, which could result in vugs in the final sintered product. Next, the tube is placed in a high-temperature oven where the temperature profile is carefully regulated as shown in **Fig.** 4.3b. Final temperatures ranging from 950 °C to 1100 °C were tested.

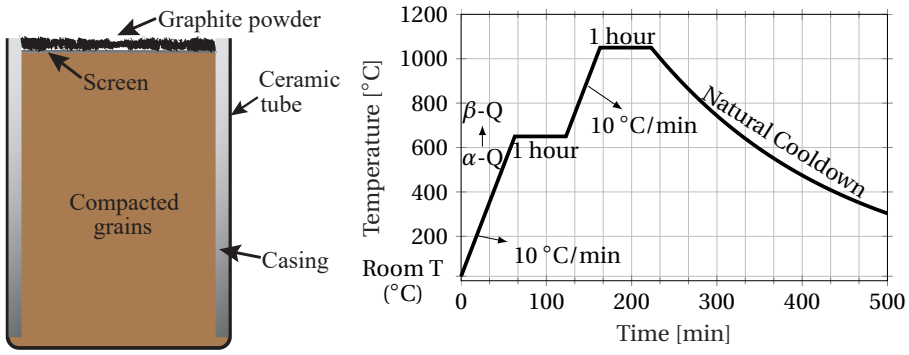

(a) Ceramic tube with porous grain pack

(b) Temperature profile in oven

Figure 4.3: (a) Ceramic tube filled with grain-aggregates and topped up with graphite powder prior to being placed in a high-temperature oven for sintering. (b) Temperature profile set inside the oven. The contents are allowed to cool down naturally and the curve representing the same is only a theoretical approximation.

Fig. 4.4 from the work of Wolf (2006) shows the expected changes in the grain framework upon sintering at 900 °C. Above 600 °C any organic content that may be present is either oxidized (if in an aerobic environment) or charred and converted to coke. The crystal structure of quartz in the matrix changes from trigonal (α-Quartz) to hexagonal (β-Quartz) close to 600 °C. Upon further heating, it is further transformed into hexagonal β-Tridymite at temperatures close to 900 °C. At temperatures in excess of 900 °C, a sintered clay matrix is formed and the grain framework is changed. Sintering increases the hardness of the material. A higher carbonate content increases the intensity of sintering (Wolf, 2006). At even higher temperatures, grains vitrify to glass and the initial grain volume decreases. Early vitrification by decarbonatization and devolatilization of the magnesium- and calcium-oxide rich glass matrix traps gases, which results in the formation of vesicles and swelling of the material. In order to obtain a homogeneous sample through this process, one must use grain-aggregates that have

an optimal composition of clay and quartz. A higher percentage of quartz results in a friable end product, whereas a higher percentage of clay and carbonates may result in excessive vitrification. A friable sample is not suitable for coring as the material might not maintain structural integrity when cored over large lengths. An excessively vitrified sample is highly heterogeneous and close to impermeable.

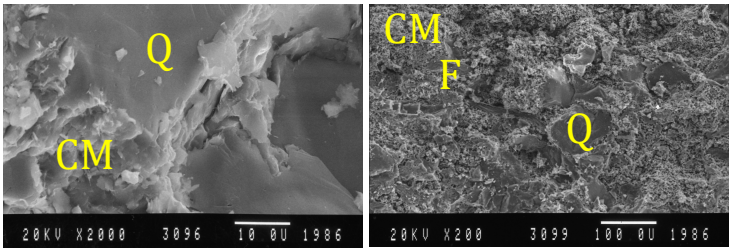

Figure 4.4: SEM images of typical grain-aggregates at 20 °C (left) and after treatment at 900 °C (right) indicating quartz (Q), feldspar (F) and clay content (CM) and showing expected changes in grain framework upon thermal treatment. *From Wolf (2006).*

As mentioned earlier, rocks A and B were thermally treated using the heating cycle as depicted in **Fig. 4.3b**. A variety of final temperatures were tested, going from 950 °C to 1100 °C in steps of 25 °C. The samples were allowed to cool overnight after each treatment. Rock A did not consolidate due to sintering at temperatures below 1050 °. At 1050 °, light sintering was observed. However, the sample was too friable, as shown in **Fig. 4.5**, to be cored over the lengths desired for foam-generation experiments. The figure to the right shows a magnified image of the sample obtained using a trinocular microscope. The clay content is not sufficient to create a rigid grain framework upon thermal treatment. Charring of the organic content can be seen on the grain surface. The results were similar at higher temperatures.

Figure 4.5: Cores from thermal treatments (upto 1050 °C) of two samples of Rock A (left and centre). Both tests resulted in a friable end product which could not be successfully cored over lengths in excess of roughly 3 cm. Magnified images of the thermally treated product (right) showing charring of organic matter (in black) over quartz grains. White bar on the top left corner of the image scales to 100 μm. The amount of clay in both the samples was not sufficient in order to maintain structural integrity of the sample upon sintering.

The carboniferous rock B yielded more-promising results. **Fig. 4.6** shows magnified images of thermally treated samples of the rock, tested up to different temperatures.

No sintering was observed below 1000 °C. The grain-aggregate pack weakly sintered when treated up to temperatures from 1000 °C to 1075 °C, and was still friable. At 1100 °C, the grain-aggregate pack sintered well and could be cored without disintegrating or fracturing. However, vitrification was also observed at 1100 °C. The bottom of the tube was vitrified, most likely due to higher temperatures at the bottom of the tube, being in contact with the oven floor. At the top of the tube, vesicles and signs of thermo-mechanical contraction were observed, in the form of fractures through the sample, plausibly due to a faster cooling rate at the top. A cylindrical sample, approximately 130 mm in length and 30 mm in diameter could be cored out of the ceramic tube as shown in **Fig. 4.7**. The central part of the core appeared to be the most homogeneous section, with no visible fractures or signs of vitrification. Permeability of the central section was measured using a Ruska gas permeameter and was found to vary between 2.5 and 3.5 darcy.

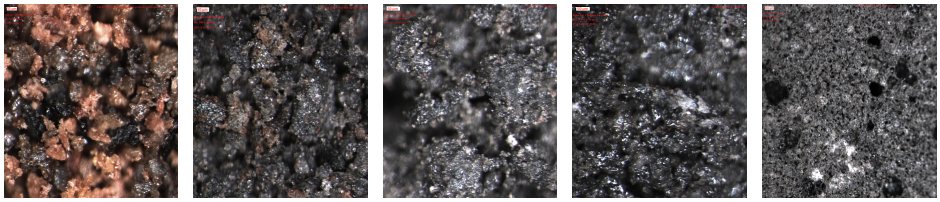

950 °C 1000 °C 1050 °C 1100 °C 1100 °C, vitrified

Figure 4.6: Microscope images (using a trinocular microscope) of rock B after thermal treatment upto various temperatures. Upto 1000 °C, no sintering was observed. From 1000 - 1050 °C, weak sintering was observed and the sample was still friable. At 1100 °C, the sample sintered well and was not friable. However, vitrified zones were observed. White bar on the top left corner of the images scales to 200 μm for the right most image showing vitrification and 50 μm for the rest.

Porous media prepared by sintering clay-rich grain-aggregates is shown to be a viable alternative to using sintered glass for coreflood experiments. In comparison with glass, the thermally treated grain-aggregate sample is more representative of subsurface reservoir rock in terms of surface chemistry and petrophysical properties such as permeability and porosity. Moreover, we expect these samples to have a higher resistance to pressure compared to sintered glass, which is usually rated for a maximum pressure of 10 bar. Nonetheless, maintaining homogeneity over large lengths in its preparation remains a challenge. For the rocks selected, we observed that sintering clay-rich grain-aggregates is more sensitive to small changes in temperature compared to sintering glass. This is most clearly evident in **Fig. 4.7**: The grain framework at the top of the core compared to the bottom of the core is significantly different, although we do not expect the temperature in the oven to vary significantly over a length of 130 mm. Fracturing through thermal contraction during cooling caused serious texture heterogeneity in the middle part **Fig. 4.7 (f-j)**. Compared to the texture heterogeneity in the sintered glass-grain samples, where the entire grain aggregate, over both length and width, varies in concentric density variation, here random fractures were generated. The positive result is that a larger diameter samples shows more homogeneity in texture

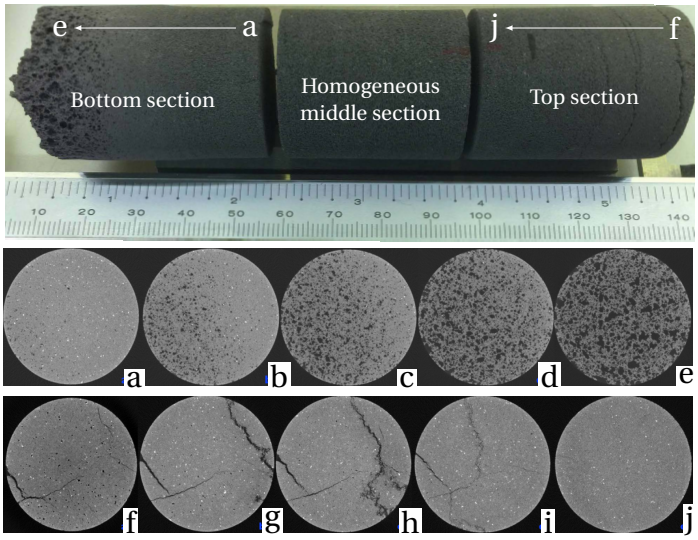

Figure 4.7: Cylindrical core of length ≈ 130 mm and diameter ≈ 30 mm extracted after thermally treating rock B up to a temperature of 1100 °C (top row). CT images of the bottom section (middle row), in addition to direct visual observations show that the lower part underwent vitrification and was most likely impermeable, as indicated by trapped pockets of gas visible after coring the sample. CT slices through the top section (bottom row) show fractures in the sample.

density distribution.

4.5. CENTRIFUGE-CONSOLIDATED SANDPACK

With the aim of overcoming the challenges involved in maintaining homogeneity while consolidating long samples by thermal treatment, we attempted to create sandpacks that were instead consolidated through increased stress and seepage under centrifugal force. The geotechnical centrifuge at the Delft University of Technology was employed for this purpose. In geo-engineering research, centrifuges are commonly used to re-create field-scale stress levels in lab-scale models (Lord, 1987; Schofield, 1980). They are used to study a variety of problems including soil–structure interaction (Stewart and McCartney, 2013), landslides and slope stability (Kim and Ko, 1982; Askarinejad et al., 2015), subsidence (Sterling and Ronayne, 1985; Jessberger and Stone, 1991) and fluid flow (Cargill and Ko, 1983), among others. We employed the centrifuge in order to cause a contractive volume change in a sandpack under an increased stress in the axial direction. The porous sample is saturated with water before being placed in the centrifuge. Under centrifugal force, water is drained from the core, being replaced by air, a more compressible fluid. The drainage of water from the sample causes suction within the pore space which can cause an additional reduction in porosity and permeability of the sample. Several consolidation models can be used to predict the time required for a specific porous medium to settle under a given amount of stress (Terzaghi, 1943; Takada and Mikasa, 1984; Fox et al., 2005; Verruijt, 2018; Bharat and Ubaid, 2019).

For the consolidated sandpacks developed in this study, we use the dimensionless parameter $T = \frac{c_v t}{h^2}$ to determine the time required for settlement inside the centrifuge, where c_v is the consolidation coefficient of the sandpack, t is the time elapsed and h is the sample height. c_v is directly proportional to the hydraulic conductivity (or permeability) of the medium and inversely proportional to the compressibility of the porous structure including the pore fluid. Effectively, a medium of lower permeability and higher compressibility would take longer to consolidate to the same fraction of the way to equilibrium as a medium with higher permeability and lower compressibility (i.e. rigid grain structure) (Terzaghi, 1943). While, theoretically, consolidation takes an infinitely long time to complete, for practical purposes, it is sufficient to assume that almost all of the consolidation has taken place at $T = 2$ (Verruijt, 2018). Therefore, we estimate the time of each centrifuge run as $t = \frac{2h^2}{c_v}$.The size of the sand column in our experiments is limited to 20 cm. c_v for moderately packed sand, saturated with water can be estimated to be $\approx 10^{-4}$ m^2/s. This gives an estimated consolidation time of $t = 800$ seconds. We time each centrifuge run for 15 minutes (900 s) and therefore, are certain that most of the settlement has taken place within that period.

For the purpose of creating sandpacks for coreflooding experiments, having an a priori estimate of the permeability of the final consolidated sample is desired. Permeability of the unconsolidated sandpack can be estimated using the Kozeny-Carman (Kozeny, 1927; Carman, 1938, 1956) or Blake-Kozeny equation (Blake, 1922; Bird et al., 2007), knowing the approximate grain diameters, tortuosity and porosity of the sample. Alternatively, one can use the Van Baaren equation (Van Baaren, 1979; Nelson, 1994) to compute the intrinsic permeability of a packed column to laminar flow of fluids. In the centrifuge, consolidation leads to a reduction in porosity and permeability of the sample, which can be quantified using constitutive relationships such as the one shown in **Fig. 4.8**. One can, for instance, quantify the reduction in voidage ($e = \frac{\text{Volume of pore space}}{\text{Volume of solid matrix}} = \frac{\phi}{1-\phi}$ where ϕ is porosity) as a function of applied stress as shown in the figure. This is called the compressibility curve and can be defined by two pairs of effective stress and corresponding void ratio. Similarly, the increase or decrease in permeability with an increase or decrease, respectively, in porosity can be quantified using empirical relationships developed using similar plots. This can then be used to design cores made using similar sand-types with a good estimate of the petrophysical properties of the final consolidated sample.

Three sand types with different grain diameters were chosen to prepare homogeneous and layered cores. The sand was sieved to achieve a narrow grain-size distribution as mentioned in **Table 4.3**. Consolidation was quantified in the form of reduction in porosity and permeability for the samples created. Pre-consolidation porosity (fourth column) was calculated by measuring the weight and density of sand poured into a container of known weight and volume. The sand was poured into a cylindrical container, which was fixed on top of a vertically vibrating table. The table was operated at a frequency of 50 Hz with the average amplitude set to 0.1 mm as sand was

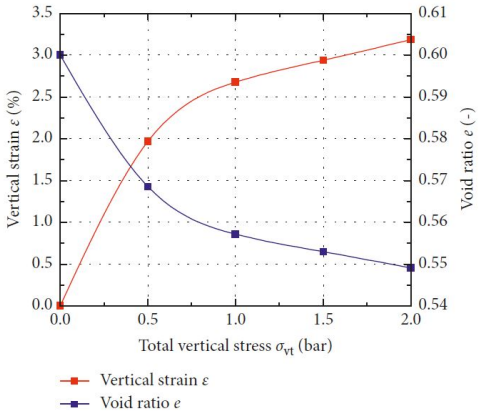

Figure 4.8: Constitutive stress-strain and voidage-strain curves for standard sand with 5% moisture content. *From Yang et al. (2018).*

gradually poured into the container using a funnel. This method of preparing a sandpack is similar to ASTM D4254-00 (Method 1A) (ASTM International., 2000). Sandpacks prepared using this method for consolidation in the centrifuge are henceforth referred to as loosely packed sand. The Van Baaren permeability (k^{vb}) (Van Baaren, 1979; Nelson, 1994) for loosely packed sand can calculated using the measured porosity porosity as:

$$k^{vb} = 10 \times d_{dom}^2 C^{-3.64} \phi^{m+3.64} \tag{4.1}$$

where k^{vb} is the single-phase permeability in millidarcies. d_{dom} is the dominant grain diameter, same as the median grain diameter (d_{50}) in this case. C is a constant that accounts for grain sorting. Here, we choose $C = 0.7$, determined through image analysis (Hoogewerf, 2019), representing very-well-sorted sand. m is the cementation factor. We select $m = 1.3$ for loosely-packed sand at atmospheric conditions. The Van Baaren permeability for each sand type is listed in the last column of **Table 4.3**.

Table 4.3: Specifications of different sand-types used in the centrifuge-consolidation experiment including grain-size range, median grain diameter (d_{50}), porosity (ϕ) and corresponding Van Baaren permeability (k^{vb}) of a loosely-packed sand column.

Sand type	Size range [μm]	D_{50} [μm]	ϕ	k^{vb} [darcies]
1	75 – 125	91	0.44	5.5
2	175 – 210	185	0.43	18.3
3	250 – 300	260	0.39	22.2

Two different sets of consolidation tests were performed on homogeneous samples made from the three sand types. In the first set of experiments, a dry loosely packed

sample was consolidated in the centrifuge at 50*g*. The cylindrical container used in these consolidation tests had an internal diameter of 4.8 cm and was made from polyether ether ketone (PEEK). The length of the container was 50 cm including two end-caps (≈ 10 cm each) at each end. Sand was poured up to ≈ 18.5 cm in each case and a 11.5-cm-long cylindrical piece of Bentheimer rock was placed on top of the sand. The purpose of the Bentheimer rock was to fill up any void space that would result from settlement in the centrifuge. The outer diameter of the rock was equivalent to the inner diameter of the PEEK cylinder. An end-cap was screwed on top of the rock to seal the container. Post-centrifuge, the end-cap was tightened further and settlement was quantified in terms of the incremental distance travelled by the end-cap. No permeability measurement was made in these dry tests and consolidation was quantified based on settlement and porosity reduction (**Table 4.4**).

For the second set of tests, a similar sample was prepared and the sandpack was saturated with water. Permeability to water was measured and the water-saturated sample was subject to 50*g* inside the centrifuge as water was allowed to drain under the centrifugal force. Consolidation was quantified in terms of a reduction in permeability for these wet tests (**Table 4.5**).

The vertical stress experienced by an infinitesimal volume of length dl, at a distance l from the top of a cylindrical sample under centrifugal force can be quantified as:

$$d\sigma_{vt} = \rho_{dry} a_l dl \tag{4.2}$$

$$= \rho_{dry} l\omega^2 dl \tag{4.3}$$

where σ_{vt} is the total vertical stress on the sample, ρ_{dry} is the bulk density of dry, loosely packed sand, l is the distance of the infinitesimal volume from the central axis of the centrifuge, dl is the length of the infinitesimal volume and a_l is the centrifugal acceleration on that volume at that distance. ω is the angular velocity of the centrifuge. The total stress on this volume is a result of the weight of the sample above it. If l_0 is the distance from the central axis of the centrifuge to the top of the sample, then, at l_0, σ_{vt}, in our case, is equal to the weight of the rock above it. At a position l, the total vertical stress can be obtained by integrating the above equation from the top of the sample (l_0 from the centre) to the position l,

$$\int_{W_{rock}}^{l} d\sigma_{vt} = \omega^2 \int_{l_0}^{l} l dl \tag{4.4}$$

$$\sigma_{vt}(l) = \rho_{dry}\omega^2 \left(\frac{l^2 - l_0^2}{2} \right) + W_{rock} \tag{4.5}$$

If the height of the sample is small (<20%) with respect to the radius of the centrifuge, then the radial stress distribution is approximately linearly proportional with distance from the centre (Lord, 1987; Taylor, 1994). For establishing constitutive relationships between vertical stress and voidage reduction, we approximate the total stress on the

entire sample to be equal to that at a distance 2/3 of the length of the sample from it's top. The arm length of the geotechnical centrifuge is 62 cm. Hinged at the end of each arm is a basket of length ≈60 cm where the cylindrical samples are housed. Therefore, the total length of a revolving arm together with the basket containing the sample is 122 cm. The height of the cylindrical sample including the core-holder containing the sand, rock and the end-caps on each end is ≈ 50 cm. The length of the sandpack, as mentioned earlier, is roughly 18.5 cm in each case. The distance from the centre of the centrifuge to the top of the sample is approximately 95 cm. Therefore, in our case, the ratio of the length of the sample to the distance from the centre of the centrifuge to the top of the sample is ≈ 0.2. In that case, the linear-model approximation leads to a maximum underestimation of the vertical stress in the sample of 9% (Lord, 1987).

The angular velocity of the centrifuge is set to 223 revolutions per minute, such that $50g$ is the gravitational force experienced at a location 30 cm from the bottom of the basket. This is approximately equal to the location where the Bentheimer sandstone sits on the sand. The weight of the rock is 393.2 g. At $50g$, this corresponds to a force of 192.9 N. Over a circular area with diameter 4.8 cm, the total stress as a result of this force is 1.07 bar. This is the vertical stress at the top of the sand column resulting from the weight of the rock above it. The dry density of each sand column, on average, is 1600 kg/m^3. Using **Eq. (4.2) and (4.4)**, the total vertical stress (σ_{vt}) at the bottom of the sandpack due to the weight of the sand above it, is 1.69 bar. Together with the weight of the bentheimer sandstone, this corresponds to a total vertical stress of 2.76 bar. **Table 4.4** lists the consolidation of the three different sand types at $50g$ quantified in terms of settlement and the subsequent reduction in porosity.

Table 4.4: Pre- and post-centrifuge porosities (ϕ_{pre} and ϕ_{post}, respectively), Van Baaren permeability corresponding to ϕ_{post} and approximate settlements of the three different sand types after a dry centrifuge run at $50g$.

Sand type	ϕ_{pre}	ϕ_{post}	k^{vb}_{post} [darcies]	Settlement [mm]
1	0.44	0.44	5.2	negligible
2	0.43	0.42	17.3	1.5
3	0.39	0.38	20.5	2

A 2.3 % and 2.6% reduction in porosity was observed for sands 2 and 3, respectively. The settlement for the finest sand was negligible and no reduction in porosity was observed after a dry centrifuge run. The expected Van Baaren permeability (**Eq. (4.1)**) obtained using the post-centrifuge porosity is also listed in the fourth column of the table. Contrary to the constitutive relationship of Yang et al. (2018), a small amount of compaction is observed under an applied vertical stress of approximately 4 bar.

As mentioned earlier, for the second set of centrifuge runs, the sand pack is initially saturated with water. When the sand column is being drained of this resident water, an additional suction force is exerted on the sand grains, equivalent to the capillary

pressure at irreducible water saturation. Layered samples using two different sand types were also prepared using this approach. The different sand layers, while packing, were separated using a water-soluble membrane in order to avoid mixing of the grains. The two layers were roughly the same height. During the permeability measurement, the membrane separating the layers was dissolved and a sharp transition between the two grain sizes was obtained. **Table 4.5** lists the pre- and post-centrifuge permeabilities of two homogeneous samples created using sand types 2 and 3. The last two rows list the pre- and post-centrifuge permeabilities of the layered samples created using sands 1 and 2 in row three and sands 1 and 3 in row four.

Table 4.5: Pre- and post-centrifuge measured permeabilities (k_{pre} and k_{post}, respectively) of two different homogeneous sand columns and two different layered columns after a wet centrifuge run at $50g$.

Sand type	k_{pre} [darcies]	k_{post} [darcies]
2	18.3	11.8
3	33.5	29.2
1 and 2	9.5	5.8
1 and 3	13.8	8.9

Assuming the permeability of the fine sand to be 5 darcies, harmonic averaging can be applied to compute the individual permeability of the coarser sand sections in the two layered packs. Using that, one can compute the average permeability contrast in these layered cores. For the layered sample containing sands 1 and 2, the permeability contrast is approximately 2:1. For the second layered sample comprising sands 2 and 3, the permeability contrast is roughly 6:1 between the high- and low-permeability zones. Clearly, draining the sample under centrifugal force results in greater compaction and consolidation. This is expected to minimize the chances of fines migration. Centrifuge-consolidation of loosely packed sandpacks also helps overcome the inhomogeneities that may result from manual preparation of the columns allowing a more-efficient packing of the grains under added vertical stress. In order to confirm this, foam-generation experiments, similar to the ones discussed in Section 4.2, were conducted using the two layered samples mentioned above.

Fig. 4.9 shows the average liquid saturation through the course of a foam-generation experiment conducted using the layered sample prepared using sands 1 and 2. The estimated permeability contrast in this sample is 2:1. Pressure was not monitored across individual sections of the core through this experiment. Instead, the objective was to observe the phase saturations through CT imaging and identify any preferential flow-paths for the gas phase as observed with sintered glass. As seen in the figure, some artefacts that might have arised while pouring the sand are visible in the form of blue streaks to the left and right of the images. The top-most image shows the saturation profile in a central vertical slice through the core, when the flow has reached steady-state to gas-brine co-injection. There appears to be a packing artefact near the top-left

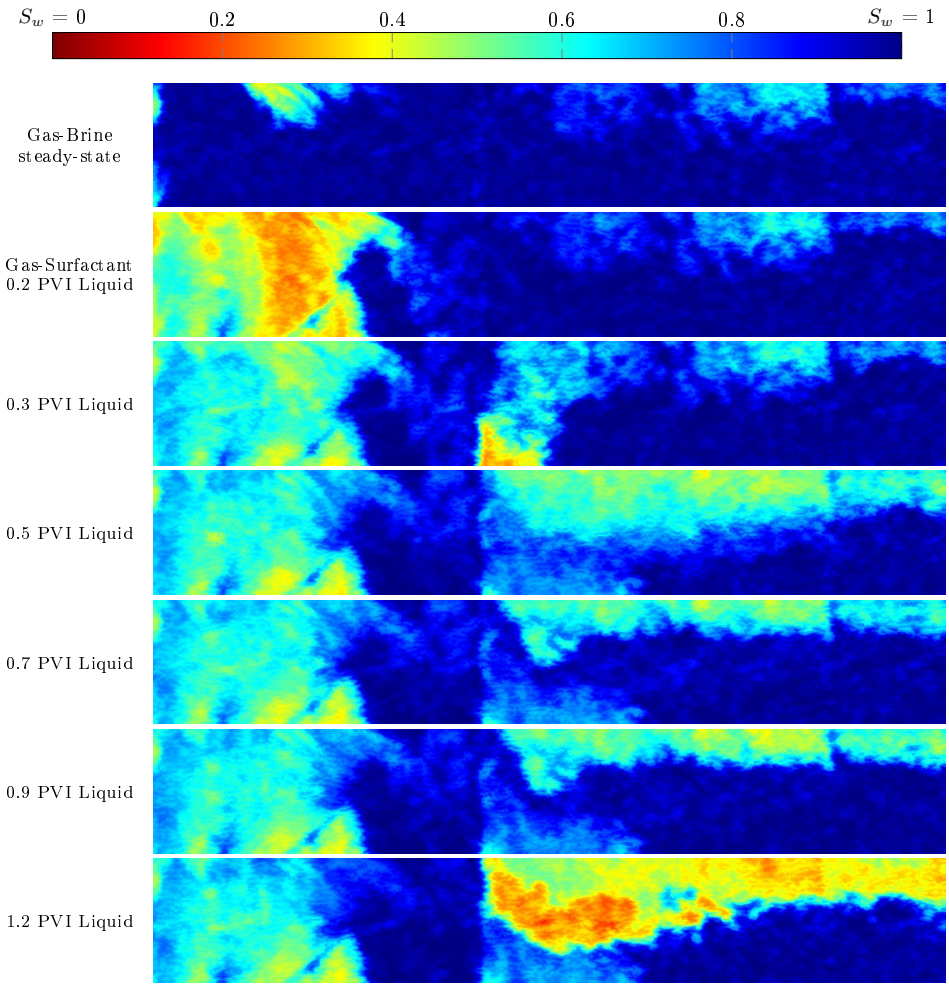

Figure 4.9: Average liquid saturation in a vertical cross-section through the center of the sandpacke obtained using X-ray CT imaging for the foam-generation experiment conducted at u_t = 0.5 ft/d and f_g=80%. The image at the top represents a measurement during steady-state gas-brine co-injection and the images thereafter were taken after surfactant had been injected into the core. Blue represents a high liquid saturation whereas red represents a high gas saturation, as indicated by the colorbar at the top. The voxel resolution is 1.5 × 1.5 × 1.5 mm^3.

corner of the image, showing a higher gas saturation than the rest of the core. Other than that, no signs for preferential flow of gas are visible. The permeability contrast is sharp as can be seen through the images. Strong foam was not generated in this experiment. This could be because the velocity or permeability contrast, or both, were too low. In the last image, a build up in gas saturation is observed indicating foam generation at the permeability contrast. However, due to gravity and most likely the weak strength of the foam, most of the gas tends to segregate to the top of the core.

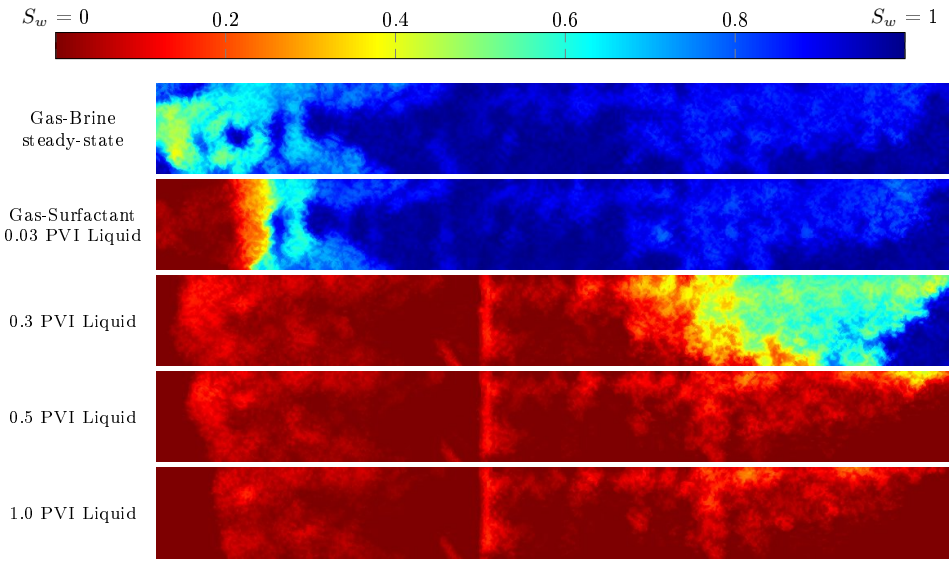

Figure 4.10: Average liquid saturation in a vertical cross-section through the center of the core obtained using X-ray CT imaging for the foam-generation experiment conducted at u_t = 1 ft/d and f_g=80%. The image at the top represents a measurement during steady-state gas-brine co-injection and the images thereafter were taken after surfactant had been injected into the core. Blue represents a high liquid saturation whereas red represents a high gas saturation, as indicated by the colorbar at the top. The voxel resolution is 1.5 × 1.5 × 1.5 mm^3.

Fig. 4.10 shows the liquid-saturation profile through in a vertical cross-section through the centre of the sandpack created using sands 1 and 3. The expected permeability contrast in this case is 6:1. A total injection velocity of 1 ft/d was employed. In this case, foam generation was observed from the inlet itself. A sharp permeability contrast can be seen in the final three images. The second image from the top shows a uniform foam front propagating through the core, without evidence of independent foam generation at the permeability boundary. There are no clear preferential pathways for gas visible in the CT images.

4.6. CONCLUSIONS

In this chapter, three different synthetic porous media were investigated for lateral and longitudinal homogeneity, to be used in coreflooding experiments. The commercially acquired sintered-glass samples were homogeneous in the longitudinal direction but lacked lateral homogeneity. If the sample size is small, cylindrical cores can be extracted out of a larger block. For our application, we required samples longer than 40 cm in length. Making a big block of sintered glass from which such a sample can be cored out is extremely difficult. The process of coring itself induces stress within the porous structure and it might not be possible to core out long samples without cracking them. As a result, cores had to be prepared by sintering glass grains packed into a cylindrical

glass tube. The glass grains did not sinter well with the glass tube and, as a result, the porosity of the sample was lower at the centre compared to the edges. During foam-generation experiments, preferential gas flow near the edges of the core was observed.

Sintering of clay-rich grain aggregates using two different grain-aggregate compositions did not yield promising results for creating long homogeneous cylindrical cores. Longer porous blocks cracked during coring. The longest sample that could be obtained was a ≈13-cm-long, 3-cm-diameter core. The grain-aggregates considered in this study were also extremely sensitive to the thermal treatment. Fractures due to differential cooling were observed towards the top of the cored sample whereas vitrified, impermeable sections were extracted from the bottom part. This may be due to differences in temperature at the bottom of the oven compared to the center.

Centrifuge-consolidated sandpacks were prepared. Both homogeneous and layered samples were prepared and a sharp change in permeability was achieved in the layered sample using a water-soluble membrane. The sandpacks were consolidated in the centrifuge in order to achieve a more efficient packing with reduced chance of fines migration. Two layered sandpacks were used for foam-generation experiments. During the course of these experiments, no sand grains were observed in any of the tubing connected to the core. There were no indications of sand migration in the CT images. Moreover, the samples were laterally more homogeneous than the sintered glass samples, as no preferential pathways for gas were observed near the edge of the core. Consolidation was quantified in terms of reduction in porosity and permeability. A greater reduction in permeability was achieved when a water-saturated sample was centrifuged while water was allowed to drain out of the sample. While centrifuging the sample does result in a more efficient packing, the characteristics of the sandpack are sensitive to how the loosely packed sand column is created. Sand must be poured carefully, through a funnel and all at once in order to maintain longitudinal homogeneity. If a vibrating table is not available, the sand can be compacted by gentle tapping along the walls of the cylinder.

For smaller samples, we recommend using sintered glass or sintered clay-rich grain-aggregates because homogeneous sections can be cored out of a larger porous block. Sintered glass is commercially available and has been used before in coreflooding experiments. For longer samples, we recommend using sandpacks. Consolidating the sandpack using a centrifuge helps significantly reduce the chances of fines migration. Only if the sandpack is to be used at low-pressure, with mild and gradual changes in pressure over time, a loosely-packed sand column can be used.

5

CONCLUSION

In this chapter, the conclusions are summarized from the experimental work presented in this thesis.

5.1. GENERAL IMPLICATIONS FOR FOAM IN POROUS MEDIA

Through the experimental results presented in this work, we can conclude that foam can be generated in simultaneous flow of gas and surfactant solution across an abrupt increase in permeability. The tests were conducted at field-like superficial velocities. In most cases (lower permeability contrasts, see Section 2.4 and 3.4), foam generation was observed as soon as the surfactant solution reached the permeability boundary. Snap-off is already occurring at the transition in gas-brine flow. Once surfactant is available, the same process results in the formation of stable bubbles that cause mobility reduction in the high-permeability zone. This mechanism of foam generation is intermittent and it is best shown by sporadic, and often large (**Figs. 2.12, 2.15, 3.3b and 3.5b**), fluctuations in the pressure gradient measured at and downstream of the boundary. The intermittency of this process was also observed and explained earlier by Falls et al. (1988).

In Chapter 1, the effect of permeability contrast on this process is investigated. We conducted experiments using four different cores with four different permeability contrasts (**Table 2.1**) across which gas and surfactant solution flowed. We found that foam was generated in all the cases with a total superficial velocity of 0.67 ft/d and an injected gas fraction of 80%. The pressure drop across the low-permeability section is low enough (**Fig. 2.6a**) to conclude that the injected gas fraction is indeed the fraction flowing across the permeability contrast and that no *strong* foam is generated in the low-permeability section prior to snap-off at the boundary. The saturation maps constructed using CT imaging provide a confirmation of the same. Snap-off at the permeability jump results in foam generation in the high-permeability section, causing a reduction in gas mobility. The reduction is larger across greater permeability contrasts. In other words, stronger foam is generated in flow across greater permeability contrasts. However, we

observe that for a significant reduction in gas mobility to register in terms of pressure gradient, it takes longer, both in terms of time and liquid PVI, as the permeability contrast increases.

In Chapter 2, we considered four different injection rates to test the impact of velocity on this process. The injected gas fraction was 80% and the core with the lowest permeability contrast (≈ 4:1) was used. Foam generation was observed at all four velocities, after roughly the same amount of surfactant solution had been injected into the core. The foam propagated from the permeability contrast to the outlet of the core at all but the lowest total superficial velocity (0.17 ft/d) tested. At the lowest velocity, the foam strength decreased as it propagated through the high-permeability zone. In the outlet tubing, in contrast to other experiments, only brief periods of foam production, followed by surfactant solution and gas, were observed. Moreover, the intermittency of this process, in terms of the magnitude and frequency of fluctuation in pressure gradient, was greater at lower velocities (**Fig. 3.8**). Clearly, the experiment conducted at the lowest velocity (**Fig. 3.3b**) showed the largest and most distinct fluctuations in pressure gradient.

In the same chapter, the effect of fractional flow on snap-off across a boundary was tested. Once again, foam generation was observed at all the gas fractions tested (f_g=60%, 80%, 95%). The total injection rate (q_t) was fixed at 0.1 ml/min (u_t = 0.67 ft/d) and the core with a permeability contrast of approximately 4:1 was used. At f_g < 60%, foam generation was observed in the low-permeability section itself. Those experiments can be found in the MSc Thesis of As Syukri (2018). The pressure and saturation response (high S_g in CT images) corresponding to strong-foam generation was observed after roughly the same amount of surfactant solution had been injected in the core. However, it was observed that foam generated at f_g=60% took longer (in terms of liquid PVI) to propagate through the high-permeability zone compared to higher gas fractions. An increase in the intermittency of foam generation was observed at higher gas fractions (**Fig. 3.9**). Additionally, no significant difference in foam strength was observed at the three gas fractions tested. At a permeability contrast close to 4:1, foam generation was observed at gas fractions higher than those predicted to be the upper limit theoretically (Rossen, 1999). A reason for this discrepancy could be the differences in the relative-permeability function for two-phase flow in the glass core compared to the relative-permeability function in the theoretical work.

Local phase saturations obtained through CT imaging show an accumulation of the liquid phase at the edge of the low-permeability zone in the core. As a result, the approximate capillary pressure, corresponding to that saturation is below the estimated critical capillary pressure for snap-off during steady-state gas-brine flow. Once surfactant reaches this transition region, foam generation is triggered.

5.2. IMPLICATIONS FOR THE FIELD

The results of this study show that deep in the reservoir, where the viscous driving force is low, foam generation can be supported by snap-off in flow across abrupt permeability

changes. To the best of our knowledge, it might be the only mechanism that can cause a significant reduction in gas mobility in low-velocity flows. Gas mobility will be reduced in the high-permeability layers. While in most of our experiments the foam propagated from the permeability transition to the outlet of the core, in the field, this may not always be the case. If the foam cannot propagate, it will block the path to high-permeability layers resulting in an improved sweep in the low-permeability layers. In a layered system, this would result in a reduction in the vertical mobility of gas and reduce the extent of gravity segregation. On a reservoir-scale, better sweep efficiency can be expected if the geological setting allows for sharp heterogeneities. This mechanism can have important consequences for foam EOR and aquifer remediation applications, and it must be taken into account to allow for an improvement in overall sweep efficiency. One can also use the results of this study to design injection strategies for horizontal wells. At the toe of a horizontal well, the drawdown can be quite low and strong foam may not be generated in the near-well region. Special screens with a permeability contrast can be used to generate foam.

It is important to note that surfactant adsorption is negligible in our synthetic porous media made from borosilicate glass. Therefore, in our experiments, foam generation appears to be almost immediate once the surfactant arrives at the permeability transition, irrespective of f_g or u_t. In the field, adsorption must first be satisfied before foam generation commences. Adsorption can delay the propagation of surfactant and foam generation at a sharp heterogeneity.

While designing the experiments reported in this thesis, the objective was to create conditions for a uniform, one-dimensional forced displacement across the permeability jump. However, as mentioned in the previous chapters, the sintered-glass porous medium was not perfectly homogeneous in the single-permeability regions and the unwanted artefact of imperfect sintering and higher porosity along the edges lead to preferential flow of gas near the walls of the core. While this may have resulted in unwanted experimental observations, complicating subsequent analysis, the aggravated effect of gravity (due to a low flow rate and high permeability), combined with this edge effect, brought the experimental conditions closer to realistic geological settings. In a realistic subsurface setting, gas may have other flow-paths available and may bypass the permeability boundary altogether, not contributing to the process of foam generation. In the experiments presented in this paper, regardless of the availability of a preferential flow-path for gas, foam generation was observed across the permeability jump. The experiments were designed so that foam was generated by snap-off and not due to drainage or a high pressure gradient. While Li and Rossen (2005) suggested that preferential flow along the edges of a core would make foam generation in such an experiment more difficult, this was not observed and snap-off still occurred at the permeability boundary at contrasts as low as 3.8:1 with a field-like total superficial velocity of 0.67 ft/d.

5.3. FUTURE PERSPECTIVES

In this study, extensive experimental evidence for snap-off in flow across sharp permeability changes is provided through one-dimensional corefloods. In the field, sharp heterogeneities can exist in all directions, with different orientations. Gas can flow through high-permeability zones, bypassing the heterogeneities altogether. Conducting two- or three-dimensional tests with sand tanks could provide further insight about the relevance of this mechanism in the field. A simulation study with an ensemble of fine-scale models that include sharp heterogeneities together with high-mobility zones allowing gas breakthrough could help identify conditions under which gas and liquid can flow through a permeability boundary, causing snap-off.

For the results of this thesis to be represented in foam models, the relationship between capillary contrast, foam texture and gas mobility must be established. The model of Falls et al. (1988) can be used for this purpose. Over the past three decades, several developments have taken place in the area of population-balance modelling of foam. Models have been developed to represent the various aspects of foam physics observed in the lab. To complete our understanding of foam generation across heterogeneities and its subsequent mobilisation at low velocities, the model of Falls et al. (1988) must be augmented with representations for foam coalescence and coarsening and its shear-thinning behaviour. Finally, an upscaled representation of this mechanism for field-scale simulations must be developed in order to account for the benefits of sharp heterogeneities in a foam-based displacement process.

In this study, we have not considered the effect of oil on foam generation. In the field, one can expect residual oil to be present when the implementation of foam EOR is being considered. Moreover, in settings where crossbedding and internal laminations exist, oil might be trapped at the high- to low-permeability interfaces. Conducting a similar set of experiments with the oil phase present could provide valuable insights, purely from a flow point of view, about the relevance of this mechanism in the field. The destabilisation of foam by oil is a separate issue. Additionally, capillary contrast can exist in the form of changes in wettability. Changes in wettability could also cause foam generation but this is yet to be shown experimentally.

In real reservoirs, sharp changes in permeability can also occur in the form of fractures. Fractures are microscopic “highways" for fluids flowing inside a rock. The interface between the matrix and the fracture also provides a nearly infinite permeability contrast. However, when fractures are present in a reservoir, the high-mobility fluid (i.e. gas) usually tends to flow largely through the fracture. There is, however, some exchange of fluids between the matrix and a fracture. In the present of surfactant solution in or around the fracture, this could cause foam generation in the fracture, if gas flows out of the matrix. Once foam is generated in the fracture, a further exchange of fluids between the matrix and the blocked fracture will be promoted. We recommend a study that would investigate the relevance of this mechanism in fractured reservoirs and examine the sweep-improvement in an analogous system.

Any change from a well-established technology to a new one is expensive. This is particularly true for the extraction of crude oil, since changes in the production facilities

and well components can cost tens of millions of dollars, if not more. Often times, research in novel technologies is discontinued due to unexpected fluctuations in oil price. The same can be said for foam EOR. While several questions concerning the behaviour of foam in porous media still remain, laboratory experiments over the years have demonstrated the benefits of using foam as a displacement agent. The results of this thesis add to those benefits. The author would like to urge companies that sponsor foam research to eventually carry out field pilots. Data from pilot tests can provide valuable information. Coupled with a detailed understanding of the field, and the existing expertise in foam, it can provide tremendous insight into the applicability of foam for EOR and aquifer remediation processes.

BIBLIOGRAPHY

Almajid, M. M. and Kovscek, A. R. 2016. Pore-level Mechanics of Foam Generation and Coalescence in the Presence of Oil. *Advances in Colloid and Interface Science* **233**: 65–82, doi: 10.1016/j.cis.2015.10.008.

Almajid, M. M. and Kovscek, A. R. 2019. Pore Network Investigation of Trapped Gas and Foam Generation Mechanisms. *Transp. in Porous Media* doi: 10.1007/s11242-018-01224-4.

Alvarez, J. M., Rivas, H. J., and Rossen, W. R. 2001. Unified Model for Steady-State Foam Behavior at High and Low Foam Qualities. *SPE J.* **6** (3): 3–6, doi: 10.2118/74141-PA. SPE-74141-PA.

Apaydin, O. G. and Kovscek, A. R. 2001. Surfactant Concentration and End Effects on Foam Flow in Porous Media. *Transp. Porous Media* **43** (3): 511–536, doi: 10.1023/A:1010740811277.

Armstrong, R. T., Georgiadis, A., Ott, H., Klemin, D. et al. 2014. Critical Capillary Number: Desaturation Studied with Fast X-ray Computed Microtomography. *Geophys. Res. Lett.* **41** (1): 55–60, doi: 10.1002/2013GL058075.

Armstrong, R. T., McClure, J. E., Berrill, M. A., Rücker, M. et al. 2016. Beyond Darcy's Law: The Role of Phase Topology and Ganglion Dynamics for Two-Fluid Flow. *Phys. Rev. E* **94** (043113), doi: 10.1103/PhysRevE.94.043113.

As Syukri, H. 2018. *Experimental Study: Foam Generation and Propagation in Flow Across a Permeability Contrast*, Master's thesis, Delft University of Technology, Delft, The Netherlands. uuid:961bf2b5-28d5-41e4-9283-a20e1c5d672b.

Ashoori, E., Marchesin, D., and Rossen, W. R. 2011. Roles of Transient and Local Equilibrium Foam Behavior in Porous Media: Traveling Wave. *Colloids Surfaces A Physicochem. Eng. Asp.* **377** (1-3): 228–242, doi: 10.1016/j.colsurfa.2010.12.042.

Ashoori, E., Marchesin, D., and Rossen, W. R. 2012a. Multiple Foam States and Long-Distance Foam Propagation in Porous Media. *SPE J.* **17** (04): 1231–1245, doi: 10.2118/154024-PA. SPE-154024-PA.

Ashoori, E., Marchesin, D., and Rossen, W. R. 2012b. Stability Analysis of Uniform Equilibrium Foam States for EOR Processes. *Transp. Porous Media* **92** (3): 573–595, doi: 10.1007/s11242-011-9921-8.

Ashoori, E. and Rossen, W. R. 2012. Can Formation Relative Permeabilities Rule Out a Foam EOR Process? *SPE J.* **17** (02): 19–22, doi: 10.2118/134906-PA. SPE-134906-PA.

Askarinejad, A., Beck, A., and Springman, S. M. 2015. Scaling Law of Static Liquefaction Mechanism in Geocentrifuge and Corresponding Hydromechanical Characterization of an Unsaturated Silty Sand Having a Viscous Pore Fluid. *Canadian Geotechnical Journal* **52** (6): 708–720, doi: 10.1139/cgj-2014-0237.

ASTM International. 2000. ASTM D4253-00 Standard Test Methods for Maximum Index Density and Unit Weight of Soils Using a Vibratory Table, doi: 10.1520/D4253-00.

Baghdikian, S. Y. and Handy, L. L. 1991. Transient Behavior of Simultaneous Flow of Gas and Surfactant Solution in Consolidated Porous Media, Tech. rep., University of Southern California, doi: 10.2172/5434448.

Berg, S., Armstrong, R., Ott, H., Georgiadis, A. et al. 2014. Multiphase Flow in Porous Rock Imaged Under Dynamic Flow Conditions with Fast X-Ray Computed Microtomography. *Petrophysics* **55** (04): 304–312.

Berg, S., Rücker, M., Ott, H., Georgiadis, A. et al. 2016. Connected Pathway Relative Permeability from Pore-scale Imaging of Imbibition. *Adv. Water Resour.* **90**: 24–35, doi: 10.1016/j.advwatres.2016.01.010.

Bernard, G. and Holm, L. 1964. Effect of Foam on Permeability of Porous Media to Gas. *SPE J.* **4** (3): 267–274, doi: 10.2118/983-PA. SPE-983-PA.

Bertin, H. J., Apaydin, O. G., Castanier, L. M., and Kovscek, A. R. 1999. Foam Flow in Heterogeneous Porous Media: Effect of Crossflow. *SPE J.* **4** (02): 75–82, doi: 10.2118/56009-PA. SPE-56009-PA.

Bharat, T. V. and Ubaid, M. 2019. Analytical Model for Consolidation Settlements Under Centrifuge Environment. *Canadian Geotechnical Journal* **56** (4): 484–494, doi: 10.1139/cgj-2017-0591.

Bird, R. B., Stewart, W. E., and Lightfoot, E. N. 2007. *Transport Phenomena*, John Wiley & Sons.

Blake, F. 1922. The Resistance of Packing to Fluid Flow. *Trans. Am. Inst. Chem. Eng.* **14**: 415–421.

Boeije, C. S. and Rossen, W. R. 2015. Fitting Foam-Simulation-Model Parameters to Data: I. Coinjection of Gas and Liquid. *SPE Reserv. Eval. & Eng.* **18** (02): 264–272, doi: 10.2118/174544-PA. SPE-174544-PA.

Boncelet, C. 2009. Image Noise Models, in *The Essential Guide to Image Processing*, ed. A. Bovik, chap. 7, 143–167, Boston: Academic Press, doi: 10.1016/B978-0-12-374457-9.00007-X.

British Petroleum 2019. BP Statistical Review of World Energy, Tech. rep., British Petroleum.

Buckley, S. and Leverett, M. 1942. Mechanism of Fluid Displacement in Sands. *Trans. AIME* **146** (1337): 107–116, doi: 10.2118/942107-G.

Cargill, K. and Ko, H.-Y. 1983. Centrifugal Modeling of Transient Water Flow. *Journal of Geotechnical Engineering* **109** (04): 536–555, doi: 10.1061/(ASCE)0733-9410(1983)109:4(536).

Carman, P. C. 1938. Determination of the Specific Surface of Powders I. *Transactions J. Soc. Chemical Industries* **57**: 225–234.

Carman, P. C. 1956. *Flow of Gases Through Porous Media*, New York City: Academic Press Inc.

Castanier, L. and Brigham, W. 1991. An Evaluation of Field Projects of Steam With Additives (includes associated papers 23547 and 23587). *SPE Reserv. Eng.* **6** (01): 62–68, doi: 10.2118/17633-PA. SPE-17633-PA.

Chad, J., Malsalla, P., and Novosad, J. 1988. Foam Forming Surfactants In Pembina/Ostracod 'G' Pool, Petroleum Society of Canada, doi: 10.2118/88-39-40.

Chambers, D. J. 1994. Foams for Well Stimulation, in *Foams: Fundamentals and Applications in the Petroleum Industry*, ed. L. L. Schramm, vol. 242 of *Advances in Chemistry*, chap. 9, 355–404, Washington, DC: American Chemical Society, doi: 10.1021/ba-1994-0242.ch009.

Chambers, K. T. and Radke, C. J. 1990. Capillary Phenomena in Foam Flow through Porous Media, in *Interfacial Phenomena in Oil Recovery.*, ed. N. Morrow, vol. 36 of *Surfactant Science Series*, chap. 6, New York: Marcel Dekker, Inc.

Chang, J. and Yortsos, Y. C. 1992. Effect of Capillary Heterogeneity on Buckley-Leverett Displacement. *SPE Reserv. Eng.* **7** (02): 285–293, doi: 10.2118/18798-PA. SPE-18798-PA.

Charlaix, E., Hulin, J. P., and Plona, T. J. 1987. Experimental Study of Tracer Dispersion in Sintered Glass Porous Materials of Variable Compaction. *The Physics of Fluids* **30** (06): 1690–1698, doi: 10.1063/1.866234.

Chen, M., Rossen, W. R., and Yortsos, Y. C. 2005a. The Flow and Displacement in Porous Media of Fluids with Yield Stress. *Chemical Engineering Science* **60** (15): 4183–4202, doi: 10.1016/j.ces.2005.02.054.

Chen, M., Yortsos, Y., and Rossen, W. R. 2005b. Insights on Foam Generation in Porous Media from Pore-network Studies. *Colloids Surfaces A Physicochem. Eng. Asp.* **256** (2-3): 181–189, doi: 10.1016/j.colsurfa.2005.01.020.

Chen, Q., Gerritsen, M., and Kovscek, A. R. 2010. Modeling Foam Displacement With the Local-Equilibrium Approximation: Theory and Experimental Verification. *SPE J.* **15** (01): 171–183, doi: 10.2118/116735-PA. SPE-116735-PA.

Chen, X., Kianinejad, A., and DiCarlo, D. A. 2016. An Extended JBN Method of Determining Unsteady-State Two-Phase Relative Permeability. *Water Resour. Res.* **52** (10): 8374–8383, doi: 10.1002/2016WR019204.

Cheng, L., Reme, A. B., Shan, D., Coombe, D. A. et al. 2000. Simulating Foam Processes at High and Low Foam Qualities, in *Proc.*, SPE/DOE Improved Oil Recovery Symposium, Tulsa, Oklahoma, 3-5 April, 1–15, doi: 10.2118/59287-ms. SPE-59287-MS.

Chou, S. I. 1990. Percolation Theory of Foam in Porous Media, in *Proc.*, SPE/DOE Enhanced Oil Recovery Symposium, Tulsa, Oklahoma, 22-25 April, 627–642, doi: 10.2118/20239-MS. SPE-20239-MS.

Clark, J. A. and Santiso, E. E. 2018. Carbon Sequestration through CO_2 Foam-Enhanced Oil Recovery: A Green Chemistry Perspective. *Engineering* **4** (03): 336–342, doi: 10.1016/j.eng.2018.05.006.

Cui, L., Ma, K., Puerto, M., Abdala, A. A. et al. 2016. Mobility of Ethomeen C_{12} and Carbon Dioxide (CO_2) Foam at High Temperature/High Salinity and in Carbonate Cores. *SPE J.* **21** (04): 1151–1163, doi: 10.2118/179726-PA. SPE-179726-PA.

Dake, L. P. 1994. *The Practice of Reservoir Engineering*, vol. 36 of *Developments in Petroleum Science*, Amsterdam: Elsevier.

Datta, S. S., Chiang, H., Ramakrishnan, T. S., and Weitz, D. A. 2013. Spatial Fluctuations of Fluid Velocities in Flow Through a Three-dimensional Porous Medium. *Phys. Rev. Lett.* **111** (06), doi: 10.1103/PhysRevLett.111.064501.

Datta, S. S., Ramakrishnan, T. S., and Weitz, D. A. 2014. Mobilization of a Trapped Non-wetting Fluid from a Three-Dimensional Porous Medium. *Physics of Fluids* **26** (02): 022002, doi: 10.1063/1.4866641.

Datta, S. S. and Weitz, D. A. 2013. Drainage in a Model Stratified Porous Medium. *EPL (Europhysics Letters)* **101** (01): 14002, doi: 10.1209/0295-5075/101/14002.

Ettinger, R. A. and Radke, C. J. 1992. Influence of Texture on Steady Foam Flow in Berea Sandstone. *SPE Reserv. Eng.* **7** (01): 83–90, doi: 10.2118/19688-PA. SPE-19688-PA.

Falls, A. H., Hirasaki, G. J., Patzek, T. W., Gauglitz, D. A. et al. 1988. Development of a Mechanistic Foam Simulator: The Population Balance and Generation by Snap-Off. *SPE Reserv. Eng.* **3** (03): 884–892, doi: 10.2118/14961-PA. SPE-14961-PA.

Farajzadeh, R., Krastev, R., and Zitha, P. 2008. Foam Films Stabilized with Alpha-olefin Sulfonate (AOS). *Colloids Surfaces A Physicochem. Eng. Asp.* **324** (1-3): 35–40, doi: 10.1016/J.COLSURFA.2008.03.024.

Fergui, O., Bertin, H., and Quintard, M. 1998. Transient Aqueous Foam Flow in Porous Media: Experiments and Modeling. *Journal of Petroleum Science and Engineering* **20** (01): 9–29, doi: 10.1016/S0920-4105(98)00036-9.

Fisher, A. W., Foulser, R. W. S., and Goodyear, S. G. 1990. Mathematical Modeling of Foam Flooding, in *Proc.*, SPE/DOE Enhanced Oil Recovery Symposium, Tulsa, Oklahoma, 22-25 April, Society of Petroleum Engineers, doi: 10.2118/20195-MS. SPE-20195-MS.

Fox, P. J., Lee, J., and Qiu, T. 2005. Model for Large Strain Consolidation by Centrifuge. *International Journal of Geomechanics* **5** (4): 267–275, doi: 10.1061/(ASCE)1532-3641(2005)5:4(267).

Friedmann, F., Chen, W., and Gauglitz, P. 1991. Experimental and Simulation Study of High-Temperature Foam Displacement in Porous Media. *SPE Reserv. Eng.* **6** (01): 37–45, doi: 10.2118/17357-PA. SPE-17357-PA.

Friedmann, F., Jensen, J., and F. Friedmann and Jensen, J. A. 1986. Some Parameters Influencing the Formation and Propagation of Foams in Porous Media, Presented at the SPE California Regional Meeting, Oakland, California, 2-4 April, doi: 10.2118/15087-MS. SPE-15087-MS.

Friedmann, F., Smith, M., Guice, W., Gump, J. et al. 1994. Steam-Foam Mechanistic Field Trial in the Midway-Sunset Field. *SPE Reserv. Eng.* **9** (04): 297–304, doi: 10.2118/21780-PA. SPE-21780-PA.

Gauglitz, P. A., Friedmann, F., Kam, S. I., and Rossen, W. R. 2002. Foam Generation in Homogeneous Porous Media. *Chem. Eng. Sci.* **57** (19): 4037–4052, doi: 10.1016/S0009-2509(02)00340-8.

Gupta, D. V. S. 2009. Unconventional Fracturing Fluids for Tight Gas Reservoirs, Presented at the SPE Hydraulic Fracturing Technology Conference, The Woodlands, Texas, 19-21 January, doi: 10.2118/119424-MS. SPE-119424-MS.

Hartkamp-Bakker, C. 1993. *Permeability Heterogeneity in Cross-bedded Sandstones: Impact on Water/Oil Displacement in Fluvial Reservoirs*, Ph.D. thesis, Delft University of Technology, Delft, The Netherlands. uuid:be8ffa8f-5b66-4c46-932b-56d3eab5823e.

Hirasaki, G. J. 1989. The Steam-Foam Process. *Journal of Petroleum Technology* **41** (05): 449–456. SPE-19505-PA.

Hirasaki, G. J., Jackson, R. E., Jin, M., Lawson, J. B. et al. 2000. Description of Surfactant/Foam Process and Surfactant-Enhanced Aquifer Remediation, in *NAPL Removal: Surfactants, Foams, and Microemulsions*, eds. S. Fiorenza, C. Miller, C. Oubre, and C. Ward, AATDF Monograph Series, 7–10, Boca Raton: CRC Press, doi: 10.1201/9781420026207.pt1.

Hirasaki, G. J., Miller, C. A., and Pope, G. A. 2005. Surfactant Based Enhanced Oil Recovery and Foam Mobility Control, Tech. rep., doi: 10.2172/860321.

Hirasaki, G. J., Miller, C. A., Szafranski, R., Lawson, J. B. et al. 1997a. Surfactant/Foam Process for Aquifer Remediation, in *Proc.*, International Symposium on Oilfield Chemistry, Houston, Texas, 18-21 February, 471–480, doi: 10.2118/37257-MS. SPE-37257-MS.

Hirasaki, G. J., Miller, C. A., Szafranski, R., Tanzil, D. et al. 1997b. Field Demonstration of the Surfactant / Foam Process for Aquifer Remediation, Presented at the SPE Annual Technical Conference and Exhibition, San Antonio, Texas, 5-8 October, doi: 10.2118/39292-MS. SPE-39292-MS.

Hoogewerf, G. 2019. *Performing a Core-flood Experiment on a Consolidated Sand Pack*, Bachelor's Thesis, Delft University of technology.

Hove, A. O., Ringen, J. K., and Read, P. A. 1987. Visualization of Laboratory Corefloods With the Aid of Computerized Tomography of X-Rays. *SPE Reserv. Eng.* **2** (02): 148–154, doi: 10.2118/13654-PA. SPE-13654-PA.

Huh, D. G. and Handy, L. L. 1989. Comparison of Steady and Unsteady-State Flow of Gas and Foaming Solution in Porous Media. *SPE Reserv. Eng.* **4** (01): 77–84, doi: 10.2118/15078-PA. SPE-15078-PA.

Isaacs, E. E., McCarthy, F. C., and Maunder, J. D. 1988. Investigation of Foam Stability in Porous Media at Elevated Temperatures. *SPE Reserv. Eng.* **3** (02): 565–572, doi: 10.2118/15647-PA. SPE-15647-PA.

Islam, M. R. and Ali, S. M. F. 1988. Numerical Simulation Of Foam Flow In Porous Media, in *Proc.*, Annual Technical Meeting, Calgary, Alberta, June 12 - 16, doi: 10.2118/88-39-04.

Jenkins, M. 1984. An Analytical Model for Water/Gas Miscible Displacements, in *Proc.*, SPE Enhanced Oil Recovery Symposium, Tulsa, Oklahoma, 15-18 April, doi: 10.2118/12632-MS. SPE-12632-MS.

Jessberger, H. L. and Stone, K. J. L. 1991. Subsidence Effects on Clay Barriers. *Géotechnique* **41** (02): 185–194, doi: 10.1680/geot.1991.41.2.185.

Jian, G., Zhang, L., Da, C., Puerto, M. et al. 2019. Evaluating the Transport Behavior of CO_2 Foam in the Presence of Crude Oil under High-Temperature and High-Salinity Conditions for Carbonate Reservoirs. *Energy Fuels* **33** (07): 6038–6047, doi: 10.1021/acs.energyfuels.9b00667.

Jiménez, A. I. and Radke, C. J. 1989. Dynamic Stability of Foam Lamellae Flowing Through a Periodically Constricted Pore, in *Oil-Field Chemistry*, vol. 396 of *ACS Symposium Series*, chap. 25, 460–479, American Chemical Society, doi: 10.1021/bk-1989-0396.ch025.

Kahrobaei, S., Vincent-Bonnieu, S., and Farajzadeh, R. 2017. Experimental Study of Hysteresis Behavior of Foam Generation in Porous Media. *Sci. Reports* **7** (01): 8986, doi: 10.1038/s41598-017-09589-0.

Kam, S. I. 2008. Improved Mechanistic Foam Simulation with Foam Catastrophe Theory. *Colloids Surfaces A Physicochem. Eng. Asp.* **318** (1-3): 62–77, doi: 10.1016/j.colsurfa.2007.12.017.

Kam, S. I., Nguyen, Q. P., Li, Q., and Rossen, W. R. 2007. Dynamic Simulations With an Improved Model for Foam Generation. *SPE J.* **12** (01): 35–48, doi: 10.2118/90938-PA. SPE-90938-PA.

Kam, S. I. and Rossen, W. R. 2003. A Model for Foam Generation in Homogeneous Media. *SPE J.* **8** (4): 417–425, doi: 10.2118/87334-PA.

Katz, A. J. and Thompson, A. H. 1986. Quantitative Prediction of Permeability in Porous Rock. *Phys. Rev. B* **34** (11): 8179–8181, doi: 10.1103/PhysRevB.34.8179.

Kharabaf, H. and Yortsos, Y. C. 1997. Invasion Percolation with Memory. *Phys. Rev. E* **55** (06): 7177–7191, doi: 10.1103/PhysRevE.55.7177.

Kharabaf, H. and Yortsos, Y. C. 1998. A Pore-Network Model For Foam Formation And Propagation in Porous Media. *SPE J.* **3** (01): 42–53, doi: 10.2118/36663-PA. SPE-36663-PA.

Kim, M. M. and Ko, H.-Y. 1982. Centrifugal Testing of Soil Slope Models. *Transportation Research Record* (872).

Kirkpatrick, S. 1973. Percolation and Conduction. *Rev. Mod. Phys.* **45** (04): 574–588, doi: 10.1103/RevModPhys.45.574.

Kovscek, A. R., Patzek, T. W., and Radke, C. J. 1994. Mechanistic Prediction of Foam Displacement in Multidimensions: A Population Balance Approach, in *Proc.*, SPE/DOE Improved Oil Recovery Symposium, Tulsa, Oklahoma, 17-20 April, Society of Petroleum Engineers, doi: 10.2118/27789-MS. SPE-27789-MS.

Kovscek, A. R., Patzek, T. W., and Radke, C. J. 1995. A Mechanistic Population Balance Model for Transient and Steady-state Foam Flow in Boise Sandstone. *Chem. Eng. Sci.* **50** (23): 3783–3799, doi: 10.1016/0009-2509(95)00199-F.

Kovscek, A. R., Patzek, T. W., and Radke, C. J. 1997. Mechanistic Foam Flow Simulation in Heterogeneous and Multidimensional Porous Media. *SPE J.* **2** (04): 511–526, doi: 10.2118/39102-PA. SPE-39102-PA.

Kovscek, A. R. and Radke, C. J. 1994. Fundamentals of Foam Transport in Porous Media, in *Foams: Fundamentals and Applications in the Petroleum Industry*, ed. L. Schramm, vol. 242 of *Advances in Chemistry*, chap. 3, 115–163, Washington, DC: American Chemical Society, doi: 10.1021/ba-1994-0242.ch003.

Kovscek, A. R. and Radke, C. J. 1996. Gas Bubble Snap-off Under Pressure-driven Flow in Constricted Noncircular Capillaries. *Colloids Surfaces A Physicochem. Eng. Asp.* **117** (1-2): 55–76, doi: 10.1016/0927-7757(96)03637-0.

Kovscek, A. R. and Radke, C. J. 2003. Pressure-driven capillary snap-off of gas bubbles at low wetting-liquid content. *Colloids Surfaces A Physicochem. Eng. Asp.* **212** (2-3): 99–108, doi: 10.1016/S0927-7757(02)00302-3.

Kovscek, A. R., Tang, G.-Q., and Radke, C. J. 2007. Verification of Roof Snap Off as a Foam-generation Mechanism in Porous Media at Steady State. *Colloids Surfaces A Physicochem. Eng. Asp.* **302** (1-3): 251–260, doi: 10.1016/j.colsurfa.2007.02.035.

Kozeny, J. 1927. Uber Kapillare Leitung der Wasser in Boden. *Royal Academy of Science, Vienna, Proc. Class I* **136**: 271–306.

Kuczynski, G. C. 1949. Study of the Sintering of Glass. *J. Appl. Phys.* **20** (12): 1160–1163, doi: 10.1063/1.1698291.

Kuczynski, G. C. 1972. Physics and Chemistry of Sintering. *Adv. Colloid Interface Sci.* **3** (03): 275–330, doi: 10.1016/0001-8686(72)85005-X.

Kular, G. S., Lowe, K., and Coombe, D. A. 1989. Foam Application in an Oil Sands Steamflood Process, in *Proc.*, SPE Annual Technical Conference and Exhibition, San Antonio, Texas, 8-11 October, doi: 10.2118/SPE-19690-MS. SPE-19690-MS.

Lake, L. W., Johns, R., Rossen, W. R., and Pope, G. 2014. *Fundamentals of Enhanced Oil Recovery*, Richardson, Texas: Society of Petroleum Engineers.

Law, D.-S., Yang, Z.-M., and Stone, T. 1992. Effect of the Presence of Oil on Foam Performance: A Field Simulation Study. *SPE Reserv. Eng.* **7** (02): 228–236, doi: 10.2118/18421-PA. SPE-18421-PA.

Leeftink, T. N., Latooij, C. A., and Rossen, W. R. 2015. Injectivity Errors in Simulation of Foam EOR. *Journal of Petroleum Science and Engineering* **126**: 26–34, doi: 10.1016/j.petrol.2014.11.026.

Lenormand, R., Zarcone, C., and Sarr, A. 1983. Mechanisms of the Displacement of One Fluid by Another in a Network of Capillary Ducts. *J. Fluid Mech.* **135**: 337–353, doi: 10.1017/S0022112083003110.

Leverett, M. 1941. Capillary Behavior in Porous Solids. *Trans. AIME* **142** (01): 152–169, doi: 10.2118/941152-G.

Li, Q. and Rossen, W. R. 2005. Injection Strategies for Foam Generation in Homogeneous and Layered Porous Media, Presented at the SPE Annual Technical Conference and Exhibition, Dallas, Texas, 9-12 October, doi: 10.2118/96116-MS. SPE-96116-MS.

van Lingen, P. P. 1998. *Quantification and Reduction of Capillary Entrapment in Cross-Laminated Oil Reservoirs*, Ph.D. thesis, Delft University of Technology, Delft, The Netherlands. uuid:d462298e-57d5-45b9-9e6e-07632ceb13fc.

van Lingen, P. P., Bruining, J., and van Kruijsdijk, C. P. J. W. 1996. Capillary Entrapment Caused by Small-scale Wettability Heterogeneities. *SPE Reserv. Eng.* **11** (02): 93–99, doi: 10.2118/30782-PA. SPE-30782-PA.

Lord, A. E. 1987. Geosynthetic/soil Studies Using a Geotechnical Centrifuge. *Geotextiles and Geomembranes* **6** (1–3): 133 – 156, doi: 10.1016/0266-1144(87)90062-8.

Lotfollahi, M., Farajzadeh, R., Delshad, M., Varavei, A. et al. 2016. Comparison of Implicit-Texture and Population-balance Foam Models. *J. Nat. Gas Sci. Eng.* **31**: 184–197, doi: 10.1016/j.jngse.2016.03.018.

Lyons, W. C., Guo, B., Graham, R. L., and Hawley, G. D. 2009. *Air and Gas Drilling Manual (Third Edition)*, Gulf Professional Publishing, doi: 10.1016/B978-0-12-370895-3.X0001-6.

Ma, K., Farajzadeh, R., Lopez-Salinas, J. L., Miller, C. A. et al. 2014. Non-uniqueness, Numerical Artifacts, and Parameter Sensitivity in Simulating Steady-State and Transient Foam Flow Through Porous Media. *Transp. Porous Media* **102** (03): 325–348, doi: 10.1007/s11242-014-0276-9.

Ma, K., Lopez-Salinas, J. L., Puerto, M. C., Miller, C. A. et al. 2013. Estimation of Parameters for the Simulation of Foam Flow through Porous Media. Part 1: The Dry-Out Effect. *Energy Fuels* **27** (5): 2363–2375, doi: 10.1021/ef302036s.

Mamun, C. K., Rong, J. G., Kam, S. I., Liljestrand, H. M. et al. 2002. Simulating Use of Foam in Aquifer Remediation. *Developments in Water Science* **47** (C): 867–874, doi: 10.1016/S0167-5648(02)80152-6.

Martin, J. H. 1993. A Review of Braided Fluvial Hydrocarbon Reservoirs: The Petroleum Engineer's Perspective. *Geol. Soc. London, Spec. Publ.* **75** (01): 333–367, doi: 10.1144/GSL.SP.1993.075.01.20.

Martinsen, H. A. and Vassenden, F. 1999. Foam Assisted Water Alternating Gas (FAWAG) Process on Snorre, in *IOR 1999-10th European Symposium on Improved Oil Recovery*, doi: 10.3997/2214-4609.201406335.

McCool, C. S., Parmeswar, R., and Willhite, G. P. 1983. Interpretation of Differential Pressure in Laboratory Surfactant/Polymer Displacements. *SPE J.* **23** (05): 791–803, doi: 10.2118/10713-PA. SPE-10713-PA.

Mees, F., Swennen, R., Geet, M. V., and Jacobs, P. 2003. Applications of X-ray Computed Tomography in the Geosciences. *Geol. Soc. Special Publication* **215**: 1–6, doi: 10.1144/GSL.SP.2003.215.01.01.

Muggeridge, A., Cockin, A., Webb, K., Frampton, H. et al. 2013. Recovery rates, Enhanced Oil Recovery and Technological limits. *Philos Trans A Math Phys Eng Sci.* **372** (2006): 20120320.

Myers, T. J. and Radke, C. J. 2000. Transient Foam Displacement in the Presence of Residual Oil: Experiment and Simulation Using a Population-Balance Model. *Ind. Eng. Chem. Res.* **39** (08): 2725–2741, doi: 10.1021/ie990909u.

Nabawy, B. S., Géraud, Y., Rochette, P., and Bur, N. 2009. Pore-throat Characterization in Highly Porous and Permeable Sandstones. *Am. Assoc. Pet. Geol. Bull.* **93** (06): 719–739, doi: 10.1306/03160908131.

Naderi Beni, A. and Varavei, A. and Farajzadeh, R. and Delshad, M. 2012. Modeling of Compositional Effects of Foam Assisted CO_2 Storage Processes, Presented at the AGU Fall Meeting, San Francisco, California, 3-7 December.

Namdar Zanganeh, M. 2011. *Simulation and Optimization of Foam EOR Processes*, Ph.D. thesis, Delft University of Technology. uuid:80b844d4-02ec-4c94-b132-e38c62e613e5.

Nelson, P. H. 1994. Permeability-porosity Relationships In Sedimentary Rocks. *Society of Petrophysicists and Well-Log Analysts* **35** (03): 38–62.

Ocampo, A., Restrepo, A., Lopera, S. H., and Mejia, J. M. 2018. Creation of Insitu EOR Foams by the Injection of Surfactant in Gas Dispersions - Lab Confirmation and Field Application, in *Proc.*, SPE Improved Oil Recovery Conference, Tulsa, Oklahoma,14-18 April, 8. SPE-190219-MS.

Orr, F. M., Heller, J. P., and Taber, J. J. 1982. Carbon Dioxide Flooding for Enhanced Oil Recovery: Promise and Problems. *Journal of the American Oil Chemists Society* **59** (10): 810A–817A, doi: 10.1007/BF02634446.

Osterloh, W. T. and Jante, J., M.J. 1992. Effects of Gas and Liquid Velocity on Steady-State Foam Flow at High Temperature, Presented at the SPE/DOE Enhanced Oil Recovery Symposium, Tulsa, Oklahoma, 22-24 April, doi: 10.2118/24179-MS. SPE-24179-MS.

Ott, H., de Kloe, K., van Bakel, M., Vos, F. et al. 2012. Core-flood Experiment for Transport of Reactive Fluids in Rocks. *Rev. Sci. Instrum.* **83** (08): 084501, doi: 10.1063/1.4746997.

Patzek, T. W. 1988. Description of Foam Flow in Porous Media by the Population Balance Method, in *Surfactant-Based Mobility Control*, ed. D. Smith, vol. 373 of *ACS Symposium Series*, chap. 16, 326–341, Washington, DC: American Chemical Society.

Patzek, T. W. 1996. Field Applications of Steam Foam for Mobility Improvement and Profile Control. *SPE Reserv. Eng.* **11** (02): 79–86, doi: 10.2118/29612-PA. SPE-29612-PA.

Patzek, T. W. and Koinis, M. T. 1990. Kern River Steam-Foam Pilots. *J. Pet. Technol.* **42** (04): 496–503, doi: 10.2118/17380-PA.

Patzek, T. W., Myhill, N. A., and Others 1989. Simulation of the Bishop Steam Foam Pilot, in *Proc.*, SPE California Regional Meeting, Bakersfield, California, 5-7 April, 5–7, doi: 10.2118/18786-MS. SPE-18786-MS.

Persoff, P., Radke, C. J., Pruess, K., Benson, S. M. et al. 1991. A Laboratory Investigation of Foam Flow in Sandstone at Elevated Pressure. *SPE Reserv. Eng.* **6** (03): 365–372, doi: 10.2118/18781-PA. SPE-18781-PA.

Rabinovich, E. M. 1985. Preparation of Glass by Sintering. *Journal of Materials Science* **20** (12): 4259–4297, doi: 10.1007/BF00559317.

Ransohoff, T. C. and Radke, C. J. 1988. Mechanisms of Foam Generation in Glass-Bead Packs. *SPE Reserv. Eng.* **3** (02): 573–585, doi: 10.2118/15441-PA. SPE-15441-PA.

Reineck, H. E. and Singh, J. B. 1980. *Depositional Sedimentary Environments*, Berlin, Heidelberg: Springer Berlin Heidelberg, doi: 10.1007/978-3-642-96291-2.

Rognmo, A. U., Al-Khayyat, N., Heldal, S., Vikingstad, I. et al. 2018. Performance of Silica Nanoparticles in CO_2-Foam for EOR and CCUS at Tough Reservoir Conditions, in *Proc.*, SPE Norway One Day Seminar, Bergen, Norway, 18 April, doi: 10.2118/191318-MS. SPE-191318-MS.

Roof, J. G. 1970. Snap-Off of Oil Droplets in Water-Wet Pores. *SPE J.* **10** (01): 85–90, doi: 10.2118/2504-PA. SPE-2504-PA.

Rossen, W. R. 1990a. Minimum Pressure Gradient for Foam Flow in Porous Media: Effect of Interactions with Stationary Lamellae. *J. Colloid Interface Sci.* **139** (02): 457–468, doi: 10.1016/0021-9797(90)90118-8.

Rossen, W. R. 1990b. Theory of Mobilization Pressure Gradient of Flowing Foams in Porous Media. I. Incompressible Foam. *J. Colloid Interface Sci.* **136** (01): 1–16, doi: 10.1016/0021-9797(90)90075-Y.

Rossen, W. R. 1990c. Theory of Mobilization Pressure Gradient of Flowing Foams in Porous Media. II. Effect of Compressibility. *J. Colloid Interface Sci.* **136** (01): 17–37, doi: 10.1016/0021-9797(90)90075-Y.

Rossen, W. R. 1990d. Theory of Mobilization Pressure Gradient of Flowing Foams in Porous Media. III. Asymmetric Lamella Shapes. *J. Colloid Interface Sci.* **136** (01): 38–53, doi: 10.1016/0021-9797(90)90075-Y.

Rossen, W. R. 1996. Foams in Enhanced Oil Recovery, in *Foams: Theory, Measurements and Applications*, eds. R. K. Prud'homme and S. A. Khan, vol. 57 of *Surfactant Science Series*, chap. 11, 413 – 464, New York: Marcel Dekker, doi: 10.1201/9780203755709.

Rossen, W. R. 1999. Foam Generation at Layer Boundaries in Porous Media. *SPE J.* **4** (04): 409–412, doi: 10.2118/59395-PA. SPE-59395-PA.

Rossen, W. R. 2003. A Critical Review of Roof Snap-Off as a Mechanism of Steady-State Foam Generation in Homogeneous Porous Media. *Colloids Surfaces A: Physicochem. Eng. Asp.* **225** (1-3): 1–24, doi: 10.1016/S0927-7757(03)00309-1.

Rossen, W. R. 2008. Comment on "Verification of Roof snap-off as a foam-generation mechanism in porous media at steady state". *Colloids Surfaces A Physicochem. Eng. Asp.* **322** (1-3): 261–269, doi: 10.1016/j.colsurfa.2008.02.034.

Rossen, W. R. and Boeije, C. S. 2015. Fitting Foam-Simulation-Model Parameters to Data: II. Surfactant-Alternating-Gas Foam Applications. *SPE Reserv. Eval. & Eng.* **18** (02): 273–283, doi: 10.2118/165282-PA. SPE-165282-PA.

Rossen, W. R. and Bruining, J. 2004. Foam Displacements With Multiple Steady States, Society of Petroleum Engineers, doi: 10.2118/89397-MS.

Rossen, W. R. and Bruining, J. 2007. Foam Displacements with Multiple Steady States. *SPE J.* **12** (01): 5–18, doi: 10.2118/89397-PA.

Rossen, W. R. and Gauglitz, P. A. 1990. Percolation Theory of Creation and Mobilization of Foams in Porous Media. *AIChE J.* **36** (08): 1176–1188, doi: 10.1002/aic.690360807.

Rossen, W. R., Ocampo, A., Restrepo, A., Cifuentes, H. D. et al. 2017. Long-Time Diversion in Surfactant-Alternating-Gas Foam Enhanced Oil Recovery From a Field Test. *SPE Reserv. Eval. & Eng.* **20** (01): 1–7, doi: 10.2118/170809-PA. SPE-170809-PA.

Rossen, W. R., Zeilinger, S., Shi, J., and Lim, M. 1999. Simplified Mechanistic Simulation of Foam Processes in Porous Media. *SPE J.* **4** (03): 279–287, doi: 10.2118/57678-PA. SPE-57678-PA.

Rossen, W. R., Zhou, Z. H., and Mamun, C. K. 1995. Modeling Foam Mobility in Porous Media. *SPE Adv. Technol. Ser.* **3** (01): 146–153, doi: 10.2118/22627-PA. SPE-22627-PA.

Sayegh, S. G. and Girard, M. 1989. The Mobility Of Carbon Dioxide Foams In Porous Media, in *Proc.*, Annual Technical Meeting, Banff, May 28 - 31, Petroleum Society of Canada, doi: 10.2118/89-40-30.

Scherer, G. W. and Bachman, D. L. 1977a. Sintering of Low-Density Glasses: I, Theory. *Journal of the American Ceramic Society* **60** (5-6): 236–239, doi: 10.1111/j.1151-2916.1977.tb14114.x.

Scherer, G. W. and Bachman, D. L. 1977b. Sintering of Low-Density Glasses: II, Experimental Study. *Journal of the American Ceramic Society* **60** (5-6): 239–243, doi: 10.1111/j.1151-2916.1977.tb14115.x.

Schindelin, J., Arganda-Carreras, I., Frise, E., Kaynig, V. et al. 2012. Fiji: An Open-source Platform for Biological-Image Analysis. *Nat. Methods* **9** (07): 676–682, doi: 10.1038/nmeth.2019.

Schofield, A. N. 1980. Cambridge Geotechnical Centrifuge Operations. *Géotechnique* **30** (3): 227–268, doi: 10.1680/geot.1980.30.3.227.

Schowalter, T. T. 1979. Mechanics of Secondary Hydrocarbon Migration and Entrapment. *Am. Assoc. Pet. Geol. Bull.* **5** (0149): 723–760, doi: 10.1306/2F9182CA-16CE-11D7-8645000102C1865D.

Shah, S. Y., Wolf, K.-H., Pilus, R., and Rossen, W. R. 2019a. Foam Generation by Capillary Snap-off: Effect of Velocity and Fractional Flow. *SPE J.* doi: 10.2118/195517-PA. SPE-195517-PA.

Shah, S. Y., Wolf, K.-H., Pilus, R., and Rossen, W. R. 2019b. Foam Generation by Capillary Snap-off in Flow Across a Sharp Permeability Transition. *SPE J.* **24** (01): 116–128, doi: 10.2118/190210-PA. SPE-190210-PA.

Shan, D. 2001. *Simulation Study of Gravity Override for Foam Processes*, Master's thesis, University of Texas at Austin.

Sheng, J. J. 2013. Foams and Their Applications in Enhancing Oil Recovery, in *Enhanced Oil Recovery Field Case Studies*, ed. J. J. Sheng, chap. 11, 251–280, Boston: Gulf Professional Publishing, doi: 10.1016/B978-0-12-386545-8.00011-7.

Shrivastava, V. K., Coombe, D. A., Singhal, A. K., and Belgrave, J. D. M. 1999. Numerical Simulation of Foam Flooding for Sweep Improvement. *J. Can. Pet. Technol.* **38** (13): 45–46, doi: 10.2118/99-13-24.

Simjoo, M., Dong, Y., Andrianov, A., Talanana, M. et al. 2013. CT Scan Study of Immiscible Foam Flow in Porous Media for Enhancing Oil Recovery. *Ind. Eng. Chem. Res.* **52** (18): 6221–6233, doi: 10.1021/ie300603v.

Soille, P. and Vincent, L. M. 1990. Determining Watersheds in Digital Pictures via Flooding Simulations, vol. 1360, Presented at the Visual Communications and Image Processing '90, Lausanne, Switzerland, 1 Sept., doi: 10.1117/12.24211.

Sorbie, K. S., Parker, A., and Clifford, P. J. 1987. Experimental and Theoretical Study of Polymer Flow in Porous Media. *SPE Reserv. Eng.* **2** (03): 281–304, doi: 10.2118/14231-PA. SPE-14231-PA.

Sterling, H. J. and Ronayne, M. C. 1985. Simulating Landfill Cover Subsidence, in *Proc.*, 11th Annual Research Symp. on Land Disposal of Hazardous Waste, Cincinnati, Ohio, 29 April-1 May. U.S.E.P.A., 236–244.

Stewart, M. A. and McCartney, J. S. 2013. Centrifuge Modeling of Soil-Structure Interaction in Energy Foundations. *Journal of Geotechnical and Geoenvironmental Engineering* **140** (4): 04013044, doi: 10.1061/(ASCE)GT.1943-5606.0001061.

Stone, H. L. 1982. Vertical, Conformance In An Alternating Water-Miscible Gas Flood, in *Proc.*, SPE Annual Technical Conference and Exhibition, New Orleans, Louisiana, 26-29 September, doi: 10.2118/11130-MS. SPE-11130-MS.

Takada, N. and Mikasa, M. 1984. Consolidation of Multi-layered Clay, in *Proc.*, Sedimentation Consolidation Models—Predictions and Validation, 216–228, ASCE.

Tanzil, D., Hirasaki, G. J., and Miller, C. A. 2002a. Conditions for Foam Generation in Homogeneous Porous Media, Presented at the SPE/DOE Improved Oil Recovery Symposium, Tulsa, Oklahoma, 13-17 April, doi: 10.2118/75176-MS. SPE-75176-MS.

Tanzil, D., Hirasaki, G. J., and Miller, C. A. 2002b. Mobility of Foam in Heterogeneous Media: Flow Parallel and Perpendicular to Stratification. *SPE J.* **7** (02): 203–212, doi: 10.2118/78601-PA. SPE-78601-PA.

Taylor, R. N. 1994. *Geotechnical Centrifuge Technology*, London: CRC Press, doi: 10.1201/9781482269321.

Terzaghi, K. 1943. *Theoretical Soil Mechanics*, John Wiley and Sons, Inc.

Van Baaren, J. P. 1979. Quick-Look Permeability Estimates Using Sidewall Samples and Porosity Logs, in *Proc.*, 6th Annual European Logging Symposium, Society of Professional Well Log Analysts.

van Duijn, C. J., Eichel, H., Helmig, R., and Pop, I. S. 2007. Effective Equations for Two-phase Flow in Porous Media: The Effect of Trapping on the Microscale. *Transp. Porous Media* **69** (03): 411–428, doi: 10.1007/s11242-006-9089-9.

van Duijn, C. J., Mikelic, A., and Pop, I. S. 2002. Effective Equations for Two-Phase Flow with Trapping on the Micro Scale. *Soc. Ind. Appl. Math.* **62** (05): 1531–1568, doi: 10.1137/S0036139901385564.

van Duijn, C. J., Molenaar, J., and De Neef, M. J. 1995. The Effect of Capillary Forces on Immiscible Two-phase Flow in Heterogeneous Porous Media. *Transp. Porous Media* **21** (01): 71–93, doi: 10.1007/BF00615335.

Vassenden, F., Holt, T., and Solheim, A. 1998. Foam Propagation on Semi-Reservoir Scale, in *Proc.*, SPE/DOE Improved Oil Recovery Symposium, Tulsa, Oklahoma,19-22 April, doi: 10.2118/39682-MS. SPE-39682-MS.

Verruijt, A. 2018. *An Introduction to Soil Mechanics*, vol. 30 of *Theory and Applications of Transport in Porous Media*, Springer International Publishing, doi: 10.1007/978-3-319-61185-3.

Visser, R. 1988. *Acoustic Measurements on Real and Synthetic Reservoir Rock*, Ph.D. thesis, Delft University of Technology, Delft, The Netherlands. uuid:80f4218a-cac7-4c8a-ae5f-853ba2bea25c.

Vitoonkijvanich, S., AlSofi, A. M., and Blunt, M. J. 2015. Design of Foam-assisted Carbon Dioxide Storage in a North Sea Aquifer Using Streamline-based Simulation. *International Journal of Greenhouse Gas Control* **33**: 113–121, doi: 10.1016/j.ijggc.2014.11.022.

Wolf, K.-H. 2006. *The Interaction Between Underground Coal Fires and Their Roof Rocks*, Ph.D. thesis, Delft University of Technology, Delft, The Netherlands. uuid:f8d4300d-6f15-4620-80ae-4a8545bd238b.

Wong, P.-z., Koplik, J., and Tomanic, J. P. 1984. Conductivity and Permeability of Rocks. *Phys. Rev. B.* **30** (11): 6606–6614, doi: 10.1103/PhysRevB.30.6606.

Yang, J. and Siddiqui, S. 1999. The Use Of Foam To Improve Liquid Lifting From Low-Pressure Gas Wells, Presented at the Petroleum Conference of The South Saskatchewan Section, Regina, Saskatchewan, October 18 - 21, doi: 10.2118/99-126.

Yang, Y., Li, X., and Li, X. 2018. Shear Strength and Compression Coefficient for Conditioned Sand Subjected to Earth Chamber Stress Levels. *Advances in Materials Science and Engineering* **2018**: 11, doi: 10.1155/2018/1759151.

Yortsos, Y. C. and Chang, J. 1990. Capillary Effects in Steady-state Flow in Heterogeneous Cores. *Transp. Porous Media* **5** (04): 399–420, doi: 10.1007/BF01141993.

Yu, G., Vincent-Bonnieu, S., and Rossen, W. R. 2019. Foam Propagation at Low Superficial Velocity: Implications for Long-Distance Foam Propagation, in *Proc.*, IOR 2019–20th European Symposium on Improved Oil Recovery, doi: 10.3997/2214-4609.201900108.

Zhou, Z. H. and Rossen, W. R. 1995. Applying Fractional-Flow Theory to Foam Processes at the "Limiting Capillary Pressure". *SPE Adv. Technol. Ser.* **3** (01): 154–162. SPE–24180–PA, doi: 10.2118/24180-PA.

Zitha, P. L. J. and Du, D. X. 2010. A New Stochastic Bubble Population Model for Foam Flow in Porous Media. *Transp. Porous Media* **83** (3): 603–621, doi: 10.1007/s11242-009-9462-6.

Zitha, P. L. J., Du, D. X., Uijttenhout, M., and Nguyen, Q. P. 2006. Numerical Analysis of a New Stochastic Bubble Population Foam Model, in *Proc.*, SPE/DOE Symposium on Improved Oil Recovery, Tulsa, Oklahoma, USA, 22-26 April, doi: 10.2118/99747-MS. SPE-99747-MS.

ACKNOWLEDGEMENTS

The content of this PhD dissertation would not have been possible without the help and support of the people I am about to mention. While I can only express my gratitude in words here, my appreciation for their involvement goes way beyond this text and I hope that those involved can relate to this deeper level of personal and professional connection.

Firstly, I would like to thank my promotor Prof. **William Rossen** for giving me this unique opportunity and for believing in me from the very beginning. Bill, your supervision and guidance through both the technical and non-technical aspects of this PhD journey have had a monumental contribution towards the end-result. I would like to thank you for our weekly meetings and for the inspiring and thought-provoking discussions we have had during these sessions. Your attitude towards research and academic life has helped me grow professionally and personally over the past four years. It was a pleasure working with you and I've enjoyed every moment of it.

Next, I would like to thank my other promotor Dr. **Karl-Heinz Wolf**. You are an endless fountain of ideas, and without your knowledge of petrophysics and geology I would have been lost at several stages of my PhD project. Your relentless pursuit of the creation of the perfect synthetic porous media inspired me to work on the challenging topic and the results of that project now form a significant portion of this book. I always left our meetings with a smile on my face and full of new directions to look into. I would also like to thank Dr. **Amin Askarinejad** for helping with the project on creating synthetic media and for the numerous insightful discussions on consolidation theory.

Dr. **Hadi Hajibeygi**, thank you for being part of my doctoral defence committee. I would not have been able to obtain this PhD position without you and I would like to thank you for that. You gave me the opportunity to work on a challenging topic during my MSc studies and that motivated me to pursue a doctoral degree. You always inspired me to strive for greatness and perfection in everything I do.

I am thankful to the rest of my committee members including Prof. **Eric Schlangen**, Prof. **Hans Geerlings**, Prof. **George Hirasaki** and Dr. **Raj Tewari** for being part of my PhD defence and for reading my dissertation. George, thank you for sharing your wealth of knowledge with all the the inspiring conversations during the Delft Summer School and during my visit to Rice University. I will forever be grateful for your help and advice with respect to doctoral research as well as professional life after my PhD.

I would like to extend my gratitude to Dr. **Sébastien Vincent-Bonnieu** for countless useful discussions about my project during the foam group meetings. While you were not directly involved with my work, you were always enthusiastic towards my research and glad to help and I will forever be grateful for that. Your professionalism and efficiency in dealing with various projects at TU Delft while being there only once a week

was a source of inspiration. I would also like to thank Dr. **Sian Jones** for being the most helpful colleague that one could ask for. Sian, thank you for the long discussions about the beauty of bubbles, for being my paranymph for the PhD defence, the Monday cakes and the recipes that came after, and for your advice on personal as well as professional matters through the course of my PhD. If I could make a list of the things I should thank you for, it could potentially form another chapter in this dissertation.

I am very thankful to Shell, PETRONAS and Universiti Teknologi PETRONAS for sponsoring my PhD project. I would like to thank Dr. **Jeroen Groenenboom**, Dr. **Hans Groot**, Dr. **Rashidah Pilus** and **Ridhwan Bahrim** for hosting us during our fruitful visit to Malaysia. I would like to thank my colleagues **Ahmed Hussain** and **Martijn Janssen**, who were part of the same project, for all the wonderful times we had on that trip. Ahmed, I am going to miss your cakes and your curiosity, especially when talking about research. Your questions often made me go back to the books and find out more about what we had just discussed. Martijn, thank you for being one of my closest friends through this journey and for all the fun we have had together both in and outside the office. You were the person I would approach to kick back and de-stress. Thanks for all the amazing evenings in Delft and for many more to come!

There are several people in the lab whom I cannot thank enough for their involvement in my research. **Michiel Slob**, you helped me build my setup and gave me the freedom that I needed in the lab. I am thankful for the productive working relationship we had and for the often lengthy but useful discussions about foam experiments. **Marc Friebel**, you are a great friend and a truly delightful colleague. You were there to support me in the toughest of times, late in the evening, at times when everything that could go wrong in an experiment did go wrong. You've helped me with a cheerful face, cracking jokes, even at times when you were swamped with your own work. Your relentless spirit while resolving challenging design issues in the lab was a true source of inspiration. **Karel Heller**, in the first year of my PhD, when experimental failure and the resultant frustration was an everyday thing, you said with encouraging assertion "Don't worry, we'll get through!". We are through! Thank you for being there, for your advice and help with not just problems with my experiments, but also various DIY projects that I'll skip the details of for now. **Ellen Meijvogel-de Koning**, **Wim Verwaal**, **Joost van Meel**, **Jens van den Berg**, **Han de Visser** and **Jolanda van Haagen-Donker**, many thanks for all your help throughout these years in the lab. Without you all, achieving these results would have been impossible.

To all the other members of the **foam group**, thank you for making this adventure so pleasant. **Jiakun**, for being there as a friend and an honest advisor in both personal and professional matters. And for all the brilliant assists every Tuesday at our weekly football game. Thanks also for never refusing to help during busy lab weekends. **Xiaocong**, for being the nicest friend, a sharing desk-mate and a fierce basketball buddy. For all the silly conversations and the dumplings! **Guanqun** (Brandon) for the deep discussions about foam behaviour in porous media and for being a selfless colleague and a helpful friend. **Jinyu**, for thinking alongside me on several technical challenges during my PhD. **Kai**, for the great blocks during football, for all the fun during our Petrobowl preparations and

for organising the foam group meetings.

Several other colleagues, while working on different projects, made the last four years a truly memorable experience. **Matteo**, for being an inspiring friend, colleague and footballer. For the countless evenings discussing the past, present and future over a cold beer. **Rafael**, for being an inexhaustible source of energy and for demonstrating that it might not be too late to dunk, even as a researcher in one's late thirties. **Mark**, for never refusing to help, for always being brutally honest, and for all the enjoyable conversations we have had about life, work and F1, while sipping a fine single malt. **Denis**, for the friendly advise at various points during my PhD and for the fun evenings with the foam group and during conferences. **Mohsen** and **Kiarash** for the delicious Persian food and for maintaining a fun atmosphere in the office. **Nikita**, **Matei**, **Siavash** and **Eduardo**, you three made the first two years of my PhD unforgettable, through all the hilarious stories and the time spent on the basketball court and the football pitch.

I would like to thank the **Comedy Football Club** for guaranteed fun every Tuesday evening, come hell or high water. The **Punch Basketball Club**, I can't thank you enough for assuring a regular supply of intense and competitive basketball, for this is crucial for my survival. **H420**, for the team spirit and for playing the right way!

Through the four years of my doctoral studies, I have supervised and mentored seven BSc students and one MSc student for their thesis projects. Without you all, this thesis would be a shadow of its current shape and form. I would like to thank **Herru As Syukri** for his tremendous help in the laboratory with foam experiments and for his indefatigable attitude towards technical challenges in the laboratory. **Alexander van Ballaer**, **Guus Hoogewerf** and **Pelle van Nieuwkerk**, thank you for all the effort you put in to tackle the challenging problem of creating synthetic porous media.

Lydia Broekhuijsen-Bentvelzen, **Marlijn Ammerlaan**, **Margot Bosselaar-Perk**, **Marja Roep-Van der Klis** and the rest of the **GSE support staff**, many thanks for all your assistance during the past four years. You always helped me promptly and with a smile and this created a very productive environment to work in.

Romy, thank you for being there from the beginning to the end and for bearing with me through all the frustrating evenings and busy weeks. Thanks also for designing the beautiful cover of this book. Thank you for pushing me consistently at times when I started procrastinating about a variety of things related directly, or indirectly, to my PhD, and the life after. I would like to thank the **Meier's** (& in laws) for being my family away from home. **Eric**, **Inge**, **Marja** and **Theo** for always showing interest in my doctoral studies. Lastly, I would like to thank my parents, **Neela** and **Yogesh Shah** and my sister **Himalee** for their support.

Curriculum Vitæ

Swej Yogesh Shah

14-03-1991 Born in Mumbai, India.

Education

2007-2009 **Lilavatibai Podar High School**, Mumbai, India

2009–2013 Bachelor of Chemical Engineering
Institute of Chemical Technology, Mumbai, India

2013–2015 Master of Science in Petroleum Engineering
Delft Univeristy of Technology, The Netherlands

2015–2019 PhD. Petroleum Engineering
Delft University of Technology, The Netherlands
Thesis: In Situ Foam Generation
In Flow Across a Sharp Permeability Transition
Promotor 1: Prof. dr. W. R. Rossen
Promotor 2: Prof. dr. K.-H A. A. Wolf

Work Experience and Internships

May–July 2012 **Indian Oil Corporation**, Mumbai, India
Chemical engineering intern

July–August 2014 **Chevron exploration & Production B.V.**, The Hague, The Netherlands
Petroleum engineering intern

April–July 2015 **Mathematics & Cybernetics, SINTEF Digital**, Oslo, Norway
Software developer (Reservoir simulation) intern

2015–2019 **Delft University of Technology**, The Netherlands
Teaching assistant, Field development project

AWARDS

2014	Young Innovator's Choice Competition - 1st Place
2014	SPE STAR Fellowship
2016	SPE Europe Region Student Paper Contest - 1st Place
2016	SPE International Student Paper Contest - 3rd Place

LIST OF PUBLICATIONS

PEER-REVIEWED PUBLICATIONS

4. **S.Y. Shah**, A. Askarinejad, W.R. Rossen, K.-H.A.A. Wolf, *Creating synthetic porous media for multiphase flow experiments under controlled conditions*, submitted, Granular Matter (2019).

3. **S.Y. Shah**, H. As Syukri, R.M. Pilus, K.-H.A.A. Wolf, W.R. Rossen, *Foam Generation in Flow Across a Sharp Permeability Transition: Effect of Velocity and Fractional Flow*, SPE Journal, *in press* (2019).

2. **S.Y. Shah**, R.M. Pilus, K.-H.A.A. Wolf, W.R. Rossen, *Foam generation by capillary snap-off in flow across a sharp permeability transition*, SPE Journal **24**, 116 (2019).

1. **S.Y. Shah**, O. Møyner, M. Tene, K.-A. Lie, H. Hajibeygi, *The multiscale restriction smoothed basis method for fractured porous media (F-MsRSB)*, Journal of Computational Physics **318**, 36 (2016).

CONFERENCE PROCEEDINGS AND TALKS

8. **S.Y. Shah**, J. Tang, J. Gong, W.R. Rossen, *Studies of Foam for EOR and CO2 storage: Liquid Injectivity, the Effect of Oil on Foam, and Generation In-situ in Heterogeneous Formations*, in 4th Biennial CO_2 for EOR as CCUS Conference (2019).

7. **S.Y. Shah**, H. As Syukri, R.M. Pilus, K.-H.A.A. Wolf, W.R. Rossen, *Foam Generation in Flow Across a Sharp Permeability Transition: Effect of Velocity and Fractional Flow*, in SPE Europec featured at 81st EAGE Conference and Exhibition (2019).

6. **S.Y. Shah**, A. van Ballaer, A. Askarinejad, W.R. Rossen, K.-H.A.A. Wolf, *Creating synthetic porous media for multiphase flow experiments under controlled conditions*, in 11th International Conference on Porous Media and Annual Meeting, Interpore (2019).

5. **S.Y. Shah**, H. As Syukri, K.-H.A.A. Wolf, R.M. Pilus, W.R. Rossen, *Foam Generation by Snap-off in Flow Across a Sharp Permeability Transition*, in IOR 2019 – 20th European Symposium on Improved Oil Recovery (2019).

4. **S.Y. Shah**, R.M. Pilus, K.-H.A.A. Wolf, W.R. Rossen, *Foam generation by capillary snap-off in flow across a sharp permeability transition*, in SPE Improved Oil Recovery Conference (2018).

3. **S.Y. Shah**, K.-H.A.A. Wolf, W.R. Rossen, *Foam generation by snap-off due to flow across a sharp permeability transition*, in 91st ACS Colloid & Surface Science Symposium (2017).

2. **S.Y. Shah**, K.-H.A.A. Wolf, W.R. Rossen, *Foam generation by snap-off due to flow across a sharp permeability transition*, in Bubble & Drop (2017).

1. **S.Y. Shah**, W.R. Rossen, K.-H.A.A. Wolf, *Preparing multi-pore homogeneous and layered cores for controlled flooding experiments*, in 9th International Conference on Porous Media and Annual Meeting, Interpore (2017).